(12) INTERNATIONAL APPLICATION PUBLISHED UNDER THE PATENT COOPERATION TREATY (PCT)

(19) World Intellectual Property Organization
International Bureau

(43) International Publication Date
06 December 2018 (06.12.2018)

WIPO | PCT

(10) International Publication Number
WO 2018/220371 A1

(51) International Patent Classification:
A61K 31/7088 (2006.01) *C12N 15/113* (2010.01)

(21) International Application Number:
PCT/GB2018/051475

(22) International Filing Date:
31 May 2018 (31.05.2018)

(25) Filing Language: English

(26) Publication Language: English

(30) Priority Data:
1708709.9 01 June 2017 (01.06.2017) GB

(71) Applicants: **THE UNIVERSITY OF LEEDS** [GB/GB]; The University of Leeds, Woodhouse Lane, Horsforth, Leeds Yorkshire LS2 9JT (GB). **THE UNIVERSITY OF YORK** [GB/GB]; The University of York, Heslington, York Yorkshire YO10 5DD (GB).

(72) Inventors: **LEONOV, German**; Sharpe Capital Limited, Spectrum House, 32-34 Gordon House Road Highgate, London Greater London NW51LP (GB). **WHITE, Simon**; University of Connecticut, Department of Molecular and Cell Biology North Eagleville Road, Storrs, Connecticut 06269 (US). **STOCKLEY, Peter**; University of Leeds, Astbury Centre for Structural Molecular Biology, Leeds Yorkshire LS2 9JT (GB). **PATEL, Nikesh**; University of Leeds, Astbury Centre for Structural Molecular Biology, Leeds Yorkshire LS2 9JT (GB). **WROBLEWSKI, Emma**; University of Leeds, Astbury Centre for Structural Molecular Biology, Leeds Yorkshire LS2 9JT (GB). **MASKELL, Dan**; University of Leeds, Astbury Centre for Structural Molecular Biology, Leeds Yorkshire LS2 9JT (GB). **TWAROCK, Reidun**; University of York, Heslington, York Yorkshire YO10 5DD (GB). **BINGHAM, Richard**; University of York, Heslington, York Yorkshire YO10 5DD (GB). **WEISS, Eva**; University of York, Heslington, York Yorkshire YO10 5DD (GB). **DYKEMAN, Eric**; University of York, Heslington, York Yorkshire YO10 5DD (GB).

(74) Agent: **SYMBIOSIS IP**; Rob Docherty, Symbiosis IP, NAFIC Sand Hutton, York Worcestershire YO41 1LZ (GB).

(81) Designated States *(unless otherwise indicated, for every kind of national protection available)*: AE, AG, AL, AM, AO, AT, AU, AZ, BA, BB, BG, BH, BN, BR, BW, BY, BZ, CA, CH, CL, CN, CO, CR, CU, CZ, DE, DJ, DK, DM, DO, DZ, EC, EE, EG, ES, FI, GB, GD, GE, GH, GM, GT, HN,

(54) Title: VIRUS LIKE PARTICLE

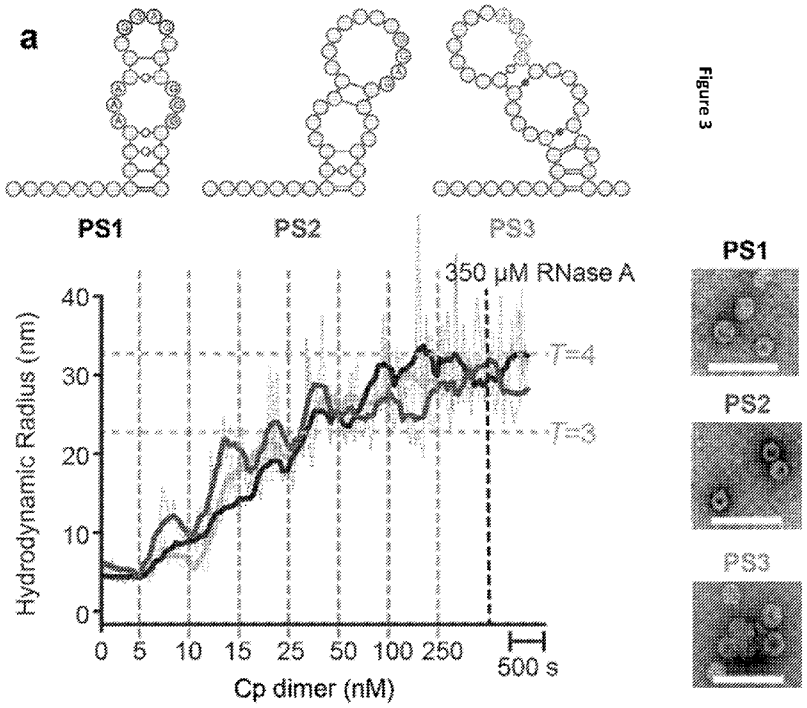

Figure 3

(57) Abstract: The disclosure relates to the assembly of Virus Like Particles [VLPs] using packaging native and artificial packaging signals and their use in vaccines and immunological compositions and the methods of vaccination or immunisation against human and animal viral pathogens.

[Continued on next page]

WO 2018/220371 A1

HR, HU, ID, IL, IN, IR, IS, JO, JP, KE, KG, KH, KN, KP, KR, KW, KZ, LA, LC, LK, LR, LS, LU, LY, MA, MD, ME, MG, MK, MN, MW, MX, MY, MZ, NA, NG, NI, NO, NZ, OM, PA, PE, PG, PH, PL, PT, QA, RO, RS, RU, RW, SA, SC, SD, SE, SG, SK, SL, SM, ST, SV, SY, TH, TJ, TM, TN, TR, TT, TZ, UA, UG, US, UZ, VC, VN, ZA, ZM, ZW.

(84) Designated States *(unless otherwise indicated, for every kind of regional protection available)*: ARIPO (BW, GH, GM, KE, LR, LS, MW, MZ, NA, RW, SD, SL, ST, SZ, TZ, UG, ZM, ZW), Eurasian (AM, AZ, BY, KG, KZ, RU, TJ, TM), European (AL, AT, BE, BG, CH, CY, CZ, DE, DK, EE, ES, FI, FR, GB, GR, HR, HU, IE, IS, IT, LT, LU, LV, MC, MK, MT, NL, NO, PL, PT, RO, RS, SE, SI, SK, SM, TR), OAPI (BF, BJ, CF, CG, CI, CM, GA, GN, GQ, GW, KM, ML, MR, NE, SN, TD, TG).

Published:

— *with international search report (Art. 21(3))*

— *with sequence listing part of description (Rule 5.2(a))*

Virus Like Particle

Field of the Invention

The disclosure relates to the assembly of Virus Like Particles [VLPs] using native and artificial nucleic acid packaging signals and their use in vaccines, immunological and pharmaceutical compositions; methods of vaccination or immunisation against human and animal viral pathogens and also as a delivery vehicle for therapeutic agents such as pharmaceutical proteins, siRNAs or gene therapy vectors or diagnostic agents.

Background of the Invention

Viruses cause various debilitating diseases in humans and animals with often detrimental effects or even death. Viral infections cause a huge financial burden to the healthcare systems around the world, and also result in vast losses of animal related products, such as in the meat or dairy industries.

In contrast to bacterial infections which can be treated with antibiotic agents after the infections starts, prevention of viral infections is typically the preferred route as there are often no effective anti-viral drug options available. Vaccination is the most effective form of disease prevention and has been successfully developed for some viral diseases such as influenza, polio, measles and Human Papilloma Virus [HPV]. Vaccination is the administration of antigenic material to stimulate an individual's immune system to develop adaptive immunity to a pathogen. The active agent of a vaccine may be, for example, an inactivated form of the pathogen, a highly immunogenic component of the pathogen or in the form of a weakened so called attenuated virus. However, all these different types of vaccines vary in their effectiveness and safety record and moreover can often be unsuitable for administration to immune compromised subjects, pregnant women or children.

Inactivated vaccines are made from viruses which have been killed through physical or chemical processes. These types of vaccines are very safe, as they cannot cause disease because they lack infectious genetic material, and are therefore suitable for immune compromised subjects. However, such inactivated vaccines are often ineffective in inducing an appropriate or long lasting immune response, and therefore frequently require multiple administration steps. Vaccines containing highly immunogenic components of the pathogen, so called subunit vaccines, provide similar benefits to the inactivated vaccines such as a high safety record as they do not contain live components of the virus which can cause disease. However, effective immune responses are not guaranteed, and even if a response is elicited,

immunological memory, providing protection against the desired pathogen for a prolonged period, may not be achieved.

Alternatively, live attenuated vaccines can be used. Live attenuated vaccines comprise weakened pathogens which although still capable of replication in the host organism cause no or a very mild disease. Vaccinations using an attenuated virus result in excellent protection; however, they are intrinsically less safe when compared to inactivated or subunit vaccines since they can revert to their original more virulent form and cause disease. Therefore attenuated vaccines are unsuitable for subjects with compromised immune systems, can harm the unborn child when given during pregnancy and have an increased potential for immunisation errors by health professionals such as e.g. reconstitution errors of lyophilised attenuated pathogens which, when given in a higher dose, are more potent. Moreover, attenuated vaccines are less stable than inactivated vaccines and require sophisticated logistics to maintain cold storage and transport to maintain the, although weakened, activity. This is of particular concern in third world countries with a less established health system.

Attenuated vaccines are common and are available for a variety of diseases such as measles, mumps, rubella, chicken pox, smallpox and polio. Most of the live attenuated vaccines in use today are derived from serial passage in cultured cells such as for example fibroblasts or and chicken embryos, resulting in a gradual loss of virulence. This method relies on the random accumulation of point mutations to confer avirulence and is time consuming and inefficient. Other methods to produce attenuated viral strains are based on genetic engineering and are disclosed in application WO2005/012535.

Virus-like particles (VLPs) comprise multiple capsid proteins that mimic the conformation of native viruses but lack the viral DNA or RNA and thus are unable to replicate in a host cell. The use of VLPs as a tool for the production of safe and efficient vaccines has been recognised and some VPL-based vaccines against human papilloma virus have been developed. US8062642 discloses the production of papillomavirus capsid proteins and VLPs with antigenic characteristics similar to those of native infectious virus. Similarly, WO9913056 discloses methods of disassembly of papilloma VLPs.

Despite the enormous success of the types of vaccines listed above they are in general very difficult to prepare/formulate with the desired properties and in many viruses their natural antigenic variation across circulating populations means that these strategies are not viable in these cases.

The present disclosure relates to the formation of VLPs using nucleic acid packaging signals derived from viruses and the design of nucleic acid cassettes comprising native and/or artificial packaging signals that provide a substrate for artificial VLP assembly and the use of artificial VLPs as vaccines and in the delivery of agents to cells, for example therapeutic or diagnostic agents. The knowledge of the RNA packaging signal-mediated assembly mechanisms of positive-sense, single-stranded (ss) RNA viruses has enabled the identification of the critical properties of their genomic RNA molecules with respect to being assembly substrates, allowing the production of artificial, efficient RNA substrates for the efficient assembly of VLPs. The latter have similar properties to the natural virions formed by viruses. In particular, artificial VLP capsids retain the native immunological properties of those viruses as well as their cell tropism. They also retain many of the stability and mechanical properties of the original virus particle. VLPs have utility in a wide range of applications in relation to the cell specific delivery of agents and as safe, attenuated vaccines and vectors for targeted delivery of drugs and in gene therapy.

Statements of the Invention

According to an aspect of the invention there is provided an artificial nucleic acid cassette for use in the assembly of a virus like particle comprising: one or more packaging signals, wherein the more than one packaging signals are arranged in series and separated by nucleic acid, said packaging signals composed of a nucleic acid loop domain comprising a nucleotide binding motif for cognate viral capsid protein(s), and a nucleic acid stem domain consisting of a double stranded region by intramolecular base pairing, wherein said artificial nucleic acid cassette, when contacted with a plurality of cognate viral capsid proteins, assembles said cognate viral capsid proteins into a VLP that protects said nucleic acid packaging signals contained within said VLP from ribonuclease digestion.

In a preferred embodiment of the invention said artificial nucleic acid cassette is a non-replicating nucleic acid.

In a preferred embodiment of the invention said VLP provokes an immune response similar to an immune response of the native virus particle when administered to an animal subject.

In a further preferred embodiment of the invention said artificial nucleic acid cassette is not a native virus particle.

In a preferred embodiment of the invention said artificial nucleic acid cassette does not comprise protein encoding nucleic acid.

In a preferred embodiment of the invention said artificial nucleic acid cassette comprises at least two nucleic acid packaging signals.

Preferably, said artificial nucleic acid cassette comprises at least 2, 3, 4, 5, 6, 7, 8, 9 or at least 10 nucleic acid packaging signals.

In a preferred embodiment of the invention said artificial nucleic acid cassette comprises at least 1 nucleic acid packaging signal.

In a preferred embodiment of the invention said artificial nucleic acid cassette comprises at least 2 nucleic acid packaging signals.

In a preferred embodiment of the invention said artificial nucleic acid cassette comprises at least 3 nucleic acid packaging signals.

In a preferred embodiment of the invention said artificial nucleic acid cassette comprises at least 4 nucleic acid packaging signals

In an alternative preferred embodiment of the invention said artificial nucleic acid cassette comprises at least 5 nucleic acid packaging signals.

In a preferred embodiment of the invention said non-coding viral nucleic acid separating said nucleic acid packaging signals is at least 5 nucleotides in length.

In a preferred embodiment of the invention said non-coding viral nucleic acid separating said nucleic acid packaging signals is at least between 5 and 50 nucleotides in length. Preferably, greater than 50 nucleotides.

In a preferred embodiment of the invention said loop domain comprising said capsid binding motif is at least 4 nucleotides in length. Preferably, said loop domain is at least 5, 6, 7 or 8 nucleotides in length.

In a preferred embodiment of the invention said stem domain is at least 4 base pairs (bp) in length. Preferably said stem domain is at least 5, 6, 7, 8, 9, 10, 11, 12, 13, 14, 15, 16, 17, 18,

19, 20, 21, 22, 23, 24, 25, 26, 27, 28, 29, 30, 31, 32, 33, 34, 35, 36, 37, 38, 39, 40, 41, 42, 43, 44, 45, 46, 47, 48, 49, 50, 60, 61, 62, 63, 64, 65, 66, 67, 68, 69, or at least 70 bp in length.

In a preferred embodiment of the invention said artificial nucleic acid cassette is at least 50 nucleotides in length. Preferably said nucleic acid cassette is between 50 and 1000 nucleotides in length.

In a preferred embodiment of the invention said artificial nucleic acid cassette is at least 50, 60, 70, 80, 90, 100, 110, 120, 130, 140, 150, 200, 250, 300, 350, 400, 450, 500, 550, 600, 650, 700, 750, 800, 850, 900, 950 or at least 1000 or nucleotides in length.

In a preferred embodiment of the invention said nucleic acid packaging signal is isolated from an RNA virus; preferably said RNA virus is a human pathogen.

Preferably said packaging signal is a modified packaging signal that retains the characteristic nucleotide recognition motif and spacing between packaging signals but alters stability of/stabilises individual packaging signals.

Several diseases in humans, animals and plants are caused by so called RNA viruses. Single-stranded RNA viruses are divided into three groups: Positive-sense ssRNA viruses (Group IV), negative-sense ssRNA viruses (Group V) and retroviruses (Group VI). On infection, the viral RNA enters the host cells and, dependent on the type of virus, RNA is directly translated (Group IV) into the viral proteins necessary for replication or is, prior to translation, transcribed into a more suitable form of RNA by an RNA-dependent RNA polymerase (Group V). Group VI RNA viruses utilise a virally encoded reverse transcriptase to produce DNA from the RNA genome, which is often integrated into the host genome and so replicated and transcribed by the host. Non-limiting examples of positive-sense ssRNA viruses include hepatitis C, West Nile virus, Dengue virus, Zika virus, SARS and MERS coronavirus and rhinovirus. Negative sense ssRNA viruses include, by example, Ebola virus, measles, mumps, influenza and hepatitis D virus. Retroviruses of the genus Lentivirus include Human Immune deficiency virus I and II and Hepatitis B virus. Examples of zoonotic viral pathogens include Ebola virus, Rabies virus and influenza A virus. Non-limiting examples of plant ssRNA viruses include Turnip Crinkle Virus, Cowpea Chlorotic Mottle Virus 1, 2 and 3, Brome Mosaic Virus 1, 2 and 3, and Satellite Tobacco Necrosis Virus. In our co-pending application US 14/916,945, the content of which is incorporated by reference in its entirety, and in particular the packaging signals and mimetic aptamers disclosed therein, are disclosed packaging signals for a range of ssRNA viruses.

In a preferred embodiment of the invention said RNA virus is a positive sense single stranded RNA virus.

In a preferred embodiment of the invention said nucleic acid packaging signal RNA virus is isolated from Hepatitis B virus.

In a preferred embodiment of the invention said Hepatitis B virus packaging signal comprises a nucleotide binding motif wherein said nucleotide binding motif comprises the nucleotide sequence RGAG wherein R is either G or A.

In a preferred embodiment of the invention said artificial nucleic acid cassette comprises at least one, two or three Hepatitis B virus packaging signals wherein one or more of said nucleic acid packaging signals includes the nucleotide binding motif RGAG.

In a preferred embodiment of the invention said nucleic acid cassette comprises at least one of the PSs identified for Hepatitis B wherein each of said nucleic acid packaging signals includes the binding motif RGAG.

In a preferred embodiment of the invention said artificial nucleic acid cassette comprises a nucleotide sequence selected from the group consisting of:

i) a nucleic acid molecule comprising a nucleotide sequence GUUUGUUUAAAGACUGGGAGGAGUUGGGGGAGGAG [SEQ ID NO: 1];

ii) a nucleic acid molecule comprising a nucleotide sequence that is at least 25% identical to the nucleotide sequence set forth in SEQ ID NO: 1 and that comprises a nucleotide binding motif GGGAGG.

In a further preferred embodiment of the invention said artificial nucleic acid cassette comprises a nucleotide sequence selected from the group:

i) a nucleic acid molecule comprising a nucleotide sequence GGGCCCUCUGACAGUUAAUGAAAAAAGGAGAUUAAAAUUAAUUAUGCCU [SEQ ID NO: 2];

ii) a nucleic acid molecule comprising a nucleotide sequence that is at least 25% identical to the nucleotide sequence set forth in SEQ ID NO: 2 and that comprises a nucleotide binding motif GAAAAAAGGAG (SEQ ID NO 9).

In a further preferred embodiment of the invention said artificial nucleic acid cassette comprises a nucleotide sequence selected from the group:

i) a nucleic acid molecule comprising a nucleotide sequence GGCUGGCAUUCUAUAUAAGAGAGAAACUACACGC [SEQ ID NO: 3];

ii) a nucleic acid molecule comprising a nucleotide sequence that is at least 25% identical to the nucleotide sequence set forth in SEQ ID NO: 3 and that comprises a nucleotide binding motif AUAUAAGAG.

In a preferred embodiment of the invention said artificial nucleic acid cassette comprises a nucleotide sequence that is at least 30%, 35%, 40%, 45%, 55%, 60%, 70%, 75%, 80%, 85%, 90%, 95%, 96%, 97%, 98% or 99% identical to the nucleotide sequence set forth in SEQ ID NO: 1 and/or SEQ ID NO: 2 and/or SEQ ID NO: 3.

In a preferred embodiment of the invention said artificial nucleic acid cassette comprises a nucleotide sequence comprising SEQ ID NO: 1 and/or SEQ ID NO: 2 and/or SEQ ID NO: 3.

In a preferred embodiment of the invention said artificial nucleic acid cassette comprises a nucleotide sequence comprising SEQ ID 4: CUGGGAGGAGUUGGGGGAGGAGAUUAGGUUAAAGGUCUUUGUACUAGGAGGCUGUAGGC

In an alternative embodiment of the invention said RNA virus is a zoonotic species that infects of a human subject.

In a further alternative embodiment of the invention said RNA virus is a species that infects a veterinary animal subject.

In a further alternative embodiment of the invention said RNA virus is a species that infects a plant cell or plant.

In a preferred embodiment of the invention said RNA virus is Satellite Tobacco Necrosis Virus.

In a preferred embodiment of the invention said nucleic acid cassette comprises at least one nucleic acid packaging signal isolated from Satellite Tobacco Necrosis Virus.

In a preferred embodiment of the invention said nucleic acid cassette comprises at least one nucleic acid packaging signal wherein said nucleic acid packaging signal comprises the nucleotide binding motif AXXA or AXXXA wherein X is any nucleotide base.

In a preferred embodiment of the invention said artificial nucleic acid cassette comprises a nucleotide sequence selected from the group:

i) a nucleic acid molecule comprising a nucleotide sequence set forth in SEQ ID NO: 5;

ii)

a nucleic acid molecule comprising a nucleotide sequence that is at least 25% identical to the nucleotide sequence set forth in SEQ ID NO: 5
[GGGCUGCCCUCAAGGACCAGGGCAGAAAAGAGGAAAAGAAAAGUGACAGAACACUUAUAAGGAAAAAA CGUACAAACGUUUUAAGGAAAAAAGGAAGCUGCAAUAGCGCAAGGAAUCCGAAAAUUCGGAAAGGAA]

and that comprises a nucleotide binding motif AXXA.

In a preferred embodiment of the invention said artificial nucleic acid cassette comprises a nucleotide sequence selected from the group:

i) a nucleic acid molecule comprising a nucleotide sequence set forth in SEQ ID NO: 6
[GGGCUGCCCUCAAGGACCAGGGCAGAAAAGAGGAAAAGAAAAGUGACAGAACACUUA UAAGGAACCACACAAGUGGAAGGAAAAAAGGAAGCUGCAAUAGCGCAAGGAAUCCGAA AAUUCGGAAAGGAA]

ii) a nucleic acid molecule comprising a nucleotide sequence that is at least 25% identical to the nucleotide sequence set forth in SEQ ID NO: 6 and that comprises a nucleotide binding motif AXXA.

In a preferred embodiment of the invention said artificial nucleic acid cassette comprises a nucleotide sequence selected from the group:

i) a nucleic acid molecule comprising a nucleotide sequence set forth in SEQ ID NO: 7
[GGGCUGCCCUCAAGGACCAGGGCAGAAAAGAGGAAAAGAAAAGUGACAGAACACUUA UAAGGAACCACACAAGUAUAAGGAAAAAAGGAAGCUGCAAUAGCGCAAGGAAUCCGAA AAUUCGGAAAGGAA]

ii) a nucleic acid molecule comprising a nucleotide sequence that is at least 25% identical to the nucleotide sequence set forth in SEQ ID NO: 7 and that comprises a nucleotide binding motif AXXA.

In a preferred embodiment of the invention said artificial nucleic acid cassette comprises a nucleotide sequence selected from the group:

i) a nucleic acid molecule comprising a nucleotide sequence set forth in SEQ ID NO: 8
[GGGCCCCGCAACAAUGCGGGGAAGGAAGGAAGGAAGAAAACGUACAAACGUUUUAAG
GAACAACGCAACAAUGCGUUGAAGGAAGGAAGGAAGGGGCGUACAAACGCCCCAAGGA
AUUUUGCAACAAUGCAAAAAAGGAA]

ii) a nucleic acid molecule comprising a nucleotide sequence that is at least 25% identical to the nucleotide sequence set forth in SEQ ID NO: 8 and that comprises a nucleotide binding motif AXXA.

In a preferred embodiment of the invention said artificial nucleic acid cassette comprises a nucleotide sequence that is at least 30%, 35%, 40%, 45%, 55%, 60%, 70%, 75%, 80%, 85%, 90%, 95%, 96%, 97%, 98% or 99% identical to the nucleotide sequence set forth in SEQ ID NO: 5, SEQ ID NO: 6, SEQ ID NO: 7 or SEQ ID NO: 8.

In a preferred embodiment of the invention said artificial nucleic acid cassette further comprises a transcription cassette comprising a nucleic acid molecule adapted to transcribe a nucleic acid encoding a polypeptide or a functional RNA.

In a preferred embodiment of the invention said adaptation is the provision of a promoter sequence and termination sequence to enable expression of said nucleic acid molecule encoding said polypeptide or functional RNA.

In a preferred embodiment of the invention said polypeptide is a therapeutic polypeptide, for example an antibody or antibody fragment.

Antibody fragments include nucleic acids encoding single chain antibody fragments. Antibodies include nucleic acid molecules encoding humanised and chimeric antibodies, prepared according to conventional methodology. Chimeric antibodies are recombinant antibodies in which all of the V-regions of a mouse or rat antibody are combined with human antibody C-regions. Humanised antibodies are recombinant hybrid antibodies which fuse the complementarity determining regions from a rodent antibody V-region with the framework regions from the human antibody V-regions. The C-regions from the human antibody are also used. The complementarity determining regions (CDRs) are the regions within the N-terminal domain of both the heavy and light chain of the antibody to where the majority of the variation of the V-region is restricted. These regions form loops at the surface of the antibody molecule. These loops provide the binding surface between the antibody and antigen.

In an alternative embodiment of the invention said functional nucleic acid is an mRNA encoding a therapeutic polypeptide, an antisense oligonucleotide or a siRNA.

A technique to specifically ablate gene function which has broad acceptance is through the introduction of double-stranded RNA, also referred to as small inhibitory or interfering RNA (siRNA), into a cell which results in the destruction of mRNA complementary to the sequence included in the siRNA molecule. The siRNA molecule comprises two complementary strands of RNA (a sense strand and an antisense strand) annealed to each other to form a double-stranded RNA molecule. The siRNA molecule is typically derived from exons of the gene which is to be ablated. Many organisms respond to the presence of double-stranded RNA by activating a cascade that leads to the formation of siRNA. The presence of double-stranded RNA activates a protein complex comprising RNase III which processes the double-stranded RNA into smaller fragments (siRNAs, approximately 21-29 nucleotides in length) which become part of a ribonucleoprotein complex. The siRNA acts as a guide for the RNase complex to cleave mRNA complementary to the antisense strand of the siRNA thereby resulting in destruction of the mRNA.

According to a further aspect of the invention there is provided a virus like particle comprising an artificial nucleic acid cassette according to the invention.

In a preferred embodiment of the invention said virus like particle is immunogenic when administered to a subject. Preferably said virus like particle provokes an immune response similar to an immune response to the cognate native virus.

In a preferred embodiment of the invention said immune response is induction of an antibody response wherein said antibody response induces antibodies that specifically bind native virus particles.

In a preferred embodiment of the invention said virus like particle retains or has enhanced cell tropism when compared to native virus particles.

According to a further aspect of the invention there is provided a vaccine or immunogenic composition comprising a virus like particle according to the invention.

In a preferred embodiment of the invention said vaccine or immunogenic composition further comprises an adjuvant and/or carrier.

Adjuvants (immune potentiators or immunomodulators) have been used for decades to improve the immune response to vaccine antigens. The incorporation of adjuvants into vaccine formulations is aimed at enhancing, accelerating and prolonging the specific immune response to vaccine antigens. Advantages of adjuvants include the enhancement of the immunogenicity of weaker antigens, the reduction of the antigen amount needed for a successful immunisation, the reduction of the frequency of booster immunisations needed and an improved immune response in elderly and immunocompromised vaccinees. Selectively, adjuvants can also be employed to optimise a desired immune response, e.g. with respect to immunoglobulin classes and induction of cytotoxic or helper T lymphocyte responses. In addition, certain adjuvants can be used to promote antibody responses at mucosal surfaces. Aluminium hydroxide and aluminium or calcium phosphate have been used routinely in human vaccines. More recently, antigens incorporated into IRIV's (immunostimulating reconstituted influenza virosomes) and vaccines containing the emulsion-based adjuvant MF59 have been licensed in countries. Adjuvants can be classified according to their source, mechanism of action and physical or chemical properties. The most commonly described adjuvant classes are gel-type, microbial, oil-emulsion and emulsifier-based, particulate, synthetic and cytokines. More than one adjuvant may be present in the final vaccine product. They may be combined together with a single antigen or all antigens present in the vaccine, or each adjuvant may be combined with one particular antigen. The origin and nature of the adjuvants currently being used or developed is highly diverse. For example, aluminium based adjuvants consist of simple inorganic compounds, PLG is a polymeric carbohydrate, virosomes can be derived from disparate viral particles, MDP is derived from bacterial cell walls; saponins are of plant origin, squalene is derived from shark liver and recombinant endogenous immunomodulators are derived from recombinant bacterial, yeast or mammalian cells. There are several adjuvants licensed for veterinary vaccines, such as mineral oil emulsions that are too reactive for human use. Similarly, complete Freund's adjuvant, although being one of the most powerful adjuvants known, is not suitable for human use.

The term carrier is construed in the following manner. A carrier is an immunogenic molecule which, when bound to a second molecule augments immune responses to the latter. Some antigens are not intrinsically immunogenic yet may be capable of generating antibody responses when associated with a foreign protein molecule such as keyhole-limpet haemocyanin or tetanus toxoid. Such antigens contain B-cell epitopes but no T cell epitopes.

The protein moiety of such a conjugate (the "carrier" protein) provides T-cell epitopes which stimulate helper T-cells that in turn stimulate antigen-specific B-cells to differentiate into plasma cells and produce antibody against the antigen.

According to a further aspect of the invention there is provided a pharmaceutical composition comprising a virus like particle according to the invention and including a pharmaceutically acceptable excipient.

When administered the compositions of the present invention are administered in pharmaceutically acceptable preparations. Such preparations may routinely contain pharmaceutically acceptable concentrations of salt, buffering agents, preservatives, compatible carriers and supplementary therapeutic agents'. The compositions of the invention can be administered by any conventional route, including injection or by gradual infusion over time. The administration may, for example, intravenous, intraperitoneal, intramuscular, intracavity, subcutaneous, transdermal or trans-epithelial.

The compositions of the invention are administered in effective amounts. An "effective amount" is that amount of an agent that alone, or together with further doses, produces the desired response. In the case of treating a disease, the desired response is inhibiting the progression of the disease. This may involve only slowing the progression of the disease temporarily, although more preferably, it involves halting the progression of the disease permanently. This can be monitored by routine methods. Such amounts will depend, of course, on the particular condition being treated, the severity of the condition, the individual patient parameters including age, physical condition, size and weight, the duration of the treatment, the nature of concurrent therapy (if any), the specific route of administration and like factors within the knowledge and expertise of the health practitioner. These factors are well known to those of ordinary skill in the art and can be addressed with no more than routine experimentation. It is generally preferred that a maximum dose of the individual components or combinations thereof be used, that is, the highest safe dose according to sound medical judgment. It will be understood by those of ordinary skill in the art, however, that a patient may insist upon a lower dose or tolerable dose for medical reasons, psychological reasons or for virtually any other reasons.

The compositions used in the foregoing methods preferably are sterile and contain an effective amount of an agent according to the invention for producing the desired response in a unit of weight or volume suitable for administration to a patient. The doses of agent administered to a subject can be chosen in accordance with different parameters, in particular in accordance

with the mode of administration used and the state of the subject. Other factors include the desired period of treatment. In the event that a response in a subject is insufficient at the initial doses applied, higher doses (or effectively higher doses by a different, more localized delivery route) may be employed to the extent that patient tolerance permits.

In general, doses of nucleic acid therapeutics such as siRNA and antisense RNA are between 1nM – 1mM. Preferably doses can range from 1nM-500nM, 5nM-200nM, and 10nM-100nM.

Other protocols for the administration of compositions will be known to one of ordinary skill in the art, in which the dose amount, schedule of injections, sites of injections, mode of administration and the like vary from the foregoing. The administration of compositions to mammals other than humans, (e.g. for testing purposes or veterinary therapeutic purposes), is carried out under substantially the same conditions as described above. A subject, as used herein, is a mammal, preferably a human, and including a non-human primate, cow, horse, pig, sheep, goat, dog, cat or rodent.

When administered, the compositions of the invention are applied in pharmaceutically-acceptable amounts and in pharmaceutically-acceptable compositions. The term "pharmaceutically acceptable" means a non-toxic material that does not interfere with the effectiveness of the biological activity of the active ingredients. Such preparations may routinely contain salts, buffering agents, preservatives, compatible carriers, and optionally other therapeutic agents' (e.g. those typically used in the treatment of the specific disease indication). When used in medicine, the salts should be pharmaceutically acceptable, but non-pharmaceutically acceptable salts may conveniently be used to prepare pharmaceutically-acceptable salts thereof and are not excluded from the scope of the invention. Such pharmacologically and pharmaceutically-acceptable salts include, but are not limited to, those prepared from the following acids: hydrochloric, hydrobromic, sulfuric, nitric, phosphoric, maleic, acetic, salicylic, citric, formic, malonic, succinic, and the like. Also, pharmaceutically-acceptable salts can be prepared as alkaline metal or alkaline earth salts, such as sodium, potassium or calcium salts.

The pharmaceutical compositions containing agents according to the invention may contain suitable buffering agents, including: acetic acid in a salt; citric acid in a salt; boric acid in a salt; and phosphoric acid in a salt. The pharmaceutical compositions also may contain, optionally, suitable preservatives, such as: benzalkonium chloride; chlorobutanol; parabens and thimerosal.

The compositions may conveniently be presented in unit dosage form and may be prepared by any of the methods well-known in the art of pharmacy. All methods include the step of bringing the active agent into association with a carrier which constitutes one or more accessory ingredients. Compositions containing agents according to the invention may be administered as aerosols and inhaled. Compositions suitable for parenteral administration conveniently comprise a sterile aqueous or non-aqueous preparation of agent, which is preferably isotonic with the blood of the recipient. This preparation may be formulated according to known methods using suitable dispersing or wetting agents and suspending agents. The sterile injectable preparation also may be a sterile injectable solution or suspension in a non-toxic parenterally-acceptable diluent or solvent, for example, as a solution in 1, 3-butanediol. Among the acceptable solvents that may be employed are water, Ringer's solution, and isotonic sodium chloride solution. In addition, sterile, fixed oils are conventionally employed as a solvent or suspending medium. For this purpose, any bland fixed oil may be employed including synthetic mono-or di-glycerides. In addition, fatty acids such as oleic acid may be used in the preparation of injectables. Carrier formulation suitable for oral, subcutaneous, intravenous, intramuscular, etc. administrations can be found in Remington's Pharmaceutical Sciences, Mack Publishing Co., Easton, PA.

According to a further aspect of the invention there is provided a virus like particle according to the invention for use in the delivery of an agent to a cell.

According to an aspect of the invention there is provided a method to vaccinate or immunise a subject to prevent or treat a viral infection comprising administering an effective amount of a virus like particle according to the invention.

Throughout the description and claims of this specification, the words "comprise" and "contain" and variations of the words, for example "comprising" and "comprises", means "including but not limited to", and is not intended to (and does not) exclude other moieties, additives, components, integers or steps. "Consisting essentially" means having the essential integers but including integers which do not materially affect the function of the essential integers.

Throughout the description and claims of this specification, the singular encompasses the plural unless the context otherwise requires. In particular, where the indefinite article is used, the specification is to be understood as contemplating plurality as well as singularity, unless the context requires otherwise.

Features, integers, characteristics, compounds, chemical moieties or groups described in conjunction with a particular aspect, embodiment or example of the invention are to be understood to be applicable to any other aspect, embodiment or example described herein unless incompatible therewith.

An embodiment of the invention will now be described by example only and with reference to the following figures:

Figure 1 The Hepatitis B Virus
(a) The genetic map of HBV showing the partially dsDNA genome and the four open reading frames of the virally encoded proteins: Pre-core/core (Cp), which forms the nucleocapsid (NC) shell; Pre S1/PreS2/S, the envelope embedded HBV antigen (HbsAg); X (which plays a role in numerous aspects of the HBV life-cycle within the cell); the polymerase, (P) and the pgRNA with the positions of the 5' ε, the redundant 3' ε (grey circle), φ and the preferred sites (PSs) studied here, highlighted by circles. (b) The HBV NC (left) comprises either 90 (*T=3*) or 120 Cp dimers (*T=4* shown). Cp dimers form characteristic four-helix bundles, two from each monomer, that appear as spikes on the surface (right bottom). The two conformers of the HBV Cp dimer (A/B & C/D) that are needed to create the *T=4* particle are also shown (right top). HBV capsid and protein dimer were obtained from PDB (3J2V)(1) (c) The Cp of the isolate used here is 185 amino acids long (RD dipeptide insertion underlined), with an alpha-helical rich region (149 amino acids long), and a C-terminal ARD. The 149th amino acid, V, is labelled light grey for clarity. ARD is rich in both basic amino acids and serines (S) are known sites for phosphorylation, which are thought to play roles in NC assembly;

Figure 2 Identification of conserved PS motifs in the pgRNA
(a) The frequency of aptamer matches (Bernoulli score ≥ 12) from the selected (solid grey line) and naïve (grey dashed line) libraries against the reference strain (NC_003977.1). The peaks that occur in the majority of tested strains are marked with a X together with the percentage of strains with peaks in the same positions. The peaks with highest frequency and level of conservation between strains are labelled PS1, PS2 & PS3. (b) Alignment of loop sequences of stem-loops in the sequences surrounding the conserved nine Bernoulli peaks from (a) obtained using Mfold. The sequences all display an RGAG motif in a single-stranded loop. (c) The probability of the number of occurrences of the motif RGAG in the loop portions of stem-loops across 10,000 randomised versions of five of the tested strains (see strains marked by an asterix in the Methods). The grey bars show this probability in the reference strain, whilst the black line is the equivalent across all five strains. The black arrow indicates

the average number of occurrences in loops of RGAG in the randomised versions of the reference strain (= 6.85). The arrow labelled +4.7σ indicates the number of occurrences in the reference strain (= 25), which is 4.68 standard deviations from the average, and the other tested strains have similar levels of occurrence;

Figure 3 PSs trigger sequence-specific VLP assembly

(a) Dye end-labelled RNA oligos encompassing PS1 (black), PS2 (dark grey) or PS3 (light grey) were each assessed for their ability to bind Cp and form VLPs at nanomolar concentrations using smFCS. All reactions contained 15 nM of RNA dye-labelled as described in Methods. Vertical dotted lines indicate points where Cp was added with the final concentrations shown in nM. Samples were allowed to equilibrate between additions. The faint trace represents real time, raw signal while the thick line represents smoothed data. EM images were recorded of the samples prior to RNase A addition (right). Scale bars represent 100 nm. (b) Hydrodynamic radial distributions of the reactions in (a), taken following the last addition of Cp (here and throughout). The amount of Cp assembling beyond dimer in the absence and presence of RNA (unlabelled) was compared. At the end of these reactions, Cp was labelled with Alexa Fluor-488 (Methods) and the resulting R_h distributions quantitated for the Cp only and Cp plus unlabelled PS1 scenarios. Note dye-labelling of the Cp dimer prevents it from assembling so this has to be an end-point measurement. A sample of each was taken for analysis by TEM. smFCS and TEM were repeated in triplicate;

Figure 4 The structures of *T*=3 and *T*=4 HBV VLPs suggest a mechanism for the specification of their quasi-conformations

The icosahedrally-averaged cryo-EM structures of (a) *T*=3 and (b) *T*=4 HBV VLPs at 5.6 Å and 4.7 Å resolution, respectively. A red icosahedron is included to assist interpretation of the two reconstructions, which are shown in the same orientation. (c & d) show ~30 Å thick slabs through the structure of each particle, with a fitted Cp-dimer in each. The *T*=3 shell is thicker, indicating that density corresponding to the ARDs is resolved in the *T*=3, but not the *T*=4, structure. Rendering both structures at equivalent resolution does not change this interpretation (Figure 11);

Figure 5 Asymmetric RNA feature in *T*=4 HBV VLPs

(a & b) 2D views of 42,411 *T*=4 particles were calculated by maximum-likelihood-based classification in RELION. An asymmetric RNA feature is visible in a subset of these particles (b). (c) An asymmetric 3D reconstruction at 11.5 Å resolution of 10,851 particles containing

the asymmetric feature. The asymmetric density for the protein shell is icosahedral, despite the lack of any symmetry averaging. (d) An approximately 40 Å thick slab through the asymmetric HBV VLP reconstruction shows the asymmetric feature bound to one region of the Cp shell revealing density ascribed to RNA and ARDs within the protein shell (bright cerise, magenta and purple). The figures were rendered in a radial colour scheme (Blue=165Å; Cyan=152Å; Green=139Å; Yellow=126Å; Pink=113Å) using USCF Chimera. (e) The asymmetric RNA density is centred beneath a Cp dimer surrounding one of the 5-fold vertices of the *T*=4 particle (indicated by the circle). A single Cp dimer is fitted as a ribbon diagram into the appropriate position using the 'Fit in map' function in UCSF Chimera. (f) As the front of the map is slabbed away, the density within is revealed. Shown and manually fitted is a single copy of PS1 as a ribbon diagram (modelled in RNA Composer). (g) Side-view of the same portion of the map, with the view oriented by the projected blue circle. Discrete fingers of density are visible between the Cp layer and RNA density, which is large enough to accommodate 2-4 RNA oligonucleotides. (h) Histogram of photobleaching steps from 630 individual fluorescent spots on a grid containing PS1 HBV VLPs. Spots containing >10 steps resulted from traces exhibiting exponential decay, which were assumed to be aggregates in which multiple bleaching steps occur simultaneously. Photobleaching was performed in duplicate;

Figure 6 Proposed model of HBV NC assembly

ARD within a Cp dimer inhibit formation of a dimer of dimers, the first intermediate on the pathway to NC assembly. Reducing the net charge on the ARD by phosphorylation or PS RNA binding allows this structure to form more easily, triggering NC formation. At concentrations higher than those mimicking *in vivo* conditions as used here, the unmodified dimer of dimers forms and particles self-assemble without RNA or will bind RNA non-specifically to produce the same outcome;

Figure 7 Characterising HBV VLPs from *E.coli* and SELEX protocol

(a) Hydrodynamic radial distribution and negative stain EM image of Alexa Fluor-488 labelled HBV VLPs purified from *E.coli*. Integration of peak yields suggests a roughly 2:1 ratio of *T*=4 (circle, 63%) and *T*=3 (circle, 37%) VLPs. Scale bar represents 100 nm. (b) SELEX protocol showing selection for aptamers with high affinity to HBV 185 Cp. HBV VLPs were immobilised onto carboxylic magnetic beads (circles) and dissociated into Cp dimers (grey rectangles) using guanidinium chloride. An RNA pool encompassing a random region (40N) was enriched for sequences with affinity for Cp by repeated cycles of binding to these beads, partitioning and amplification. Negative selections at each round used carboxylic acid beads which had been treated with NHS-EDC and inactivated with Tris. Stringency was increased after round

5 by decreasing the number of positive beads by half and increasing the number of washes from 8 to 10. The reverse transcriptase-PCR products at the end of each round were analyzed by native PAGE to confirm the isolation of products for the next round of selection. The 10th round products were converted to DNA and sequenced;

Figure 8 PS oligo structures, example smFCS trace and EMs of PS containing VLPs
(a) PS1-3 and ε secondary structures, made using VARNA software(2), were predicted in Mfold. Preferred sites were taken from the HBV genome, NC_003977.1, at positions: PS1$_{(1717-1751)}$, PS2$_{(2602-2633)}$ and PS3$_{(2765-2798)}$. In order to make them all the same length (47 nucleotides) to avoid effects of charge differences the following additions were made; PS1, 5' - GGGUUUUGG and CCC - 3'; PS2, 5' - GGGUUUUGGGG and CCCC - 3'; PS3, 5'- GGGUUUUGG and CCCC - 3'. The consensus motif RGAG is highlighted in red in each of the loops. The stability of each RNA fold, as predicted by Mfold, is shown below each structure.

(b) Example smFCS assay. R_h values for, fluorescently labelled RNAs are determined before and after Cp is titrated in at fixed time points (vertical dashed lines), allowing the R_h values to equilibrate after each step. The faint red trace represents real time, raw signal while the thick red line represents smoothed data. PS1 R_h initially climbs slowly, until a threshold Cp concentration, which triggers rapid assembly into a *T*=3 or *T*=4 VLP (R_h ~24-32 nm, orange dashed lines) as determined by measurements of Alexa-Flour 488 labelled HBV particles from *E.coli* (Figure 7a). At the end of each titration, the complexes formed are challenged by addition of RNase A. An unchanged R_h is assumed to mean that the test RNA has been encapsidated in a closed VLP. The time scale on which this occurs is indicated in the bottom right.
(c) TEMs from assembly reactions of PS1, 2, 3 and Cp alone and unlabelled PS1 in Figure 3. Large white particles in Cp alone and Unlabelled PS1 TEMs are latex beads. Also present is TEM from empty particle assembly described in Table 2. These empty HBV particles were assembled at much higher concentrations of Cp (1.5 μM) and in the absence of RNA. Scale bars represent 100 nm.

Figure 9 smFCS assays of PS1 variants
(a) smFCS assays of the PS1 variants (structures top left) and accompanying hydrodynamic radial distributions plotted in 2 nm bins and fitted with Gaussian peaks below, as colour coded in the key. 15 nM PS1 (black), PS1 loop mutant (grey) bulge mutant (dark grey) and epsilon (light grey) RNAs were tested for their ability to form VLPs under single molecule conditions. Vertical dotted lines indicate points of addition of Cp with the final concentrations shown in

nM. Samples were allowed to equilibrate between additions. RNase A was added to check for correctly formed particles. Samples were taken prior to RNase A addition for analysis by TEM shown right, both here and throughout this figure. (b) - as (a) with RNA oligos PS1 (dashed black), L1 , L2 and L3.. (c) - as (a) with RNA oligos PS1 (dashed black), L4 (dark grey), L5 and B1 (d) as (a) with RNA oligos PS1 (dashed black) and DNA oligo PS1 (grey). Scale bars represent 100 nm. PS1 controls (dashed black) in each panel were repeated for individual batches of purified Cp, accounting for the variations in assembly efficiency seen. smFCS and TEM were repeated in triplicate.

Figure 10 Role(s) of ARD and its charge on assembly
(a) smFCS assays of 15 nM PS1 with Cp (light grey) and Cp_{149} (grey) and accompanying hydrodynamic radial distributions plotted in 2 nm bins and fitted with Gaussian peaks below. EM images of particles are shown (right). (b) as (a) with PS1 and Cp (black), kinase and Cp pre equilibrated and added to PS1 (l grey) and PS1 and Cp with kinase added simultaneously (dark grey). TEMs are shown right. Scale bars represent 100 nm. PS1 controls (black) in each panel were repeated for individual batches of purified Cp, accounting for the variations in assembly efficiency seen. smFCS and TEM were repeated in triplicate.

Figure 11 ARD structure in *T*=4 and *T*=3 VLPs.
Slabs (~30 Å thick) through the structures of the icosahedrally-averaged *T*=4 particle at 4.7 Å (left), the same *T*=4 structure low pass filtered to 7 Å (middle), and the *T*=3 particle at 5.6 Å (right). A Cp dimer is fitted into each. Even at a slightly lower resolution than the *T*=3 VLP, there is no equivalent density for the ARD in the *T*=4 VLP, confirming that it has different conformations in each particle.

Figure 12: The STNV system. (A) Ribbon diagram of the STNV T=1 capsid (left, PDB 3S4G) viewed along a five-fold axis with a trimeric capsomer highlighted (dark grey) and right a CP monomer (dark grey, PDB 3S4G). Side-chains mutated here are shown and labelled. The disordered N-terminal amino acid sequence shown as a dashed line, next to the sequence of the first 25 amino acids. (B) Sequence and putative secondary structure of the 127 nt 5′ STNV-1 genomic fragment showing the locations of the PS SLs, named 5′ to 3′ as PS1 to 5, respectively. Each contains the CP recognition motif, -A.X.X.A-, in their loops (white circles, black outline). The B3 aptamer is shown similarly above. Nucleotides are colour-coded as indicated, here and throughout (see also Fig 22). (C) Example smFCS assays. Rh values for CP-free, fluorescently-labelled RNAs (black line for PS1-5, red for B3) are determined before and during STNV CP titration at fixed time points (vertical dashed lines), allowing the Rh values to equilibrate after each step. The PS1-5 Rh initially collapses, by up to 30%, until the

CP concentration reaches a threshold, triggering cooperative assembly to T=1 VLPs (Rh ~11 nm). At the end of each titration, the complexes formed are challenged by addition of RNAse A. Unchanged Rh values were assumed to indicate that the RNA is in a closed VLP;

Figure 13: Defining the CP recognition motif. (A) Ensemble reassembly efficiency of variant B3 RNAs, determined by sedimentation velocity (variant RNAs are colour-coded as inset). The expected T=1 VLP sediments at ~42 S. (B) EM images of representative assembly products, scale bar, here and throughout = 50 nm, see also Fig 17B. (C) Illustration of the variant RNA smFCS competition assay for results plotted in (D). (D) Change in Rh (in %) of a capsomer (~ 5 nm) formed with 1 nM AF488- labelled B3, following addition of 100-fold molar excess of competitor variant RNAs (loop sequences from top to bottom represent bars from left to right in the graph);

Figure 14: Electrostatic interactions and co-operativity of assembly. Wild-type or R8A CPs were titrated into B3 (1 nM) or PS1-5 (10 nM), and Rh changes monitored. Titrations points are shown above (B3 in grey) and below (PS1-5), respectively. (B) Wild-type STNV CP was titrated into 10 nM of each of PS1-5, PS1-3,PS3-5 or PS2-4;

Figure 15: Assembly of synthetic cassettes. (A) Sequences, putative secondary structures and folding free energies of PS1-5, the Synthetic, stable PS1-5 and of the All PS3 cassettes (Figure 22). SLs with positive folding free energies cannot be folded by Mfold. (B) STNV CP titration of all variant PS1-5 constructs, conditions as in Fig 14. Inset – EM images of the products with PS1-5 (black), Synthetic, stable PS3 (light grey) RNAs;

Figure 16: Assembly assays with genomic chimeras: (A) Schematics of the STNV-1 genome (black) and the modified variants, Synthetic, stabilised PS1-5+Δ1-127STNV-1 (bottom) and Unstable PS1-5+Δ1-127STNV-1 (middle). (B) STNV CP was titrated into 1 nM of STNV-1 (black), Synthetic, stabilised PS1-5+Δ1-127STNV-1 (light grey) or Unstable PS1-5+Δ1-127STNV-1 (dark grey), and the resulting Rh was monitored using smFCS. The Rh of the recombinant T=1 particle is indicated in orange. (C) The hydrodynamic radii from the data on the titration plot (B) between 4000 and 6500 secs is plotted as a distribution. (D) EM images of the products from (B);

Figure 17 (A-C): Assembly behaviour of B3 variants. **(A)** MFold structures of all B3 variants; loop sequences are given under each structure. **(B)** EM images of the B3 variant assemblies at 4.3 μM concentration. The scale bar shown is 100 nm. Panel positions in B correspond with the SL in the equivalent position in A. **(C)** Comparison of STNV CP reassembly efficiency

using B3 inner variant RNAs via svAUC. Reassembly reactions were carried out at a 1:3 RNA:CP ratio with final CP concentration of 4.5 μM. **(D-F): B3 Variant-capsomer competition assays. (D)** 15 nM STNV CP and 5 nM Alexa Fluor 488 labelled B3 were used to form a capsomer of ~5 nm R_h. This was measured via smFCS for 1200 s. At this point 100-fold molar excess of B3 variant GUUG (light grey), GUUU (black) or UUUG (dark grey) was added and the resulting R_h change tracked for 1800 s. The raw data were then used to compute the percentage change in the R_h (Fig 13C & D). **(E)** as in (D) with B3 variant AUUA (dark grey), AUUU (grey) or UUUA (light grey). **(F)** as in (D) with B3 variant AUUG (dark grey), GUUA (light grey) or unlabeled B3 (black);

Figure 18: Characterisation of the STNV CP charge-change mutants: (**A)** SDS PAGE of charge-change mutants expressed in *E.coli,* red arrow indicates the STNV CP band. **(B)** svAUC of charge-change mutants purified from *E.coli*. Only mutants that produce enough VLPs (wild type ,R8A and R8D (dashed [termed R8D']) were analysed;

Figure 19: Assembly behaviour of STNV CP charge-change mutants with single or multiple packaging signals. (A) Top: Wild-type ,R8A , R8D R14K17A or R14K17D titrated into 1 nM B3 and the resulting hydrodynamic radius monitored as described in Fig 14. Middle: R_h values from the upper chart shown as a distribution, with 0.5 nm bin sizes, were fitted with Gaussian peaks to highlight the heterogeneity present in solution throughout the reaction. The R_h of a T=1 particle is indicated by the orange dashed line. Bottom: EM images of the above reactions (from left top to right bottom; Wild-type, R8A , R8D R14K17D, R14K17A . **(B)** As in (A) but with CP titrated into 10 nM PS1-5; (from left top to right bottom; Wild-type, R8A , R8D R14K17A, R14K17D) ,

Figure 20: Assembly behaviour of three PS fragments. Top: R_h values corresponding to 3000- 4000 secs of reactions between STNV CP and PS 1-5 (black), PS 1-3 (dark grey, left), PS 3-5 (black, left) and PS 2-4 (light grey) from Fig 14B, plotted as a distribution, with 2 nm bin sizes and fitted with Gaussian peaks. Bottom: EM images of the reactions from Fig 14;

Figure 21: Stable structures of the three PS fragments**.** Most stable structures of PS1-3, PS2-4 and PS3-5 as predicted by Mfold. Colour coding is as seen in Fig 12 and throughout. The two main PS1-3 folds predominantly present two -A.X.X.A- SLs, however these appear to be too distant for cooperative assembly. PS2-4 presents two SLs, one with an -A.X.X.A- motif, and another one at a distance of 4 nts away from the other. The two main folds of PS3-5 also present two SLs, but whilst these SLs are in close proximity (10-12 nt), only one presents an -A.X.X.A- motif, 6% of the time;

Figure 22: 127-mer cassette structures. Top: sequences, putative secondary structures and folding free energies as determined by Mfold of the STNV wild-type PS 1-5 gene fragment and its synthetic counterparts. Bottom: table comparing the relative folding free energies of each SL as determined by Mfold. Oligos are colour-coded as in Fig 12;

Figure 23: Interrogation of the structure and stability of the 127-mer assembly cassettes. (A) Molar ellipticity of RNA oligonucleotides WT PS1-5 (squares), Stable PS1-5 (circles), Unstable PS1-5 (triangles), All PS3 (inverted triangles) and Synthetic, stable PS1-5 (diamonds) at 260 nm with increasing Ca^{2+} concentration. **(B)** Molar ellipticity at 260 nm during thermal melts of the RNA oligonucleotides, colour-coded as in (A);

Figure 24: Assembly behaviour of the synthetic 127 mer cassettes**. (A)** The R_h values between 3000 – 4000 secs of reactions containing STNV CP and PS 1-5 (black), stable PS 1-5 (dark grey), unstable PS 1-5 (grey), all PS3 (red) or synthetic, stable PS1-5 (light grey) from Fig 15A, plotted as in Fig 19. **(B)** EM images of the above reactions, colour coded as in Fig 15A;

Figure 25: Assembly behaviour of the genomic chimeras. (A) smFCS reassembly using STNV-1 genomic RNA. R_h values were measured before and during STNV CP titration (vertical dashed lines), allowing the R_h values to equilibrate after each step. The STNV-1 genome initially collapses by up to ~30%, and then the R_h recovers to a value corresponding to a T=1 VLP (R_h ~11 nm). (B) QELS measured light scattering data of reassemblies between STNV-1 (black), Synthetic, stabilised PS1-5+Δ1-127STNV-1 (light grey) and Unstable PS1-5+Δ1-127STNV-1 (grey) with STNV CP eluting from a TSKgel G6000PWxl SEC column (Tosoh). Peak areas and the measured R_h values are listed in Table 6. (C) EM images of the VLPs in the main peaks (~20 min).

Table 1: Masses of the different forms of Cp and kinase (SRPKΔ) used, as determined by ESI-MS mass spectrometry

	Expected mass (Da)	**Observed mass (Da)**
SRPKΔ	45615.4	45614.7 ± 1.37
Phosphorylated Cp_{185}	21995.4	21995 ± 0.71
Cp_{185}	21395.3	21395.6 ± 0.86

Cp_{149}	16852.3	16851.7 ± 0.06

Table 2: Association of Alexa-Fluor-488 labelled PS1 with Cp.

Anisotropy was used to determine if 15 nM of Alexa-Fluor-488 labelled RNA PS oligos can bind to, or enter, 125 nM of preformed shells of Cp. The latter were formed by reassembly in the absence of RNA at high concentration(3) (Fig 8c). Fluorescence polarisation values are influenced by the mass of the dye-labelled species(4). The polarisation value for PS1 oligo goes down following addition of RNase, as expected but remains unchanged when incorporated in VLPs assembled in the presence of the oligo. When labelled PS1 is added to the empty Cp VLP its fluorescence emission is unaffected, suggesting that it is not quenched, and it remains RNase sensitive confirming that it does not bind the outside of the protein shell or get internalised.

	Fluorescence Polarisation		*Total Fluorescence*	
Sample	*-RNase*	*+RNase*	*-RNase*	*+RNase*
PS1 oligo	72	43.5	73637	74102
PS1 VLP	130	128	30187	33564
PS1 + empty VLP	52.8	15.5	69336	70672

Table 3: Sequence changes and corresponding assembly behaviour of PS1 variant oligonucleotides, L1-5 and B1. Assembly behaviour is indicated as follows, the first "+" indicates RNA-Cp binding, the second signifies formation of *T*=3/ *T*=4 sized species, and the third indicates RNase protection. "-" indicates failure in that assay.

RNA Oligo	**Loop**	**Bulge**	**Assembly behaviour**	**Comment**
PS1	**GGGAGG**	**GGG**	**+++**	
L1	**UUUAUU**	**GGG**	**+ - -**	**Loop G's are important**

L2	**GUUAGG**	**GGG**	**+ - -**	**Loop G's are important**
L3	**UGGAUU**	**GGG**	**+ + -**	**Loop G's are important**
L4	**GGGUGG**	**GGG**	**+ + -**	**Loop A is important**
L5	**GGGGGG**	**GGG**	**+ + -**	**Loop A is important**
B1	**GGGAGG**	**AAC**	**+ + -**	**Bulge sequence/structure is important**

Table 4: B3 sequence variants. Loop motif (left), full sequence (middle) and folding free energy values (right) of the B3 sequence variants.

Loop motif	**Sequence**	**ΔG of folding (kcal mol^{-1})**
ACAA	ACAUGCAACAAUGCACAC (SEQ ID NO 10)	-2.6
AUUU	ACAUGCAAUUUUGCACAC (SEQ ID NO 11)	-2.6
UUUA	ACAUGCAUUUAUGCACAC (SEQ ID NO 12)	-2.6
GUUU	ACAUGCAGUUUUGCACAC (SEQ ID NO 13)	-2.1
UUUG	ACAUGCAUUUGUGCACAC (SEQ ID NO 14)	-2.9
AUUG	ACAUGCAAUUGUGCACAC (SEQ ID NO 15)	-2.6
GUUA	ACAUGCAGUUAUGCACAC (SEQ ID NO 16)	-3.4
GUUG	ACAUGCAGUUGUGCACAC (SEQ ID NO 17)	-2.5
AUUA	ACAUGCAAUUAUGCACAC (SEQ ID NO 18)	-2.6

Table 5: Analysis of suboptimal structures of RNA assembly cassettes. Mfold was used to fold each cassette with a suboptimality setting of 500. These folds were then assessed by the following criteria: The presence of the correct -A.X.X.A- loop in PSs 1 through 5 were verified and shown as a percentage (green = 60+, orange = 40+, red 0-39 throughout the table). The nucleotide spacing between each stem loop was measured, compared to the expected value (Fig 22) and also displayed as a percentage. Where these spacings differed, the maximum nucleotide difference is given.

	% of Correctly presented - A.X.X.A- motifs					% of 'correct' spacings				Maxi-mum spacing variance
Cassette	**PS 1**	**PS2**	**PS 3**	**PS4**	**PS5**	**1-2**	**2-3**	**3-4**	**4-5**	
WT PS1-5	72	0	8	0	10	8	0	0	0	+7
Synthetic Stable PS1-5	100	87	100	75	73	9	60	76	72	+7
Stable PS1-5	100	87	99	68	31	5	72	55	68	+7
Unstable PS1-5	98	97	0	73	27	73	0	0	67	+7
All PS3	100	99	100	100	100	92	90	100	90	+4
PS1-3	78	2	9	*N/A*	*N/A*	0	0	*N/A*	*N/A*	*N/A*
PS2-4	*N/A*	0	2	0	*N/A*	*N/A*	0	0	*N/A*	+3
PS3-5	*N/A*	*N/A*	34	4	6	*N/A*	*N/A*	0	0	*N/A*

Table 6: Yield and R_h values from QELS experiments. Measured R_h values taken from the midpoint of the main peak (20 min, Fig 25) eluted from the TSKgel G6000PWxl column. Yields of genomic chimera reassemblies were calculated by integrating the area under the main peak (20 min, Fig 25) using the peak analyser function in Origin Pro 9. Yields were then normalised to the highest value and shown as percentages.

Sample	R_h value / nm	Relative Yield / %
STNV-1	9.1	80
Unstable PS1-5 + Δ1-127 STNV-1	8.9	40
Synthetic, Stabilised PS1-5 + Δ1-127 STNV-1	9.3	100

Table 7: RNA oligonucleotide primers

Primer Name	Sequence 5'- 3'	SEQ ID NO	Tm °C
Forward	GACATTAATACGACTCACTATAGGGACATGCA	19	65.5
AUUArev	GTGTGCATAATTGCATGTCCCTATAGTGAGTCG	20	68.2
GUUGrev	GTGTGCACAACTGCATGTCCCTATAGTGAGTCG	21	70.0
AUUGrev	GTGTGCACAATTGCATGTCCCTATAGTGAGTCG	22	69.5
GUUArev	GTGTGCATAACTGCATGTCCCTATAGTGAGTCG	23	69.5
UUUArev	GTGTGCATAAATGCATGTCCCTATAGTGAGTCG	24	68.2
AUUUrev	GTGTGCAAAATTGCATGTCCCTATAGTGAGTCG	25	68.2
GUUUrev	GTGTGCAAAACTGCATGTCCCTATAGTGAGTCG	26	69.5
UUUGrev	GTGTGCACAAATGCATGTCCCTATAGTGAGTCG	27	69.5
ACCArev	GTGTGCATGGTTGCATGTCCCTATAGTGAGTCG	28	64.3
AAAArev	GTGTGCATTTTTGCATGTCCCTATAGTGAGTCG	29	62.0
AGGArev	GTGTGCATCCTTGCATGTCCCTATAGTGAGTCG	30	64.0
AUGArev	GTGTGCATCATTGCATGTCCCTATAGTGAGTCG	31	62.9
AGUArev	GTGTGCATACTTGCATGTCCCTATAGTGAGTCG	32	62.5
Unstable 1-5 forward	AGTAATACGACTCACTATAGGGGGGCTGCCCTCAAGGACCAGGGCAGAAAAGAGGAAAAGAA	33	62
Unstable 1-5 template	GGCAGAAAAGAGGAAAAGAAAAGTGACAGAACACTTATAAGGAAATACACAAGTATAAGGAAAAAAGGAAGCTGCAATAGCGCAAGGAA	34	62
Unstable 1-5 reverse	TTCCTTTCCGAATTTTCGGATTCCTTGCGCTATTGCAGCTT	35	62
All PS3 forward	GGGCCCCGCAACAATGCGGGGAAGGAAGGAAGGAAGAAAACGTACAAACGTTTT	36	65
All PS3 template	AGAAAACGTACAAACGTTTTAAGGAACAACGCAACAATGCGTTGAAGGAAGGAAGGAAGGGGCGTACAAACGCCCCAAGGAATTTT	37	65

All PS3 reverse	TTCCTTTTTTGCATTGTTGCAAAATTCCTTGGGGC GTTTGTACGC	38	65
Stable 1-5 template	GGCAGAAAAGAGGAAAAGAAAAGTGACAGAACA CTTATAAGGAACCACACAAGTGGAAGGAAAAAAG GAAGCTGCAATAGCGCAAGGAA	39	62
Synthetic stable 1-5 template	GGCAGAAAAGAGGAAAAGAAAAGTGACAGAACA CTTATAAGGAAAAAACGUACAAACGUUUUAAGG AAAAAAGGAAGCTGCAATAGCGCAAGGAA	40	62
PS1-5 forward	AGTAATACGACTCACTATAGGGAGTAAAGACAGG AAACTTTACTGACTAACATGGCAAAAC	41	62
PS1-5 template	ACTGACTAACATGGCAAAACAACAGAACAACAGG CGAAAATCCGCAACAATGCGTGCAGTGAAGCGC ATGATAAATACAC	42	62
PS1-5 reverse	TCAGTGCAAACCTTTTATGCTCCAAGTGTGTATTT ATCATGCGCT	43	62
PS1-3 forward	AGTAATACGACTCACTATAGGGAGTAAAGACAGG AAACTTTACTGACTAACATGGCAAAAC	44	61
PS1-3 template	ACTGACTAACATGGCAAAACAACAGAACAACAGG CGAAAAT	45	61
PS1-3 reverse	CGCATTGTTGCGGATTTTCGCCTGTTGT	46	61
PS2-4 forward	AGTAATACGACTCACTATAGGGTGGCAAAACAAC AGAACAACAGGCGAAAAT	47	58
PS2-4 template	AACAGAACAACAGGCGAAAATCCGCAACAATGC GTGCAGTGAAGCGCATGATAAATA	48	58
PS2-4 reverse	CCAAGTGTGTATTTATCATGCGCTTCACTGCACG CATTGTTGCGG	49	58
PS3-5 forward	AGTAATACGACTCACTATAGGGCCGCAACAATGC G	50	61
PS3-5 template	CCGCAACAATGCGTGCAGTGAAGCGCATGATAA ATACAC	51	61
PS3-5 reverse	TCAGTGCAAACCTTTTATGCTCCAAGTGTGTATTT ATCATGCGCT	52	61

Materials and Methods

Cloning, expression and purification of proteins used.

We obtained an *E.coli* Cp-expressing plasmid (a gift of Prof. Nicola Stonehouse), known to produce assembled HBV VLPs containing host RNAs(5). The Cp encoded has the following amino acid sequence differences compared to the current GenBank reference strain (NC_003977.2): A61, E77-FAGAS (single letter amino acid code) -D78 insertion, S92N, F102I, I121L, R156-RD-R157 insertion. Since the wild-type C61 has been implicated in

assembly(6), this was restored to the gene before expression in a PET28b plasmid in BL21(DE3) *E.coli* cells. The inserted FAGAS epitope was also removed. Induction with 1 mM IPTG at 0.6 OD was followed by growth for 20 hrs at 21°C. Cells were lysed using a Soniprep 150 with 5x 30 sec bursts on ice. The lysate was then clarified by spinning at 11,000 g for 1 hr. VLPs were then pelleted by centrifugation at 120,000 g for 14 hr, resuspended in 20 mM Hepes (pH 7.5), 250 mM NaCl, and 5 mM DTT and applied to an XK50 column packed with 25 ml of Capto™core 700 resin (GE Life Sciences). Fractions containing VLPs were pooled and precipitated with 40%(w/v) ammonium sulphate. The Cp appeared pure on SDS-PAGE and its identity, and that of variants, was confirmed by mass spectrometry (Table 1). Cp lacking the ARD, i.e. Cp_{149}, was produced by mutagenesis (Q5 site-directed mutagenesis kit, NEB) and prepared similarly. Note, the Cp_{149} VLP expressed in *E.coli* lacks significant encapsidated cellular RNA. VLPs were visualised by negative stain transmission electron microscopy (TEM). Full length Cp VLPs were additionally purified by sucrose density gradient before dye-labelling using Alexa Fluor-488 SDP ester (Invitrogen) over 4 hrs at room temperature in 200 mM sodium carbonate buffer (pH 8.3), followed by desalting over a NAP5 column. There were two over-lapping VLP peaks on the gradient and it was impossible to separate them. TEM and smFCS confirm that they are the expected *T*=3 and *T*=4 shells, with the latter the predominant form (Fig 7a). The Cp region 140-148 has been shown to be a determinant of morphology, the shorter versions producing more *T*=3 shells(7). It is possible that the dipeptide insertion adjacent to the linker region at position 157 may alter the properties of the Cp. However, when we removed the RD insertion, yielding Cp_{183}, we found no differences with Cp_{185}, either in RNA binding, ability to form VLPs with PS RNAs or preference for the dominant quasi-conformer shell formed. Since longer Cp was used for SELEX and the high resolution EM work, those are the data shown throughout.

All HBV variants used for assembly assays were dissociated from VLPs into protein dimers as previously described(3), with the exception that dissociation was at pH 9.5, as opposed to 7.5. This was done in the presence of Complete Protease Inhibitor Tablets (Thermofisher Scientific). HBV core dimer concentration was determined by UV absorbance. Fractions with an A_{260}:A_{280} ratio of approximately 0.6 or lower were used in assembly assays. SRPKΔ kinase was expressed and purified from a pRSETb plasmid, as previously described(8).

SELEX protocol

Purified HBV capsids (~360 µg) were immobilised onto 6 mg of M270 carboxylic acid Dynabeads (Thermofisher Scientific) following the manufacturer's protocol. Beads were washed twice with selection buffer (25 mM Hepes, pH 7.5, 250 mM NaCl, 2 mM DTT, EDTA-

free complete protease inhibitor) and unreacted N-hydroxysuccinamide blocked with a 15 m 50 mM Tris-HCl pH 7.4 wash. Beads were washed a further three times with selection buffer. Immobilised capsids were dissociated with a 30 minute incubation of 2 M guandinium chloride in 0.5 M $LiCl_2$. Beads were then washed three times with B&W buffer (10 mM Tris-HCl, pH 7.5, 1 mM EDTA, 2 M NaCl) and then washed three times with selection buffer. Beads were resuspended in selection buffer so that concentration of beads was 10 mg/mL. Negative selection beads were also prepared in the same manner but with no capsids. Ten rounds of SELEX were performed *in vitro* using a synthetic, combinatorial N40 2´OH RNA library ($\sim 10^{24}$ potential sequences) as described previously(9). The amplified DNA of round 10 was then subjected to Next Generation Sequencing on an Illumina MiSeq platform. This yielded ~1.6M sequence reads, in which one sequence occurs 65,802 times and there are 1149 aptamers with a multiplicity of 100 or higher. The overall frequencies of the four nucleotides in this aptamer pool is A34.30%; C9.09%; G40.97% & U15.64%, and compares with the same data for the unselected naïve library of A26.10%; C22.03%; G24.64% & U27.22%. The highest multiplicity for sequences in the latter pool is 4. These data confirm that selection from the naïve pool occurred, and that the base composition of the selected aptamers is consistent with the RGAG motif identified within the HBV genomes.

PS identification

PS identification was carried out using the laboratory HBV strain (*NC_003977.1). The aptamer library contained 1,664,890 unique sequences, each 40 nts in length that have been aligned against the genome as follows: Each aptamer sequence was slid along the genome in increments of 1 nt. For each such position of the reference frame, the subset of the aptamer sequence with the best alignment to the genome was identified according to the Bernoulli score *B*, which benchmarks the probability of a non-contiguous alignment to that of a contiguous alignment of *B* nucleotides. The Bernoulli scores for all reference frames of a given aptamer sequence in the library were rank-ordered starting from the largest score, and all matches with the genome up to a Bernoulli score of 12 counted. The procedure was then repeated for the other aptamer sequences and corresponding matches added, resulting in the peaks in Fig. 2a.

Identification of a consensus motif

HBV genome sequences with the following accession numbers were randomly extracted from 750 complete HBV genomes found in GenBank: KCS10648.1; *AF223955.1; AY781181.1; *AB116266.1; AB195943.1; KR014086.1; *KR014072.1; KR014055.1; KR013939.1; KR013921.1; KR013816.1; KR013800.1; EU796069.1; AB540582.1, and the NCBI HBV

reference strain (GenBank Seq ID *NC_003977.2) and the laboratory strain (GenBank Seq ID NC_003977.1) were added to the ensemble. Sequences used for the statistical analysis in Fig. 2c are marked by an asterisk. Bernoulli peaks, which occurred within at most 10nts of each other in at least 80% of these 16 HBV strain variants, were marked by a green cross in Fig. 2a to indicate their conservation. To identify the putative PS recognition motif, we extracted sequences of 60 nts, centred around the peak nucleotide of each Bernoulli peak, from three representative strains (AF223955.1, NC_003977.1, & NC_003977.2) and determined all possible stem-loops of negative free energy via Mfold(10). We carried out a similarity analysis of these stem-loops, comparing both sequence and structure elements, we identified for each peak area that representative that has the highest degree of similarity both with secondary structure elements in the other peak areas in the same genome and stem-loops corresponding to the same peak area in the other strains. This returned a stem-loop for each peak. An alignment of the corresponding loop sequences is shown in Fig. 2b.

RNA dye-labelling

PS1, PS2 and PS3 (47 nucleotides long) were purchased from Integrated DNA Technologies with a 5' C6-amino group. To label RNA, 6 µL of RNA (200 µM) was mixed with 1 µL 1 M sodium borate buffer, pH 8 and 3 µL 10 mM Alexa-488-SDP (Thermofisher Scientific) and rolled at room temperature for 4 hours. 10 µL of 2x denaturing loading dye was then added to the RNA, boiled for 5 minutes and loaded onto a pre-warmed denaturing PAGE. RNA was gel extracted, isopropanol precipitated and finally re-suspended in DEPC-H_2O and frozen at -80°C until needed.

Assembly Assays

Assembly reactions were performed by adding HBV Cp in dissociation buffer (50 mM Tris (pH 9.5), 1.5 M GuHCl, 500 mM LiCl and 5 mM DTT) to 15 nM Alexa-488 labelled RNA in a reassembly buffer containing 20 mM Hepes (pH 7.5), 250 mM NaCl, 5 mM DTT and 0.05%(v/v) Tween-20 at 25°C. Successive additions of dimer were performed until assembly was deemed complete by the measured R_h value plateauing, but never exceeded 10% of total reaction volume. Each addition of Cp is marked by a vertical dashed grey line in the titration plots and the expected hydrodynamic radii of T=3 and T=4 particles (as determined for dye-labelled particles expressed in *E.coli*) are marked by an orange horizontal dashed line within figures.

Manual mixing throughout the reactions caused an approximate 1 min delay at the start of FCS data collection. FCS measurements were made using a custom-built FCS setup with 30

sec data accumulation per autocorrelation function (CF). Individual CFs were decomposed into triplet state relaxation and diffusion (characterized by diffusion time, TD) components, and the latter was converted into an apparent hydrodynamic radius, R_h(11). Samples for TEM were taken at the end of each measurement. Plots of R_h over time (thin dashed line) were smoothed (thick solid line) using the FFT filter in Origin Pro-8 with a cutoff percentage of 35%. Plots of R_h distribution were also fitted using Origin Pro-8 software, to a normal single or multiple peak Gaussian function. Samples taken for negative stain TEM analysis were placed on to a glow discharged carbon coated formvar 300 mesh Cu grid. Grids were stained with 2% uranyl acetate and dried.

Assembled particle labelling

Assembly was carried out as in smFCS experiments. In particular, Cp was titrated into reassembly buffer with and without 15 nM unlabelled PS1 to a final concentration of 250 nM. This was allowed to incubate at room temperature for 1 hour, and then buffer exchange was carried out via dialysis to remove guanidinium hydrochloride present. Labelling of protein was then carried out by adding Alexa Fluor-488 SDP ester (1:50 ratio of dye to Cp dimer) and incubating overnight at 4 °C. The resulting sample was then measured via smFCS in 30 s bins for 100 min and the R_h data plotted as above in a hydrodynamic radial distribution plot. A sample was then removed for analysis via TEM. Post labelling, Cp dimer became assembly incompetent, therefore Cp could not be tracked during real time assembly.

Photobleaching

HBV VLPs containing Alexa-488 labelled PS1 were assembled as described in smFCS assembly assays. Under those conditions all RNA is bound to protein as judged from fluorescence quenching and photon counting in the FCS experiments. VLPs were then added to two glow discharge-irradiated Carbon/Formvar 300-mesh grids (Agar Scientific), and one grid stained with 2% (w/v) uranyl acetate and viewed with a Jeol 1400 microscope at 40,000x magnification. The remaining, unstained grid was positioned Formvar side down onto a clean microscope coverslip and mounted onto an inverted TIRF microscope. The laser (Coherent Sapphire, 488 nm, 25 mW) power was adjusted to excite and photobleach the labelled RNA within the time frame of several minutes. Sequential images were taken with an emCCD camera (Andor iXon) with 0.2 sec exposures and em gain of 200. An unexposed field of view was used for each series.

Fluorescent spots were identified in the collected frames using previously described procedures and converted into time traces(12). These were then inspected and classified according to the number of photobleaching steps. Frequencies of traces with a defined number of steps were collated in a histogram. Several bright spots per field of view exhibited continuous intensity decay, presumably representing larger aggregates. These were used to estimate the overall photobleaching rate (0.003 per frame) and formally included in the histogram as representing 10 steps. The histogram without the bin representing continuum events was modelled as a weighted sum of binomial distributions for up to quadruple occupancy and probability of labelling of 0.56 estimated from UV-Vis spectra.

Electron microscopic reconstructions

Large scale VLP preparation

smFCS experiments were scaled up into 96 well plates. Two 96 well plates (Non-Binding Surface, Corning) were used. PS1 RNA was labelled and gel purified as described earlier and HBV dimer was purified as described above. Each well contained 200 µL of 15 nM PS1 in re-assembly buffer. As in smFCS, ten 2 µL injections of 2.5 µM dimer in dissociation buffer were performed. A Perkin-Elmer Envision plate reader was used to carry out the injections and record the anisotropy of the PS1 RNA (FITC excitation and emission filters). VLPs were purified away from free RNA and capsid using a 1.33 g/mL caesium chloride gradient and spun at 113,652 x *g* for 90 hours using an SW40Ti rotor. A single band was observed and fractionated. The band was dialysed into reassembly buffer to remove caesium chloride. The 2 mL fraction of VLP was concentrated to 200 µL using an Amicon 100 kDa MWCO spin concentrator.

CryoEM specimen preparation

After recovery of the PS1-containing VLPs and removal of caesium chloride by dialysis, their structures were analysed using single-particle cryo-EM. VLPs were vitrified. 200 mesh EM grids with Quantifoil R 2/1 support film and an additional ~ 5 nm continuous carbon film were washed using acetone and glow discharged for 40 s prior to use. CryoEM grids were prepared by placing 3µl of ~ 3.2 mg/ml HepB VLP on the grid, before blotting and plunge freezing using a Leica EM GP freezing device. Chamber conditions were set at 8 °C and 95 % relative humidity, with liquid ethane temperature at -175 °C. Data was collected on a FEI Titan Krios (eBIC, Diamond Light Source, UK) transmission electron microscope at 300 keV using an

electron dose of 27 $e^-/Å^2/s$, 2.5 s exposure, yielding a total electron dose of 67.5 $e^-/ Å^2$. Data was recorded on a 17 Hz FEI Falcon II direct electron detector. The dose was fractionated across 33 frames. Final object sampling was 1.34 Å per pixel. A total of 2397 micrographs were recorded using EPU (FEI) automated data collection software.

Single particle image processing

2397 micrographs were motion corrected and averages of each movie were generated using MotionCorr(13), and contrast transfer function (CTF) parameters for each were determined using CTFFIND4(14). Micrographs with unacceptable astigmatism or charging, as determined by examining the output from CTFFIND4, were discarded leaving a total dataset of 1710 micrographs. All particle picking, classification and alignment was performed in RELION 1.3(15).

Approximately 57,000 particles were manually picked and classified using reference-free 2D classification in RELION 1.3. This classification confirmed the initial visual impression that although the VLPs were purified as a single band on a caesium gradient, two sizes of VLPs were present. A selection of resulting 2D class averages were used as templates for automated particle picking. The particle stack generated using auto-picking was subject to 2D classification to separate *T*=3 and *T*=4 particles, and to remove particles not corresponding to VLPs. The subsequent particle stacks (5589 for *T*=3, 42,411 for *T*=4) were subject to 3D classification, using a sphere with the approximate diameter of the VLP as a starting model. Subsets of the data were reconstructed including data out to the Nyquist frequency using the 3D autorefine option in RELION with I3 symmetry imposed to generate all structures presented in this work. Within the *T*=4 42,411 particle dataset it was clear that a further subset (10,851 particles) of the data contained a significant asymmetric feature inside the Cp shell where RNA binding would be expected to occur. An asymmetric (C1) reconstruction was performed on a relatively homogenous set of 10,851 such particles, giving the reconstruction at 11.5 Å resolution.

The 3D model of PS1 RNA was made using RNA Composer(16). The cryoEM figures were rendered using USCF Chimera(17).

Purification of recombinant STNV CPs

Recombinant STNV VLPs were purified from E. coli(18). STNV charge-change mutant plasmids were created using primers designed using Agilent, and a Quikchange site directed

mutagenesis kit (Agilent). CP monomers were purified by disassembly in 50 mM Tris (pH 8.5), 10 mM EDTA, in the presence of Complete Protease Inhibitor Cocktail (Roche, United Kingdom). STNV CP was separated from the mRNA by sequential Q-Sepharose, and SP-Sepharose columns (GE Healthcare, Sweden). STNV CP was washed with 20 column volumes of 50 mM HEPES (pH 7.5) and 25 mM NaCl to remove residual EDTA, and subsequently eluted using a 0.025 - 2 M NaCl gradient in buffer. CP elutes at 0.8 M NaCl. STNV CP was analysed by SDS-PAGE and its concentration determined by UV absorbance. Fractions with an A260:A280 ratio of 0.6 or lower were used in assembly assays. Mutant CPs that did not form VLPs during overexpression were purified using the same sequential Q-Sepharose and SP-Sepharose columns method.

Preparation of RNA Oligonucleotides

dsDNA transcripts encoding the RNA oligonucleotides used in this study were produced using primers and the KAPA2G system (KAPA biosystems) following the manufacturer's protocol. Transcriptions were carried out using a Highscribe T7 High yield RNA synthesis kit (NEB). Products were run on a denaturing RNA gel. The Alexa Fluor 488 labelled B3 oligonucleotide used throughout was synthesised and HPLC purified by DNA Technology A/S (Denmark). Other RNA oligonucleotides requiring a 5′ fluorophore were labelled with an amino GMP during transcription and cross linked to an Alexa Fluor 488 SDP ester (Invitrogen) prior to gel purification as described previously(19).

Genomic chimeras were created by purchasing Gene blocks of the Synthetic, stabilised and Unstable + Δ1-127 STNV-1 constructs with a 5′ T7 promoter (IDT DNA technology), possessing BamHI and HindIII cleavage sites at either end to create sticky ends after restriction digestion and dephosphorylation using Antarctic phosphatase (NEB). This gene block was then ligated into a PACYC184 plasmid using T4 DNA ligase (NEB). Transcription was carried out as above after linearization using BamHI.

RNA was annealed prior to each experiment by heating to 80°C for 90 s and cooling slowly to 4°C in a buffer containing 50 mM NaCl, 10 mM HEPES and 1 mM DTT at pH 7. Genomes were only heated to 65°C.

STNV Reassembly in the Presence of B3 Variants and Sedimentation Velocity Analytical Ultracentrifugation (svAUC)Reassembly reactions were carried out in the presence and absence of B3 variants in a 1:3 RNA:CP ratio at a final CP concentration of 4.5 μM, by dialysis into a buffer containing 50 mM HEPES (pH 7.5) and 2 mM Ca2+. All samples were analysed by TEM and AUC. For AUV, 0.32 mL of each sample was placed in a 1.2 cm path length 2-sector meniscus matching epon centrepiece cell constructed with sapphire windows. The

samples were centrifuged at 15,000 rpm in an Optima XL-1 analytical ultracentrifuge at 20°C in an An50-Ti rotor. Changes in absorbance at 260 nm were detected by absorbance optics with 100 scans taken in approximately 11 hrs 30 min. Data were fitted and analysed using the program Sedfit.

5

smFCS Data Collection and Analysis

FCS measurements were performed on a custom-built smFCS facility. Excitation laser (Sapphire CW blue laser, 488 nm, Coherent, USA) power was set to 65 µW. The focus position was adjusted to 20 µm from the cover slip inner surface (maintained by piezoelectric feedback
10 loop, Piezosystems Jena, Germany). Immersion oil (refractive index 1.515, type DF, Cargille Laboratories, USA) was used with immersion oil objective (63 x magnification, numerical aperture 1.4). The photon count was recorded and analysed by an ALVL5000 multiple tau digital correlator (ALV-GmbH) in single channel mode. FCS data was analysed using non-linear, least-squares fitting with a single component diffusion model autocorrelation function
15 corrected for the triplet state in Matlab. Diffusion time was used in the calculation of apparent hydrodynamic radius (Rh) and plotted as a function of assembly time. Rh calculations were based on the measured diffusion time for Alexa Fluor 488 dye with the estimated Rh of the dye (= ~0.7 nm in assembly buffer).

20 smFCS Assembly and Competition assays

Initial measurements of Alexa Fluor 488 labelled RNA oligonucleotides were taken for at least 10 runs of 30 secs (5 min). Purified STNV CP was titrated into labelled RNA. Each titration was measured for a minimum of 10 30 secs runs. In assembly assays this was repeated until full capsid assembly had occurred. At this point RNase A was added to confirm RNA
25 protection. In competition assays, once the sample had formed a capsomer structure (Rh=~5 nm) the sample was monitored for a further 120 runs of 10 secs (20 min to ensure stability). At this point unlabelled B3 short/B3 variant competitor was added in 100-fold molar excess and measured for 120 runs of 10 secs.

30 CD analysis

Transcribed oligonucleotides were diluted to 1.5 µM in 300 µl, in a buffer containing 10 mM MES, 50 mM NaCl and 1 mM DTT at pH 6. Measurements were performed on a Jasco J715 spectropolarimeter, from 200 to 350 nm, with a bandwidth of 2 nm. Each Ca2+ and STNV titration was inverted 5 times and allowed to reach equilibria for 2 min prior to the next
35 measurements. Thermal denaturations were performed using a Peltier temperature control from 10- 95 °C in 5 °C steps, and an end scan was performed at 10 °C to check for cleavage.

Each measurement was performed in triplicate and averaged. Data was converted to molar ellipticity using the equation: $\Delta\varepsilon$ (cm2 mM-1) = θ/(32980 C(mM) L(cm) N(no. of nt)).

Light scattering assay of reassembly with genomic RNA variants

Reassemblies were performed with genomic chimeras in a 96 well plate as in the smFCS assays, with 1 nM genome and CP titrated in until a final concentration of 400 nM STNV CP was reached. This was concentrated through a 100 kDa centricon (millipore) at 10k xg for 5 min and run on a TSKgel G6000PWxl SEC column (Tosoh) with an AKTA pure system (GE Healthcare) connected to a DAWN HELEOS and Optilab TrEX for QELS and refractive index measurements. The column flow-rate was 0.4 ml min-1 for 50 min. Peaks were fractionated, A260/280 ratios measured and EM images obtained (Fig 25). The yield of the Unstable PS3 sample, as calculated by integration of light scattering signal, is dramatically lower than that of the wild-type STNV RNA, whilst the stabilised synthetic cassette results in a significantly higher (>20%) yield in VLP compared to the natural sequence. QELS estimates the Rh values similar to those from smFCS, 9.3 ± 0.1 nm, 9.1 ± 0.3 nm and 8.9 ± 0.2 nm for Synthetic, stabilised PS1-5 + Δ1-127STNV-1, wild type STNV-1 and Unstable PS1-5 + Δ1-127STNV-1, respectively (Table 6). The A260/280 ratios of the assembled VLPs eluting from the gel filtration column are also informative. Both the PS1-5 + Δ1-127STNV-1 and the wild-type STNV-1 genome samples have identical values (1.62), whilst the Unstable PS1-5 + Δ1-127STNV-1 sample has a higher value (1.89). This is consistent with there being a constant amount of RNA in the first two samples fully enclosed in shells containing the same number of CPs, whilst the final sample has the same RNA content in an incomplete shell.

Example 1

The HBV pgRNA contains preferred Cp binding sites

HBV VLPs assembled from (full-length) Cp subunits expressed in *E. coli* were purified as described(3) (Fig 7a & Table 1). They form a mixture of *T*=3 and predominantly *T*=4 shells. These were immobilised onto magnetic beads, disassembled by treatment with guanidinium chloride and then washed to remove host RNA, resulting in immobilised Cp dimers(20) with their ARDs accessible. RNA SELEX was carried out using our standard protocols (Fig. 7b) and the aptamer pool from the 10th round analysed by NextGen DNA sequencing (Methods).

The RNA sequences that bind Cp in the selected library were aligned to the HBV pre-genome most closely related to the protein used for the SELEX experiments (the laboratory strain, GenBank Seq id NC_003977.1(21)). Statistically significant matches (a Bernoulli score of 12 or more, Methods) to the pgRNA of this strain (the blue peaks in Fig. 2a) were benchmarked against an alignment of the unselected library (grey curve in Fig. 2a) to identify peaks that occur with significant frequency. This identifies multiple sites dispersed across the pgRNA having similar sequences/structures to Cp binding aptamers, consistent with our expectation for PS-like sites across the genome. We applied the same procedure to 14 randomly selected HBV strain variants from GenBank, the current NCBI HBV reference strain (GenBank Seq ID NC_003977.2) as well as the laboratory strain (GenBank Seq ID NC_003977.1) and identified all those peaks that are conserved in at least 80% of these strains (marked with green crosses in Fig. 2a). These genomic regions are thus likely to encompass PSs. The three peaks with the highest conservation (100%) and peak heights, the latter indicating how many aptamers matched these sites, are labelled PS1, PS2 and PS3 in Fig. 2a. For the nine sites with high conservation between strains, we extracted 30 nts 5′ and 3′ to the peak nucleotide in the genomic sequences of three representative strain variants, including the laboratory strain and the reference genome, and considered all their possible secondary structure folds with negative free energy via Mfold (Methods). A similarity analysis of primary and secondary structure revealed the predicted existence of stem-loops sharing a purine-rich loop recognition motif, RGAG (Fig. 2b).

We computed the frequency of this motif in stem-loops across the 16 HBV strains analysed. Across all strains, the RGAG motif occurs in stem-loops on average ~25.4 times (precisely 25 times in the laboratory strain). Compared to 10,000 randomised versions of the pgRNAs, the frequency of occurrence of RGAG in the actual genome is 4.68 standard deviations above the average (Fig. 2c), strongly implying a functional role(s).

Example 2

pgRNA oligonucleotides trigger VLP formation in vitro

PS1, 2 & 3 oligonucleotides (Fig. 8a), were tested for their ability to bind Cp dimers using single molecule fluorescence correlation spectroscopy (smFCS) (Fig. 3 & 8b). This technique yields a real time estimate of the hydrodynamic radius (R_h) of dye-labelled species. Importantly, it allows reactions to be followed at low nanomolar concentrations, where we have shown that binding specificity more closely reflects the situation *in vivo* compared to most *in vitro* reactions. The latter are typically carried out at higher (e.g. 0.1-0.8 μM)

concentrations(20), where the specificity of PS-mediated assembly is reduced or lost. In order to avoid electrostatic effects due to differing oligo lengths, each PS was produced as part of a 47 nt long fragment, each dye-labelled at its 5´ end (Methods(19)). The labelled oligos (~15 nM) were then titrated with increasing amounts of Cp (5-250 nM Cp dimer) and the R_h values tracked over time (Fig. 3a). After each addition there was a pause of ~10 min to allow reactions to equilibrate. The titrations lead to distortions in the data collection and the averaging, which is visible in the plots as noisy signals. After equilibration at 250 nM Cp, RNase was added to each reaction and the R_h values monitored for ~10 min. If these declined steeply, it was assumed that the VLPs produced were incomplete. Negative stain EM images were obtained for the samples before RNase addition, and the sizes of the complexes present at this point were also assessed by calculation of R_h distribution plots (Fig 3b and Fig. 8c, respectively).

Each of the PS fragments stimulates assembly of both T=3 and T=4 complete VLPs with roughly equal efficiency under these conditions (Fig. 3a & b), with the latter being the dominant product, as expected(22). Addition of Cp >250 nM does not increase the R_h values obtained, implying that by this stage all the RNAs have been incorporated into VLPs. In order to assess whether these effects are a direct consequence of Cp-PS interaction, we carried out a number of controls. Dye-labelled PS fragments do not bind to preformed VLPs and remain RNase sensitive in their presence (Table 2), implying that the PSs only get internalised in assembling VLPs. To determine if the RNA triggers assembly, we compared assembly efficiency of Cp with and without PS RNA present by adding a protein modifying dye after incubation of Cp alone or completion of a titration of unlabelled PS1. The R_h distribution plots are shown in Fig. 3b. In the absence of RNA, <5% of Cp assembles under these conditions, in contrast to >80% of the Cp for assembly in the presence of RNA. It appears that Cp-PS interaction triggers an increase in the assembly efficiency. This effect varies with the age of the Cp, consistent with oxidation of an assembly-inhibiting disulphide at the dimer interface(6). Comparative statements here are based on the results of both positive and negative control experiments with each batch of Cp.

We then probed the RNA sequence-specificity of these reactions (Fig 9a). Test oligos comprised the epsilon stem-loop, as well as loop and bulge variants of PS1. This included a variant in which the bulge region was fully base-paired. In similar assays to the PS1-3 reactions the R_h values for all three RNAs remain sensitive to nuclease action, implying that assembly of closed shells requires a specific RNA sequence/structure. EM images and distribution plots confirm this interpretation. The sequence sensitivity of the assembly reaction is further highlighted by additional PS1 variants (Figs. 9b & c; Table 3). Their effects on

assembly confirm the importance of the bulge and/or sequences within it, and the loop RGAG (here a GGAG) motif. A DNA oligonucleotide encompassing the PS1 sequence (Fig. 9d) elicits aggregation, showing that faithful assembly is a specific property of the PS in its RNA form, i.e. with an A helical duplex stem, as well as the Cp-recognition motif in the loop.

The C-terminal ARD of the HBV Cp is believed to mediate interactions with the pgRNA, and the 1-149 Cp fragment that lacks the ARD readily assembles in the absence of nucleic acid(23). We therefore assessed the ability of Cp_{149} to respond to PSs in the smFCS assay. No RNA-dependent assembly, or PS binding by Cp_{149}, occurs under these conditions (Fig. 10a), although EM images show that the truncated Cp alone readily assembles, confirming that the ARD is essential for the interaction with RNA. The ARD is extensively phosphorylated *in vivo*, although the responsible cellular kinase remains unknown(24). Lowering the positive charge on the C-terminus of Cp should reduce its ability to bind PS RNAs. We phosphorylated Cp *in vitro*(8) (Table 1) and tested its properties. EM images show that modified Cp readily assembles but does not bind to PS1 in smFCS assays (Fig. 10b).

Example 3

HBV NC assembly is triggered by formation of a sequence-specific RNA-core protein complex.

The VLPs assembled around PS1 were purified on a larger scale and their structures determined by cryo-EM, yielding icosahedrally-averaged reconstructions of the *T*=3 and *T*=4 particles (Fig. 4). A significant fraction (~25%) of the *T*=4 particles also contained an asymmetric feature located just below the protein shell. An asymmetric reconstruction of these particles was also calculated (Fig. 5). The result suggests the asymmetric feature represents a complex between PS1 oligonucleotides and the ARD domains of the overlying Cp subunits.

From the EM map at this resolution it is not possible to determine the number of PS oligonucleotides present in the complex. The $A_{260/280}$ ratio of the purified VLP suggests that the RNA content, assuming *T*=4 morphology, is ~5 oligos/particle(25) . An additional estimate of this stoichiometry was obtained by studying photobleaching of PS1 VLPs (Fig. 4, Methods). VLPs show multiple bleaching steps, confirming that there are multiple oligos within each shell. Given the labelling efficiency of the oligos, the data are consistent with 2-4 oligos/VLP. We built a 3D model of PS1 and manually positioned it within the EM map (Fig. 4f, Methods). From the relative volume of the asymmetric density and the size of the PS1 oligo, it appears that at

least two copies of the PS are present within the density. We cannot exclude the possibility that other RNA molecules are bound to the protein shell elsewhere, but are not visible due to mobility or an irregular location with respect to the ordered RNA density. The biochemical and structural data are consistent with the asymmetric structure being an assembly initiation complex, where an RNA preferred site(s) has initiated assembly culminating in the formation of the *T*=4 NC.

The cryo-EM data hint at a further insight into HBV biology. A minority of HBV particles, whether from assembly reactions or wild-type virus infections, assemble with *T*=3 quasi-symmetry and both types of particles are visible in our cryo-EM data. Using 2D and 3D classification the *T*=3 (~11%) and *T*=4 (89%) particles are readily separable. Figure 4 shows 3D reconstructions of the two particles with imposed icosahedral symmetry at 5.6 Å and 4.7 Å resolution, respectively. In addition to the obvious differences in size and number of Cp dimers that the two VLP structures contain, the *T*=4 and *T*=3 maps are different in the features visible on their inner surfaces, where the ARDs are located and where RNA binding occurs. As might be expected for icosahedrally-averaged maps of a sub-stoichiometrically occupied VLP, both structures are essentially devoid of density attributable to RNA. The capsid shell of the *T*=4 structure is visibly thinner than the *T*=3 equivalent, however, and closer examination of the *T*=3 map suggests that additional density corresponding to ordered segments of the ARDs is visible (Fig. 4), which is absent in the *T*=4 structure (Fig. 4 c & d). This difference persists when the *T*=4 map is Fourier filtered to be at a similar resolution as the *T*=3 (Fig. 11). This is consistent with previous studies that showed that the Cp C-terminal region, including the ARD, plays a role(s) in determining capsid geometry(22, 26).

Example 4

Sequence-specific recognition of individual PS sites

There are multiple consequences of sequence-specific RNA-CP recognition in the STNV system (Fig 12). Titration of CP into oligonucleotides encompassing only PS3 (or B3) initially results in formation of a trimeric capsomer (Rh ~5 nm), followed by formation of T=1 VLPs (Rh~11.3 nm) as the CP concentration is raised gradually. Rh distribution plots of the smFCS data at the end of the titration suggest that the VLPs formed are homogeneous, whilst electron microscopy images (EM) and RNase challenge assays suggest that they are composed of complete protein shells. A similar titration with a PS3/B3 variant having a loop sequence of -U.U.U.U-, showed that CP binds such SLs, but the complex formed is unable to assemble to VLPs(19). The natural 127-mer, encompassing PSs1-5, shows more complex behaviour. Addition of low CP concentrations triggers a collapse in its Rh by about 20-30%, mimicking

the behaviour seen for the full length genome(27). Subsequent CP additions result in co-operative conversion to T=1 VLPs with the same properties as those formed around PS3 alone. PS sequence variants within this fragment confirm that -A.X.X.A- is a CP recognition motif and its presence is only absolutely required in PS3, however the variants no longer assemble with wild-type co-operativity(19). STNV-1 CP alone shows no tendency to aggregate below 15 μM under these conditions, and therefore everything in the titrations shown here is a consequence of RNA-CP binding.

These results highlight the importance of PS3 recognition by CP for assembly. In order to identify the critical features of that recognition, we produced a series of SLs encompassing variant loop sequences with the PS3 stem (Fig 17 & Table 4). The variants have altered nucleotides in the "inner" two positions (-C.C-; -A.A-; -G.G-; -G.U- & -U.G-) compared to the wild-type –C.A- of PS3. "Outer" variants (-A.U.U.A-; -A.U.U.G-; -G.U.U.A-; -G.U.U.G-; -G.U.U.U-; -U.U.U.G-; -U.U.U.A- & -A.U.U.U-), in which both inner nucleotides were altered to uridines, were also tested. Our expectation was that there would be no base specificity at the middle positions while the adenines would be preferred at the first and last positions of the tetraloop. We examined their abilities to support assembly of both the T=1 shell and the trimeric capsomer. Test RNAs and CP were mixed at ~ 5 μM concentrations in reassembly buffer and the results assayed by velocity sedimentation analysis and in EM images. Under these conditions, the inner nucleotide variants form T=1 capsids with roughly similar efficiency as PS3, confirming that their identities are not part of the CP recognition motif (Fig 13 A/B & Fig 17). The outer nucleotide variants showed differing behaviour, with only the -A.U.U.U-, -U.U.U.A- and -A.U.U.A- variants having a peak in a similar position to PS3, confirming that the outer adenines are part of the CP recognition motif.

In order to examine their relative importance for CP affinity, we adapted the smFCS assay (Fig 13B). Labelled B3 was titrated with CP to form the trimer, as judged by the Rh value, and then a 100-fold molar excess of each sequence variant was added to compete off the B3. Variants that do not bind with a similar affinity to B3 fail to displace the labelled RNA, whereas B3 and other variants outcompete the labelled species restoring the Rh of CP-free RNA. The results (Fig 13D) show the percentage Rh change following this challenge, revealing a wide variation in the ability of the variant RNAs to compete. All those with guanine substitutions, and the -A.U.U.U- variant, fail to compete. The superior performance of the -U.U.U.A- variant suggests that either the 3′ A is the most important for CP recognition, or that the A-U base pair at the top of the adjacent stem breaks, presenting an -A.U.U.U.A.U- variant of the B3 motif that is still recognised by the CP. Either way, -A.X.X.A- outperforms all variants, suggesting that SLs carrying tetraloop motifs of -A.X.X.A- encompass the best CP recognition motif for assembly into VLPs.

Example 5: The roles of electrostatics and PS cooperativity in VLP assembly

PS-mediated assembly explains features of viral genome packaging that purely electrostatically driven reactions do not, although there is clearly a beneficial effect of charge neutralisation in supplying some of the free energy to drive encapsidation. We therefore examined the importance of these effects on STNV assembly using a series of charge-change CP variants. Mutations at three positively charged residues R8, R14 and K17 in the N-terminal arm of the CP (Fig 12), were produced with A or D in place of K or R. Since R14 and K17 are adjacent in three-dimensions, their variants were made as the double mutants, i.e. R14A/K17A and R14D/K17D. The mutated CPs express normally (Fig 18), but both double mutants fail to assemble significantly in E.coli under these conditions. Since VLPs obtained from E.coli contain host cell RNA, as well as the recombinant mRNA encoding the viral CP, this outcome suggests that R14 and K17 play important roles in assembly.

All the variant proteins were examined for their abilities to bind RNA oligos encompassing either a single PS (B3) or the 127-mer fragment (Fig 14 & Fig 19). Neither double mutant bound either RNA under these conditions. R8A assembles around B3 but requires a much higher (>10 fold) CP concentration to do so, consistent with it having a lowered affinity for the RNA. By 1 μM CP it forms T=1 shells that are resistant to RNase challenge. The R8D variant confirms the importance of the positive charge, failing to form any stable higher order species, even at higher concentrations, with the RNA remaining accessible to RNase digestion. This dependence on favourable electrostatic interaction remains when R8D is titrated against the 127-mer (Fig 14A). However, with this RNA both R8A and wild-type CP show very similar binding curves, including the initial Rh decrease. It appears that the co-operativity arising from CP binding at multiple PS sites overcomes the deleterious effect on intrinsic RNA-CP affinity of reduced electrostatic attraction. If we assume that the altered charge(s) on the N-terminal arm does not significantly alter the unliganded CP conformation, these effects probe the role(s) of electrostatic interactions during RNA sequence-specific triggering of assembly. They imply that charge neutralisation is not an absolute requirement for assembly on longer natural RNA fragments, consistent with the PS-mediated, but not the electrostatic assembly mechanism.

Given that the cooperativity of multiple RNA PSs can overcome diminution of electrostatic attraction, as expected for a process in which PSs act collectively, we then examined how many PSs are required to generate cooperative assembly. Given the importance of recognition at PS3 and the effects seen for fragments containing five PSs, three sub-fragments of the 127-mer each containing PS3 were tested (Fig 14B & Fig 20). These are PS1-PS3 (nts 1-76); PS2-PS4 (nts 38-104) and PS3-PS5 (nts 66-127), each potentially able to bind CP at PS3 but differing in the numbers of flanking sites, from two 5′ or 3′ of PS3, to just one on each flank.

Only the fragment with the PS3 centrally located assembles T=1 shells that are RNase resistant, although it does not show a collapse and the overall yield is lower than for the 127-mer. The other fragments appear to form non-specific aggregates that eventually spontaneously dissociate.

The interpretation of these results is non-trivial. The effects are clearly not purely electrostatic in nature since the PS2-4 fragment (66 nts) is shorter than PS1-3 (76nts) and 1 nt shorter than PS3-5. To understand the specificity of the reactions we need to consider the folding propensity of each of the PS-encompassing sites. The secondary structure of the 127-mer shown (Fig 15) was arrived at by constraining its folds to capture the maximum number of SLs with -A.X.X.A- loop motifs present. In this fragment only PS1 and PS3 are predicted to have a favourable folding free energy (Mfold,(10). in isolation. This is consistent with our previous smFCS assays, in which alterations of the CP recognition motifs within each PS and variations in the relative spacing of PS3 with its neighbours resulted in markedly different assembly behaviour(28). We expect these RNA molecules to exist in solution as an ensemble of differing conformations. Interaction with the STNV CP will displace this equilibrium, preferentially selecting a single or few assembly competent conformations in which the PSs are present. The assembly efficiency we see may therefore be directly related to the population of such conformers in the ensemble and thus related to the free energy costs in imposing this conformation. Assessing the extent of a conformational ensemble is difficult, but a sense of the likelihood of alternate structures can be obtained from Mfold by altering the usual default parameters to explore an ensemble of suboptimal folds within 500 percent from the minimum free energy fold (suboptimality = 500).

When such structures are examined for the three PS-containing fragments, a possible explanation for their assembly competencies emerges. For PS1-3, the dominant folds encompass PS1 with a minority also containing PS3 (Table 5). In principle, that minor conformer could promote assembly, but the critical spacing between PS1 and PS3 is too large to facilitate the co-operative effects of multiple PSs. A similar analysis of PS2-4 suggests that the dominant secondary structure does not contain any of the PS folds expected for the 127-mer. However, its predicted secondary structure contains two alternative SLs that are almost always present, one of which presents an -A.X.X.A- sequence (Fig 22). Their relative spacing (4 nt) is short enough to see a co-operative effect. The PS3-5 fragment forms two SLs within 10-12 nts of one another, one presenting an -A.X.X.A- motif as PS5. This would suggest an assembly-competent structure. However, in the ensemble of possible structures, this SL is only present in 6% of the potential folds (Table 5), which may account for the assembly behaviour (Fig. 14B).

The conformational scrambling behaviour described above for the fragments encompassing three PSs probably reflects events in vivo where it is known that sequences within the 127-mer participate in formation of a translational enhancer with sequences in the 3′ UTR(29). That complex cannot be present in the assembly competent conformer. In order to explore the effects of such secondary structure folding propensity further, we turned to the design of artificial PS-containing sequences.

Example 6:Assembly of non-viral substrates

In order to investigate the requirements for an efficient assembly substrate, we produced synthetic cassettes mimicking aspects of the wild-type 127 mer (PS1-5) in which most of the natural viral sequence has been replaced (~77%). Attempts to create these sequences using a simple base substitution scheme, e.g. swapping all As for Us; Cs for Gs, Gs for Cs and Us for As in the regions other than the CP recognition motifs, all resulted in unstable secondary structures. We therefore chose to modify the existing SLs by conversion of base pairs to G-C, inversion of existing G-C pairs, or adding extra base pairs and then checking that they would likely fold into similar secondary structures to those in the wild-type 127-mer. The natural viral sequences connecting these SLs were then replaced with strings of As and Gs until only one fold was most likely (Fig 18 & Fig 23). The relative separations of the base-paired stems were kept identical to those in the wild-type 127-mer. As a result of these changes, PSs 1, 2, 4, and 5 have been stabilised compared to the wild-type 127mer, with all SLs having favourable folding propensity (Fig 23).

To assess the importance of the folding propensity of the dominant PS3 site we also created the following synthetic versions: 1) Unstable PS1-5, in which the folding free energy of PS3, the central PS, is positive (0.3 vs -2.6 kcal/mol), i.e. a scenario in which PS3 is unlikely to fold spontaneously; 2) Stable PS1-5, in which the folding free energy of the central PS is more negative (-3.5 vs -2.6 kcal/mol for the 127-mer), i.e. where PS3 is more stable; 3) All PS3, in which all five PSs mimick PS3, with stems of all PSs extended to the same length (7 bp) and all CP recognition motifs identical to that in wild-type PS3; & 4) Synthetic, stabilised PS1-5, containing the artificial PSs 1, 2, 4 and 5 from Stable PS1-5, and the artificial extended stem-loop for PS3 from the All PS3 construct. The latter is hyper-stabilised with respect to the PS3 in both the wild-type 127-mer and the Stable PS1-5 (-7.6 vs -2.6 or -3.5 kcal/mol, respectively).

Example 7

In order to compare the behaviours of these test variant oligonucleotides we examined their potential secondary structures. Table 5 lists the frequency of occurrence of each PS in

ensembles created using the suboptimality feature in Mfold, together with their relative spacings. In addition, we compared their circular dichroism (CD) spectra. CD provides a physical signal(30), the molar ellipticity at 260 nm, that is proportional to the percentage of base-paired residues and/or tertiary structure. The measurements were made in a buffer containing calcium ions since these are required in the reassembly buffer, there being several Ca2+ binding sites within the STNV capsid (38, 39). Titration of the test RNAs up to 2 mM calcium, the concentration in reassembly buffers, results in mild increases (9–17 %) in the 260 nm ellipticity, as expected (Fig 24A). The only exception is Unstable PS1-5, which does not respond to the presence of the cation. The molar ellipticity values of all test RNAs in this buffer decline as expected with temperature (Fig 24B). All the RNAs have different CD ellipticities at 260 nm, illustrating the complexity of comparing RNA conformational ensembles. The Unstable PS1-5 sample is much less structured throughout the temperature range. Perhaps surprisingly given the apparent Mfold structures, the wild-type 127-mer has the highest amount of structure at the lower temperatures. At the highest temperature tested all the RNAs except Unstable PS1-5 have roughly similar ellipticity values, implying that they had reached similar levels of denaturation.

All these synthetic variants trigger assembly of T=1 capsids and are able to protect the encapsidated RNA from challenge by nuclease but with very different CP concentration dependences. All but the Unstable PS1-5 show similar initial decreases in Rh to the 127-mer (Fig. 15B). The Unstable PS1-5 assembly behaviour resembles that of PS3 alone, suggesting that it has lost co-operativity, and its distribution plot and appearance in EM images (Fig 24) suggests that it has also lost the ability to regulate capsid formation efficiently. In contrast, the importance of the central PS folding propensity is illustrated by the behaviour of Stable PS1-5. Despite the potential issues with a folding ensemble, it shows a similar collapse to the 127-mer and a cooperative assembly to T=1 particles with a similar Rh distribution to the wild-type fragment. It assembles into VLPs at lower CP concentrations than the wild-type 127-mer, i.e. under these conditions it is a better assembly substrate. Remarkably, All PS3 also assembles more efficiently than wild-type even though it encompasses PSs that are longer than those found in the 127-mer, suggesting that there is some leeway in the PS secondary structure context in which the recognition motif is presented. This is a little surprising given the critical dependency on PS spacing around PS3 observed previously(19). The efficiency of assembly and the folding propensity of the All PS3 variant notwithstanding, the Synthetic, stabilised PS1-5 is by far the best assembly substrate, assembling to VLPs most efficiently (i.e. it assembles more quickly following 100 nM CP titration point) (Fig 15B).

Example 8

These results suggest that it is possible to abstract the critical assembly features from a viral genomic RNA fragment. Given the alterations in the stem lengths and loop sizes in the synthetic fragments it would also appear that there is considerable scope for engineering templates with improved PS folding propensity.

Transfer of critical assembly features to genomic-scale RNAs

As a test of whether these experiments have successfully identified essential assembly features we examined how inclusion of this improved RNA "cassette" alters the assembly efficiency of a natural RNA. That RNA must be inherently able to be assembled into the small volume of the STNV virion. The genomic fragment from 128-1239 nts of the STNV-1 RNA is the obvious test fragment. We therefore constructed two genomic chimeras: [Unstable PS1-5 + Δ1-127STNV-1], which is 1242 nts long and [Synthetic, stabilised PS1-5 + Δ1-127STNV-1], 1248 nts long, and compared their assembly efficiencies in vitro relative to the wild-type STNV-1 RNA (Fig 16A). All three behaved differently in these assays, implying that the sequence and structure of the 5′ 127-mers regulates the assembly pathway of a fragment that is over 10 times its size. The wild-type genome shows the expected initial collapse in Rh (to ~7.5 nm) followed by a slight rise in Rh consistent with the formation of T=1 particles (Fig 16B). Note, the data in Fig 16A are for a CP titration compared to the single step addition of a complete complement of CPs described previously (12). In contrast, the Unstable PS1-5 leader sequence results in a larger initial collapse in Rh (to ~5 nm; 65%) followed by only a small rise that implies VLPs are not made efficiently. Indeed the RNA in this species remains susceptible to RNase degradation, implying that it has not been completely encapsidated. Synthetic, stabilised PS1-5 + Δ1-127STNV-1 has roughly the same initial, CP-free Rh, but appears simply to shrink to values consistent with VLP formation, rather than collapsing and recovering. Rh distributions and EM images of the assembly products are consistent with this interpretation. It is noticeable that the Synthetic, stabilised PS1-5 + Δ1-127STNV-1 VLP trace is less noisy than the other samples and has a distribution in Rh sizes that more closely matches that of authentic VLPs isolated from E.coli. Confirmation of the interpretation of these results is provided by quasi-elastic light scattering (QELS) of the products following elution from a gel filtration column (Fig 25).

Example 9

We have shown that the dual code inherent in RNA PS-mediated virus assembly, i.e. that genomic RNAs simultaneously encode a genetic message as well as instructions for efficient capsid assembly, are separable. An important question is why do the codes not separate

during the course of viral evolution, especially as replication in ssRNA viruses occurs via error-prone processes that lead to creation of a quasi-species of genome variants. There are now three examples of viruses using RNA PS-mediated virus assembly where we have structural information that partially answer this question. In bacteriophage MS2(31), human parechovirus-1(32) and STNV(19), at least one of the PS sites in the genome also encodes amino acid residues forming part of the PS binding site. This intimate embedding of both codes has the consequence of favouring assembly only of progeny RNAs in which PS-mediated assembly persists. Similarly the density of functions encoded within such RNAs is well known. The natural 5′ 127-mer in the STNV genome also forms an essential transcriptional/translational enhancer contact with the 3′ end sequence. Since that structure and assembly are mutually excluding functions, the natural sequence has evolved to balance the propensity that they form such that the viral lifecycle can proceed efficiently.

The focus here is the property of the assembly code liberated from the wild-type viral RNA sequence. Indeed, by sequentially investigating each aspect of the STNV assembly sequence in its natural context we have been able to reproduce its effects in triggering in vitro assembly of STNV CPs using a synthetic non-viral RNA. Additional refinements allow us to produce sequences that are either less or more efficient than the wild-type STNV 127-mer. These results confirm the nature of PS-mediated assembly for STNV. Assembly in vitro initiates within the 127-mer by recognition by CP subunits of the PS3 stem-loop. Higher–order CP binding is dependent on the correct positioning and folding of the neighbouring PSs (PS2 and 4), each presenting a consensus CP recognition motif in the loop. The 127-mer potentially encompasses five PSs that make the initial binding co-operative with respect to protein concentration leading to a collapse in the hydrodynamic radius of the RNA, a necessary precursor to encapsidation. Electrostatic interactions contribute to these protein-RNA contacts but are not the major driving force, which instead is a high-affinity sequence-specific interaction of the stem and loop regions of the PSs with the inner surface of the protein capsid. Despite its minimal sequence content, the -A.U.U.A- sequence is bound with low nanomolar affinity by the CP. Remarkably, grafting the synthetic variant 127-mers onto the remainder of the natural STNV-1 genome results in chimeras whose assembly properties are dominated by the first ~10% of the RNA.

Previously, Wilson and colleagues showed they could direct assembly of non-viral RNAs into rods of Tobacco Mosaic Virus (TMV) CP by creating RNA chimeras encompassing the TMV assembly initiation site(33, 34). This was successful, with the length of the protein-coated rods formed being determined by the length of the RNA being packaged, as expected from the

known assembly mechanism(35). This approach was less successful when applied to spherical ssRNA viruses(36), the highest affinity MS2 PS having positive effects on in vitro encapsidation of short RNAs but being less important on longer ones(37). Note, all these experiments were done at micromolar concentrations where the effects of PS-mediated assembly are lost(31, 37). The results described above suggest an efficient route for encapsidation of bespoke, non-viral RNAs in shells of viral CPs. In vitro assembly may be possible for a large number of CP-RNA combinations, but it differs from in vivo assembly where, in many viruses, there is good evidence suggesting that only nascent genomic transcripts emerging from the viral polymerase complex are packaged into progeny virions. In such reactions, the RNA is very likely to fold kinetically, avoiding some of the issues with RNA conformational ensembles in the in vitro reactions such as those described here.

Viruses and virus-like particles are finding increasing potential medical applications as gene therapy or drug-delivery vectors, as well as acting as non-replicating synthetic vaccines. Viral protein shells are also of interest for nanotechnology applications. The results described here offer an important insight into ways to create such structures with high efficiency and potentially carrying non-viral RNAs with advantageous properties. This will be essential for the production of designer synthetic virions.

References

1. Yu X, Jin L, Jih J, Shih C, Zhou ZH (2013) 3.5Å cryoEM structure of hepatitis B virus core assembled from full-length core protein. *PLOS ONE* 8(9):e69729.

2. Darty K, Denise A, Ponty Y (2009) VARNA: Interactive drawing and editing of the RNA secondary structure. *Bioinformatics* 25(15):1974–1975.

3. Porterfield JZ, et al. (2010) Full-length hepatitis B virus core protein packages viral and heterologous RNA with similarly high levels of cooperativity. *J Virol* 84(14):7174–7184.

4. Lakowicz JR ed. (2006) *Principles of Fluorescence Spectroscopy* (Springer US, Boston, MA).

5. Holmes K, et al. (2015) Assembly Pathway of Hepatitis B Core Virus-like Particles from Genetically Fused Dimers. *Journal of Biological Chemistry* 290(26):16238–16245.

6. Selzer L, Katen SP, Zlotnick A (2014) The hepatitis B virus core protein intradimer interface modulates capsid assembly and stability. *Biochemistry* 53(34):5496–5504.

7. A Zlotnick, et al. (1996) Dimorphism of Hepatitis B Virus Capsids Is Strongly

Influenced by the C-Terminus of the Capsid Protein. *Biochemistry* 35(23):7412–7421.

8. Aubol BE, et al. (2003) Processive phosphorylation of alternative splicing factor/splicing factor 2. *Proceedings of the National Academy of Sciences* 100(22):12601–12606.

9. Bunka DHJ, et al. (2011) Degenerate RNA packaging signals in the genome of Satellite Tobacco Necrosis Virus: implications for the assembly of a T=1 capsid. *J Mol Biol* 413(1):51–65.

10. Zuker M (2003) Mfold web server for nucleic acid folding and hybridization prediction. *Nucleic Acids Res* 31(13):3406–3415.

11. Podjarny A, Dejaegere AP, Kieffer B eds. (2011) *Biophysical Approaches Determining Ligand Binding to Biomolecular Targets: Detection, Measurement and Modelling* (Royal Society of Chemistry, Cambridge) Available at: http://ebook.rsc.org/?DOI=10.1039/9781849732666.

12. Sharma A, et al. (2014) Domain movements of the enhancer-dependent sigma factor drive DNA delivery into the RNA polymerase active site: insights from single molecule studies. *Nucleic Acids Res* 42(8):5177–5190.

13. Li X, et al. (2013) Electron counting and beam-induced motion correction enable near-atomic-resolution single-particle cryo-EM. *Nature Methods* 10(6):584–590.

14. Rohou A, Grigorieff N (2015) CTFFIND4: Fast and accurate defocus estimation from electron micrographs. *Journal of structural biology* 192(2):216–221.

15. Scheres SHW (2015) Semi-automated selection of cryo-EM particles in RELION-1.3. *Journal of structural biology* 189(2):114–122.

16. Popenda M, et al. (2012) Automated 3D structure composition for large RNAs. *Nucleic Acids Res* 40(14):e112–e112.

17. Pettersen EF, et al. (2004) UCSF Chimera—A visualization system for exploratory research and analysis. *Journal of computational chemistry* 25(13):1605–1612.

18. Lane SW, et al. (2011) Construction and crystal structure of recombinant STNV capsids. *J Mol Biol* 413(1):41–50.

19. Patel N, et al. (2015) Revealing the density of encoded functions in a viral RNA. *Proc Natl Acad Sci USA* 112(7):2227–2232.

20. Porterfield JZ, et al. (2010) Full-length hepatitis B virus core protein packages viral and heterologous RNA with similarly high levels of cooperativity. *J Virol* 84(14):7174–7184.

21. Wang JC-Y, Nickens DG, Lentz TB, Loeb DD, Zlotnick A (2014) Encapsidated hepatitis B virus reverse transcriptase is poised on an ordered RNA lattice. *Proc Natl Acad Sci USA* 111(31):11329–11334.

22. A Zlotnick, et al. (1996) Dimorphism of Hepatitis B Virus Capsids Is Strongly Influenced by the C-Terminus of the Capsid Protein. *Biochemistry* 35(23):7412–7421.

23. Birnbaum F, Nassal M (1990) Hepatitis B virus nucleocapsid assembly: primary structure requirements in the core protein. *J Virol* 64(7):3319–3330.

24. Ludgate L, et al. (2012) Cyclin-dependent kinase 2 phosphorylates s/t-p sites in the hepadnavirus core protein C-terminal domain and is incorporated into viral capsids. *J Virol* 86(22):12237–12250.

25. Porterfield JZ, Zlotnick A (2010) A simple and general method for determining the protein and nucleic acid content of viruses by UV absorbance. *Virology* 407(2):281–288.

26. Watts NR, et al. (2002) The morphogenic linker peptide of HBV capsid protein forms a mobile array on the interior surface. *EMBO Journal* 21(5):876–884.

27. Borodavka A, Tuma R, Stockley PG (2012) Evidence that viral RNAs have evolved for efficient, two-stage packaging. *Proc Natl Acad Sci USA* 109(39):15769–15774.

28. Dykeman EC, Stockley PG, Twarock R (2014) Solving a Levinthal's paradox for virus assembly identifies a unique antiviral strategy. *Proc Natl Acad Sci USA* 111(14):5361–5366.

29. Kaempfer R, van Emmelo J, Fiers W (1981) Specific binding of eukaryotic initiation factor 2 to satellite tobacco necrosis virus RNA at a 5'-terminal sequence comprising the ribosome binding site. *Proceedings of the National Academy of Sciences* 78(3):1542–1546.

30. Sosnick TR, Fang X, Shelton VM (2000) Application of circular dichroism to study RNA folding transitions. *Meth Enzymol* 317:393–409.

31. Beckett D, Uhlenbeck OC (1988) Ribonucleoprotein complexes of R17 coat protein and a translational operator analog. *J Mol Biol* 204(4):927–938.

32. Shakeel S, et al. (2017) Genomic RNA folding mediates assembly of human parechovirus. *Nat Commun* 8(1):5.

33. Sleat DE, Turner PC, Finch JT, Butler PJ, Wilson TM (1986) Packaging of recombinant RNA molecules into pseudovirus particles directed by the origin-of-assembly sequence from tobacco mosaic virus RNA. *Virology* 155(2):299–308.

34. Gallie DR, Plaskitt KA, Wilson TM (1987) The effect of multiple dispersed copies of the origin-of-assembly sequence from TMV RNA on the morphology of pseudovirus particles assembled in vitro. *Virology* 158(2):473–476.

35. Caspar DL, Klug A (1962) Physical principles in the construction of regular viruses. *Cold Spring Harb Symp Quant Biol* 27:1–24.

36. Qu F, Morris TJ (1997) Encapsidation of turnip crinkle virus is defined by a specific packaging signal and RNA size. *J Virol* 71(2):1428–1435.

37. Beckett D, Wu HN, Uhlenbeck OC (1988) Roles of operator and non-operator RNA sequences in bacteriophage R17 capsid assembly. *J Mol Biol* 204(4):939–947.

Claims

1. An artificial nucleic acid cassette for use in the assembly of a virus like particle comprising: one or more packaging signals, wherein the more than one packaging signals are arranged in series and separated by nucleic acid, said packaging signals comprising a nucleic acid loop domain comprising a nucleotide binding motif for cognate viral capsid protein(s), and a nucleic acid stem domain comprising a double stranded region by intramolecular base pairing, wherein said artificial nucleic acid cassette, when contacted with a plurality of cognate viral capsid proteins, assembles said cognate viral capsid proteins into a VLP that protects said nucleic acid packaging signals contained within said VLP from ribonuclease digestion.

2. The artificial nucleic acid cassette according to claim 1 wherein said artificial nucleic acid cassette is a non-replicating nucleic acid.

3. The artificial nucleic acid cassette according to claim 1 or 2 wherein said VLP provokes an immune response similar to an immune response of the native virus particle when administered to an animal subject.

4. The artificial nucleic acid cassette according to any one of claims 1 to 3 wherein said artificial nucleic acid cassette does not comprise protein encoding nucleic acid.

5. The artificial nucleic acid cassette according to any one of claims 1 to 4 wherein said artificial nucleic acid cassette comprises at least one nucleic acid packaging signal.

6. The artificial nucleic acid cassette according to claim 5 wherein said artificial nucleic acid cassette comprises at least 2 nucleic acid packaging signals.

7. The artificial nucleic acid cassette according to claim 5 wherein said artificial nucleic acid cassette comprises at least 3 nucleic acid packaging signals.

8. The artificial nucleic acid cassette according to claim 5 wherein said artificial nucleic acid cassette comprises at least 4 nucleic acid packaging signals

9. The artificial nucleic acid cassette according to claim 5 wherein said artificial nucleic acid cassette comprises at least 5 nucleic acid packaging signals.

10. The artificial nucleic acid cassette according to any one of claims 1 to 9 wherein said non-coding viral nucleic acid separating said nucleic acid packaging signals is at least 5 nucleotides in length.

11. The artificial nucleic acid cassette according to claim 10 wherein In a preferred embodiment of the invention said non-coding viral nucleic acid separating said nucleic acid packaging signals is at least between 5 and 50 nucleotides in length.

12. The artificial nucleic acid cassette according to claim 10 wherein said non-coding viral nucleic acid separating said nucleic acid packaging signals is greater than 50 nucleotides.

13. The artificial nucleic acid cassette according to any one of claims 1 to 12 wherein said loop domain comprising said capsid binding motif is at least 4 nucleotides in length.

14. The artificial nucleic acid cassette according to any one of claims 1 to 13 wherein said stem domain is at least 5 base pairs (bp) in length.

15. The artificial nucleic acid cassette according to any one of claims 1 to 14 wherein said artificial nucleic acid cassette is at least 50 nucleotides in length.

16. The artificial nucleic acid cassette according to claim 15 wherein said nucleic acid cassette is between 50 and 1000 nucleotides in length.

17. The artificial nucleic acid cassette according to any one of claims 1 to 16 wherein said nucleic acid packaging signal is isolated from an RNA virus.

18. The artificial nucleic acid cassette according to claim 17 wherein said RNA virus is a positive sense single stranded RNA virus.

19. The artificial nucleic acid cassette according to claim 18 wherein said nucleic acid packaging signal RNA virus is isolated from Hepatitis B virus.

20. The artificial nucleic acid cassette according to claim 19 wherein said Hepatitis B virus packaging signal comprises a nucleotide binding motif wherein said nucleotide binding motif comprises the nucleotide sequence RGAG wherein R is either G or A.

21. The artificial nucleic acid cassette according to claim 20 wherein said artificial nucleic acid cassette comprises at least one, two or three Hepatitis B virus packaging signals wherein one or more of said nucleic acid packaging signals includes the nucleotide binding motif RGAG.

22. The artificial nucleic acid cassette according to any one of claims 19 to 21 wherein said nucleic acid cassette comprises at least one of the packaging signals identified for Hepatitis B wherein each of said nucleic acid packaging signals includes the binding motif RGAG.

23. The artificial nucleic acid cassette according to any one of claims 19 to 22 wherein said artificial nucleic acid cassette comprises a nucleotide sequence selected from the group consisting of:

i) a nucleic acid molecule comprising a nucleotide sequence GUUUGUUUAAAGACUGGGAGGAGUUGGGGGAGGAG [SEQ ID NO: 1];

ii) a nucleic acid molecule comprising a nucleotide sequence that is at least 25% identical to the nucleotide sequence set forth in SEQ ID NO: 1 and that comprises a nucleotide binding motif GGGAGG.

24. The artificial nucleic acid cassette according to any one of claims 19 to 23 wherein said artificial nucleic acid cassette comprises a nucleotide sequence selected from the group:

i) a nucleic acid molecule comprising a nucleotide sequence GGGCCCUCUGACAGUUAAUGAAAAAAGGAGAUUAAAAUUAAUUAUGCCU [SEQ ID NO: 2];

ii) a nucleic acid molecule comprising a nucleotide sequence that is at least 25% identical to the nucleotide sequence set forth in SEQ ID NO: 2 and that comprises a nucleotide binding motif GAAAAAAGGAG.

25. The artificial nucleic acid cassette according to any one of claims 19 to 24 wherein said artificial nucleic acid cassette comprises a nucleotide sequence selected from the group:

i) a nucleic acid molecule comprising a nucleotide sequence GGCUGGCAUUCUAUAUAAGAGAGAAACUACACGC [SEQ ID NO: 3];

ii) a nucleic acid molecule comprising a nucleotide sequence that is at least 25% identical to the nucleotide sequence set forth in SEQ ID NO: 3 and that comprises a nucleotide binding motif AUAUAAGAG.

26. The artificial nucleic acid cassette according to any one of claims 19 to 25 wherein said artificial nucleic acid cassette comprises a nucleotide sequence comprising SEQ ID NO: 1 and/or SEQ ID NO: 2 and/or SEQ ID NO: 3.

27. The artificial nucleic acid cassette according to any one of claims 19 to 26 wherein said artificial nucleic acid cassette comprises a nucleotide sequence comprising SEQ ID 4: CUGGGAGGAGUUGGGGGAGGAGAUUAGGUUAAAGGUCUUUGUACUAGGAGGCUGU AGGC.

28. The artificial nucleic acid cassette according to any one of claims 1 to 18 wherein said RNA virus is a species that infects a plant cell or plant.

29. The artificial nucleic acid cassette according to claim 28 wherein said RNA virus is Satellite Tobacco Necrosis Virus.

30. The artificial nucleic acid cassette according to claim 29 wherein said nucleic acid cassette comprises at least one nucleic acid packaging signal isolated from Satellite Tobacco Necrosis Virus.

31. The artificial nucleic acid cassette according to claim 29 or 30 wherein said nucleic acid cassette comprises at least one nucleic acid packaging signal wherein said nucleic acid packaging signal comprises the nucleotide binding motif AXXA or AXXXA wherein X is any nucleotide base.

32. The artificial nucleic acid cassette according to any one of claims 28 to 31 wherein said artificial nucleic acid cassette comprises a nucleotide sequence selected from the group:

i) a nucleic acid molecule comprising a nucleotide sequence set forth in SEQ ID NO: 5;

ii) a nucleic acid molecule comprising a nucleotide sequence that is at least 25% identical to the nucleotide sequence set forth in SEQ ID NO: 5 and that comprises a nucleotide binding motif AXXA.

33. The artificial nucleic acid cassette according to any one of claims 28 to 32 wherein said artificial nucleic acid cassette comprises a nucleotide sequence selected from the group:

i) a nucleic acid molecule comprising a nucleotide sequence set forth in SEQ ID NO: 6

ii) a nucleic acid molecule comprising a nucleotide sequence that is at least 25% identical to the nucleotide sequence set forth in SEQ ID NO: 6 and that comprises a nucleotide binding motif AXXA.

34. The artificial nucleic acid cassette according to any one of claims 28 to 33 wherein said artificial nucleic acid cassette comprises a nucleotide sequence selected from the group:

i) a nucleic acid molecule comprising a nucleotide sequence set forth in SEQ ID NO: 7

ii) a nucleic acid molecule comprising a nucleotide sequence that is at least 25% identical to the nucleotide sequence set forth in SEQ ID NO: 7 and that comprises a nucleotide binding motif AXXA.

35. The artificial nucleic acid cassette according to any one of claims 28 to 34 wherein said artificial nucleic acid cassette comprises a nucleotide sequence selected from the group:

i) a nucleic acid molecule comprising a nucleotide sequence set forth in SEQ ID NO: 8

ii) a nucleic acid molecule comprising a nucleotide sequence that is at least 25% identical to the nucleotide sequence set forth in SEQ ID NO: 8 and that comprises a nucleotide binding motif AXXA.

36. The artificial nucleic acid cassette according to any one of claims 1 to 35 wherein said artificial nucleic acid cassette further comprises a transcription cassette comprising a nucleic acid molecule adapted to transcribe a nucleic acid encoding a polypeptide or a functional RNA.

37. The artificial nucleic acid cassette according to claim 36 wherein said adaptation is the provision of a promoter sequence and termination sequence to enable expression of said nucleic acid molecule encoding said polypeptide or functional RNA.

38. The artificial nucleic acid cassette according to claim 37 wherein said polypeptide is a therapeutic polypeptide, for example an antibody or antibody fragment.

39. The artificial nucleic acid cassette according to claim 37 wherein said functional nucleic acid is an mRNA encoding a therapeutic polypeptide, an antisense oligonucleotide or an siRNA.

40. A virus like particle comprising an artificial nucleic acid cassette according to any one of claims 1 to 39.

41. The virus like particle according to claim 40 wherein said virus like particle is immunogenic when administered to a subject.

42. The virus like particle according to claim 41 wherein the immune response is induction of an antibody response wherein said antibody response induces antibodies that specifically bind native virus particles.

43. The virus like particle according to any one of claims 40 to 42 wherein said virus like particle retains or has enhanced cell tropism when compared to native virus particles.

44. A vaccine or immunogenic composition comprising a virus like particle according to any one of claims 40 to 43.

45. The composition according to claim 44 wherein said vaccine or immunogenic composition further comprises an adjuvant and/or carrier.

46. A pharmaceutical composition comprising a virus like particle according to any one of claims 40 to 43 and including a pharmaceutically acceptable excipient.

47. A virus like particle according to any one of claims 40 to 43 for use in the delivery of an agent to a cell.

Figure 1
A

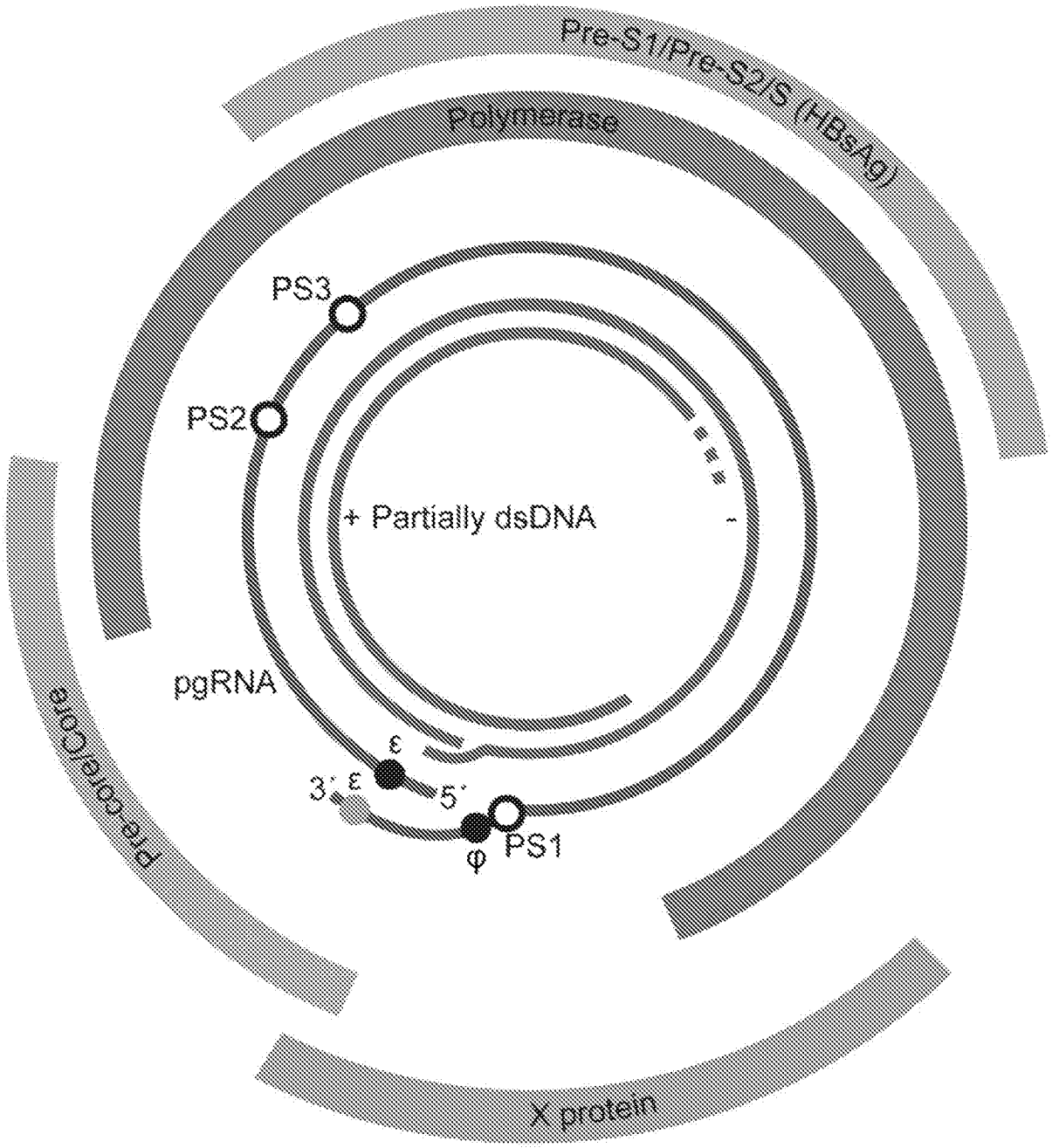
Pre-S1/Pre-S2/S (HBsAg)
Polymerase
PS3
PS2
+ Partially dsDNA
-
pgRNA
ε
3'
ε
5'
φ
PS1
Pre-core/Core
X protein

Figure 1 continued

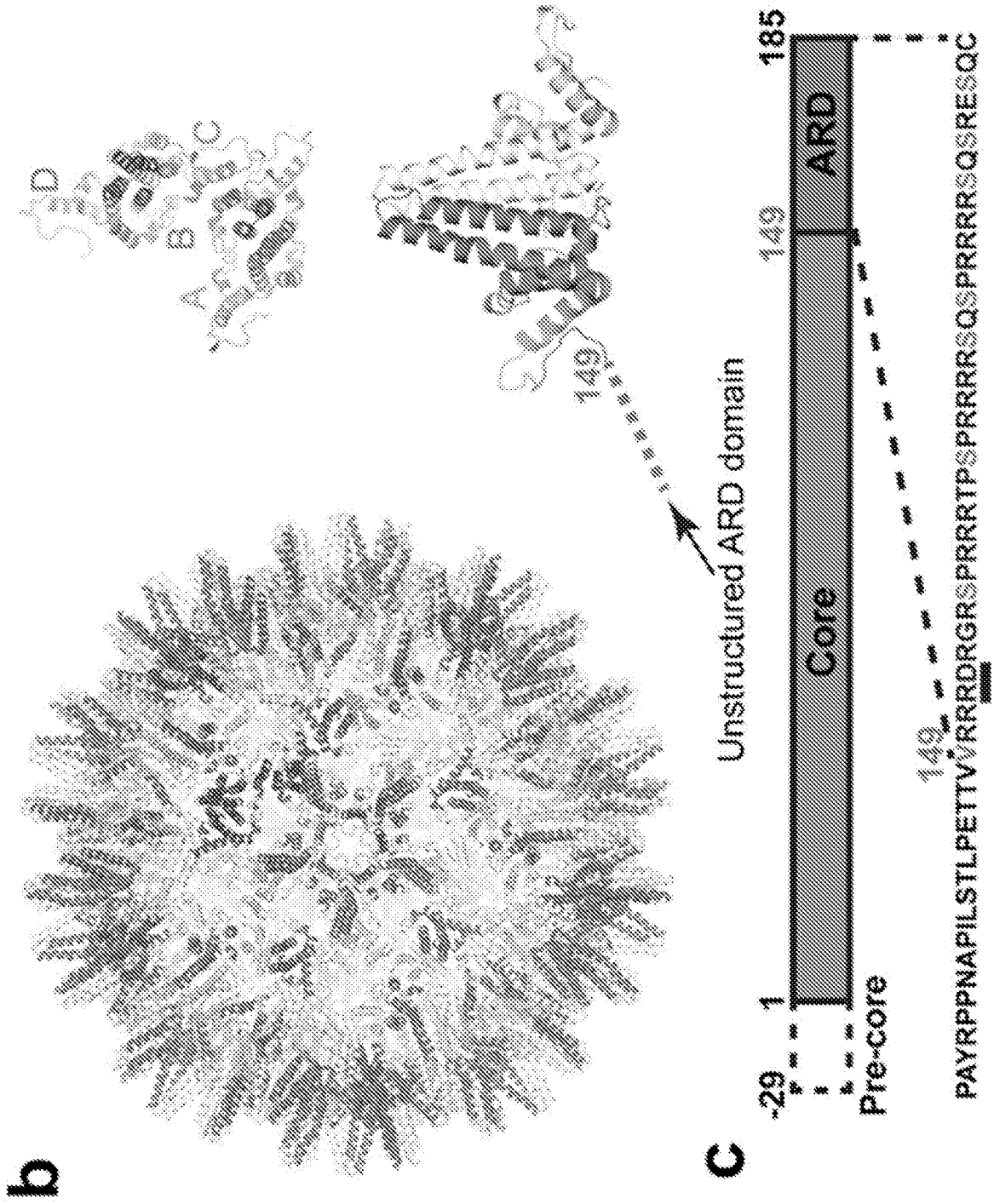

Figure 2

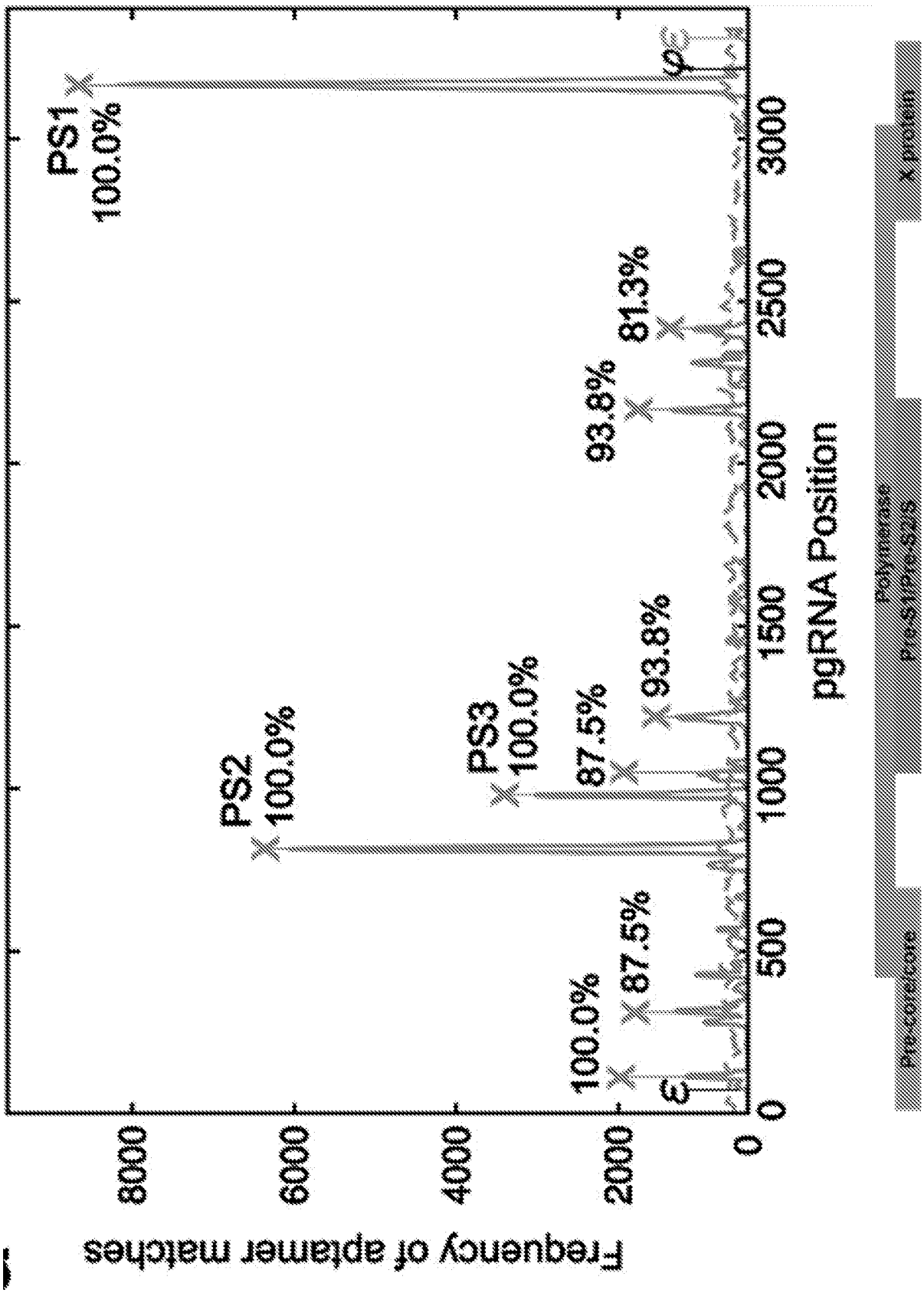
PS1
100.0%
PS2
100.0%
PS3
100.0%
100.0%
87.5%
93.8%
87.5%
93.8%
81.3%
100.0%
ε
ε'
0
500
1000
1500
2000
2500
3000
2000
4000
6000
8000
pgRNA Position
Frequency of aptamer matches
Pre-core/core
Polymerase
Pre-S1/Pre-S2/S
X protein

Figure 2 continued

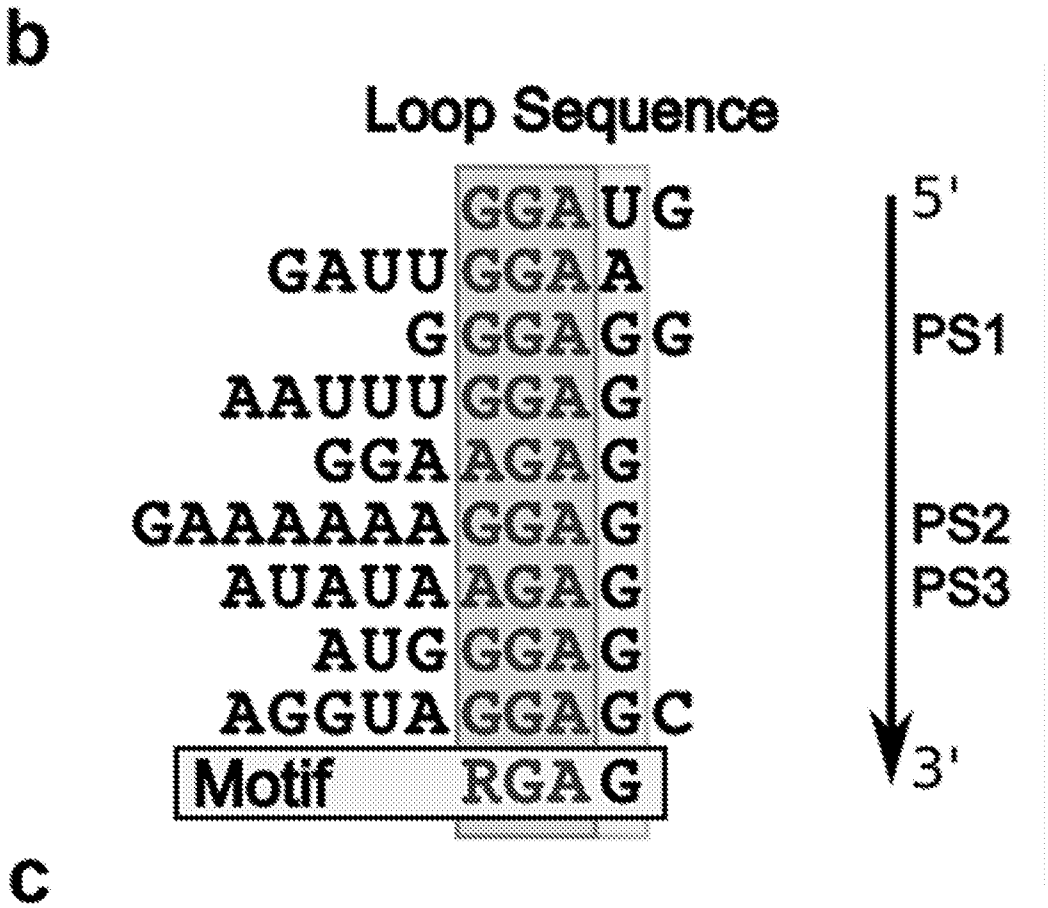

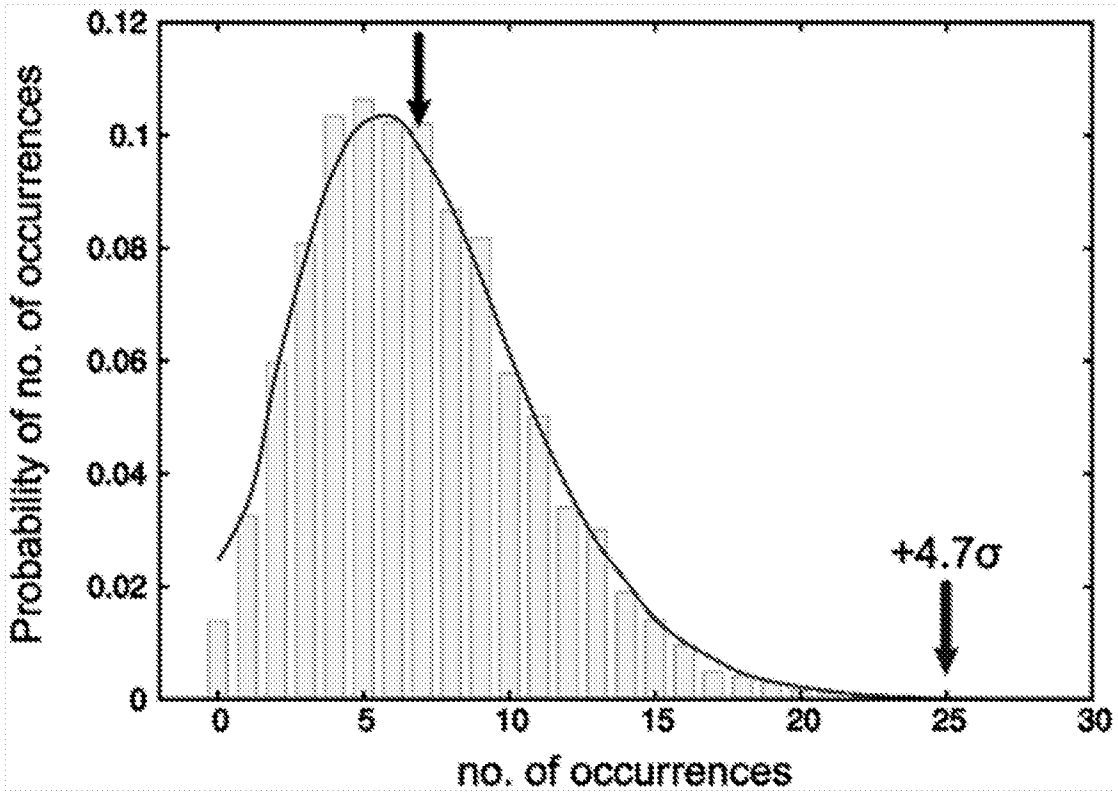

Figure 3

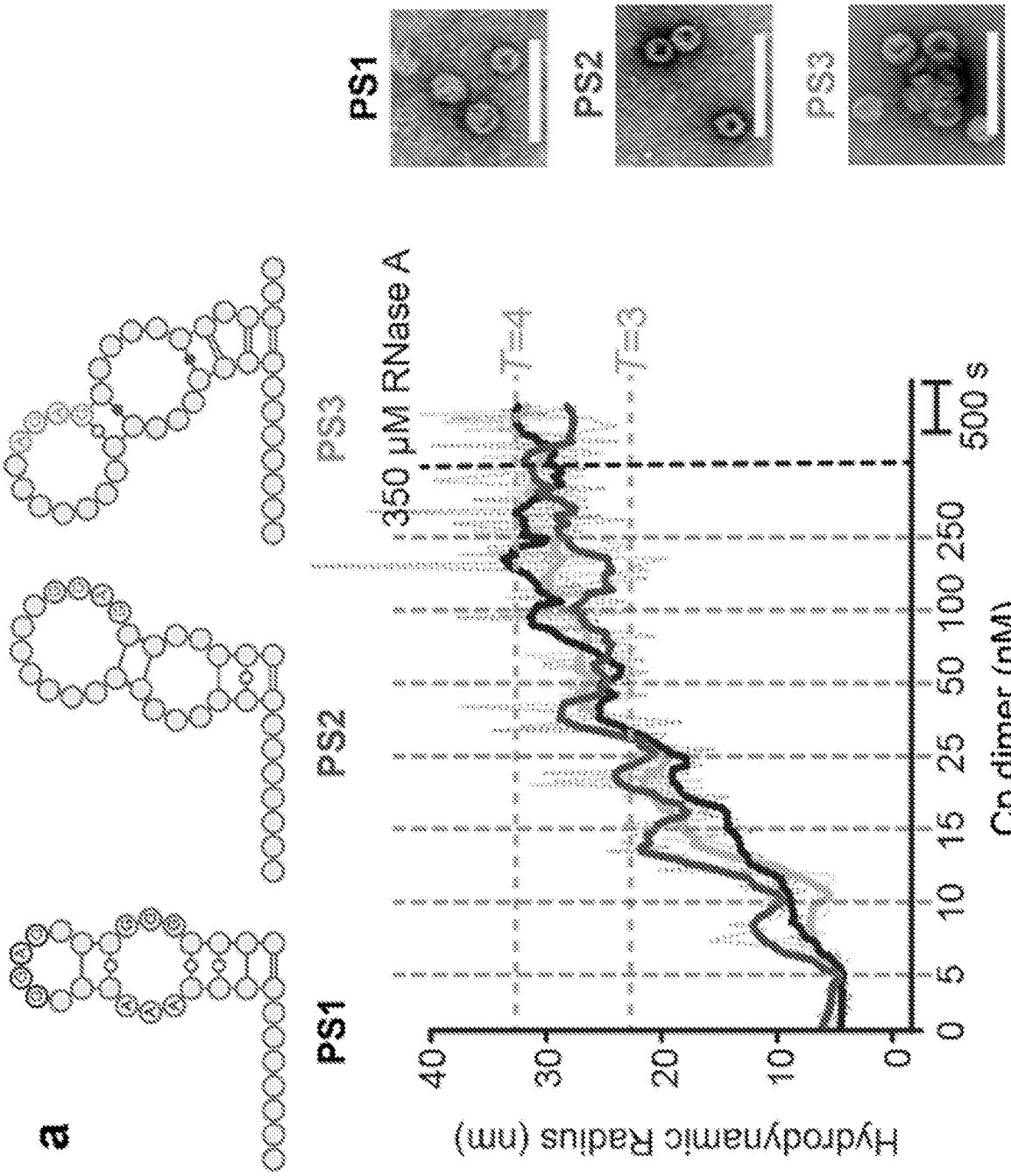
a
PS1
PS2
PS3
350 μM RNase A
T=4
T=3
Hydrodynamic Radius (nm)
40
30
20
10
0
0 5 10 15 25 50 100 250
Cp dimer (nM)
500 s
PS1
PS2
PS3

Figure 3 continued

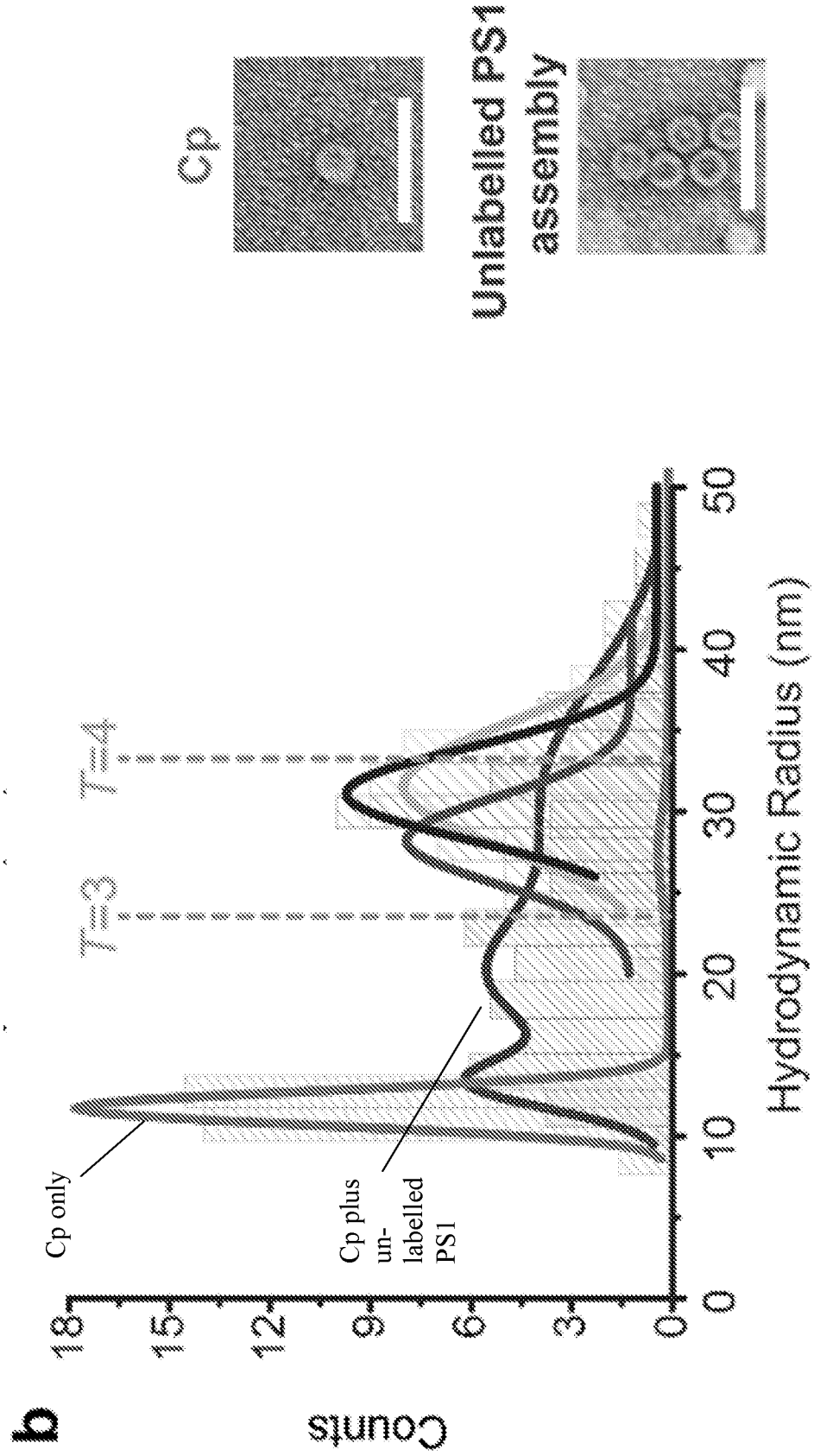

Figure 4

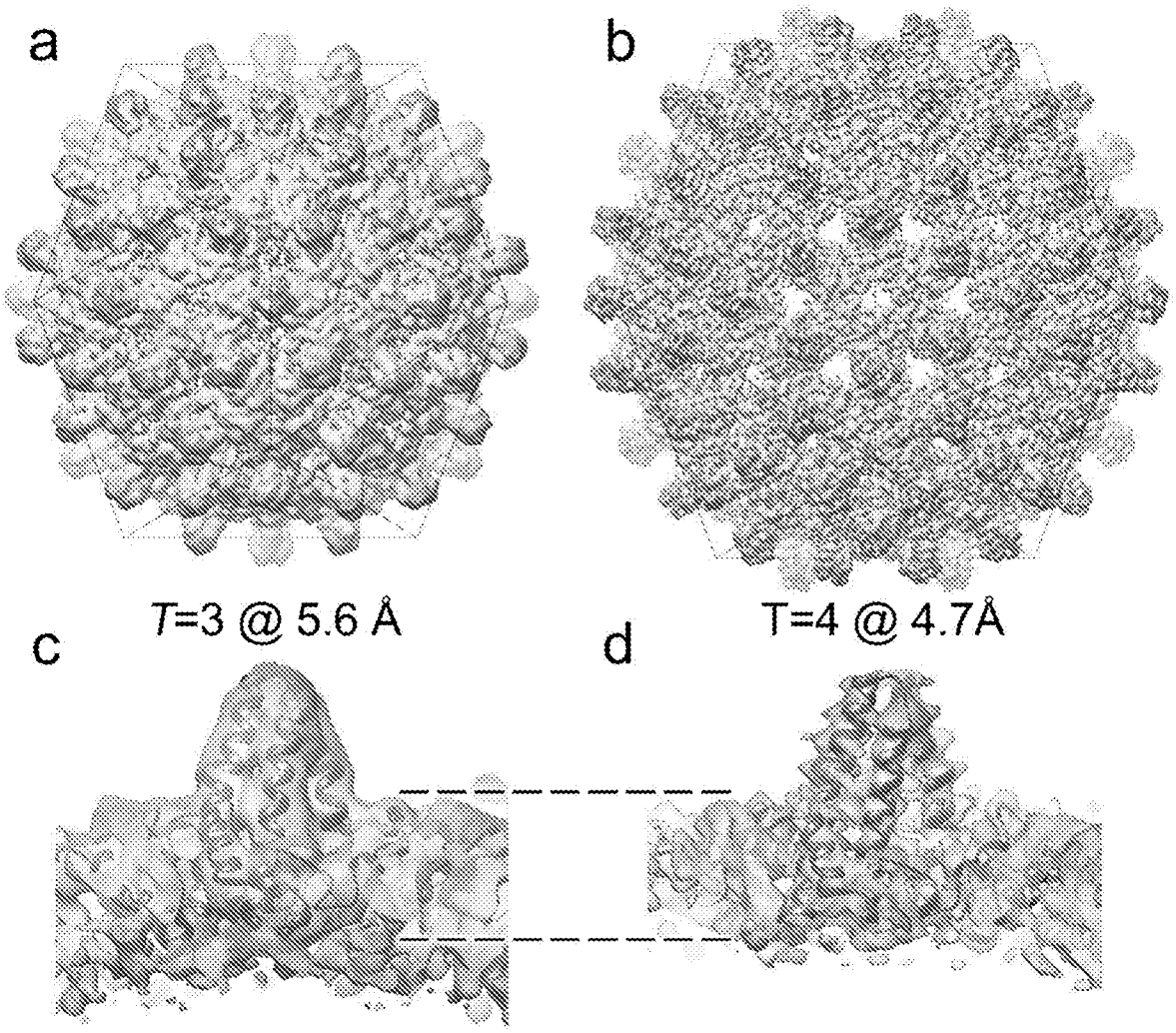

Figure 5

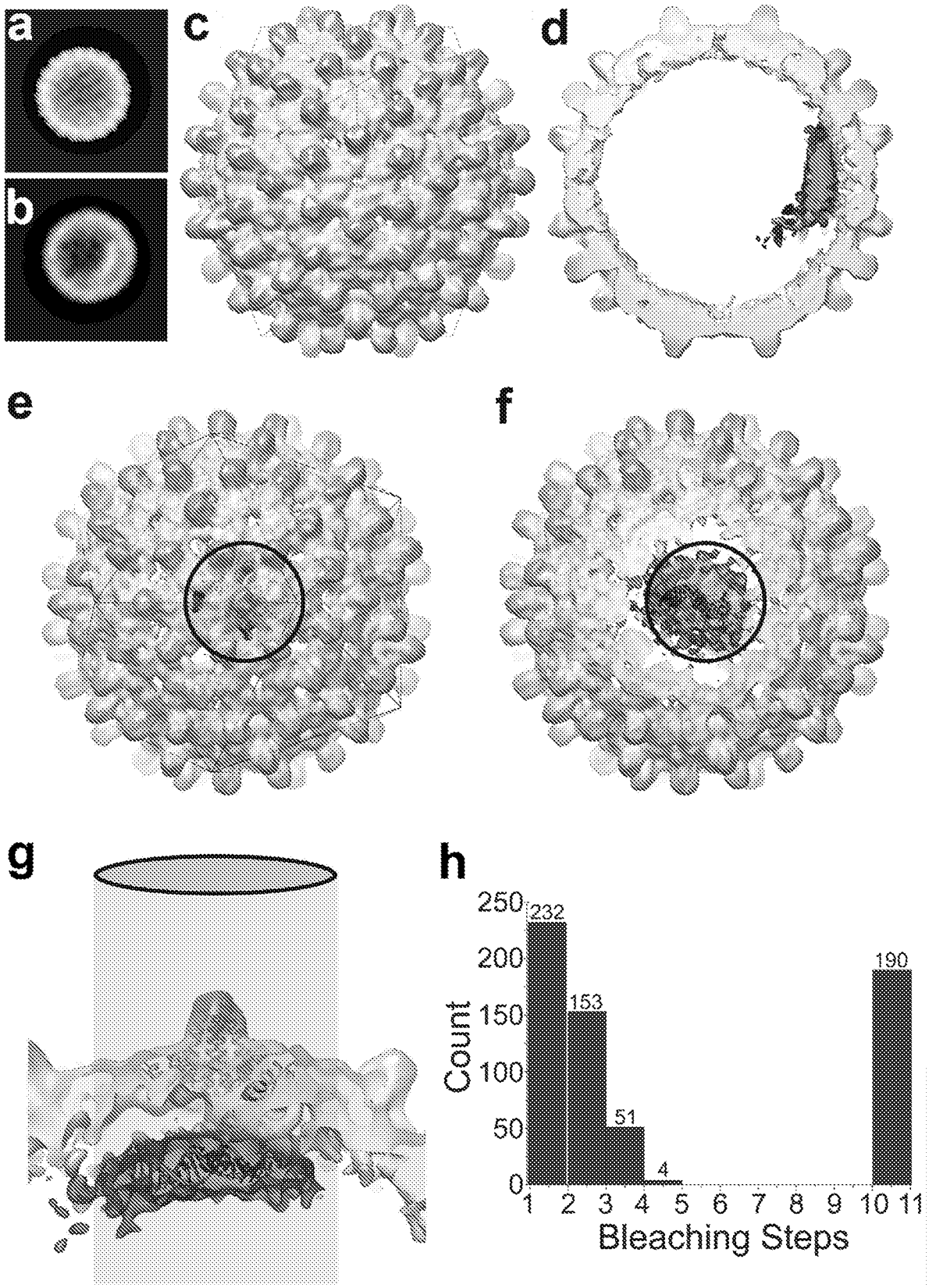
a
b
c
d
e
f
g
h
250
200
150
100
50
0
Count
232
153
51
4
190
1 2 3 4 5 6 7 8 9 10 11
Bleaching Steps

Figure 6

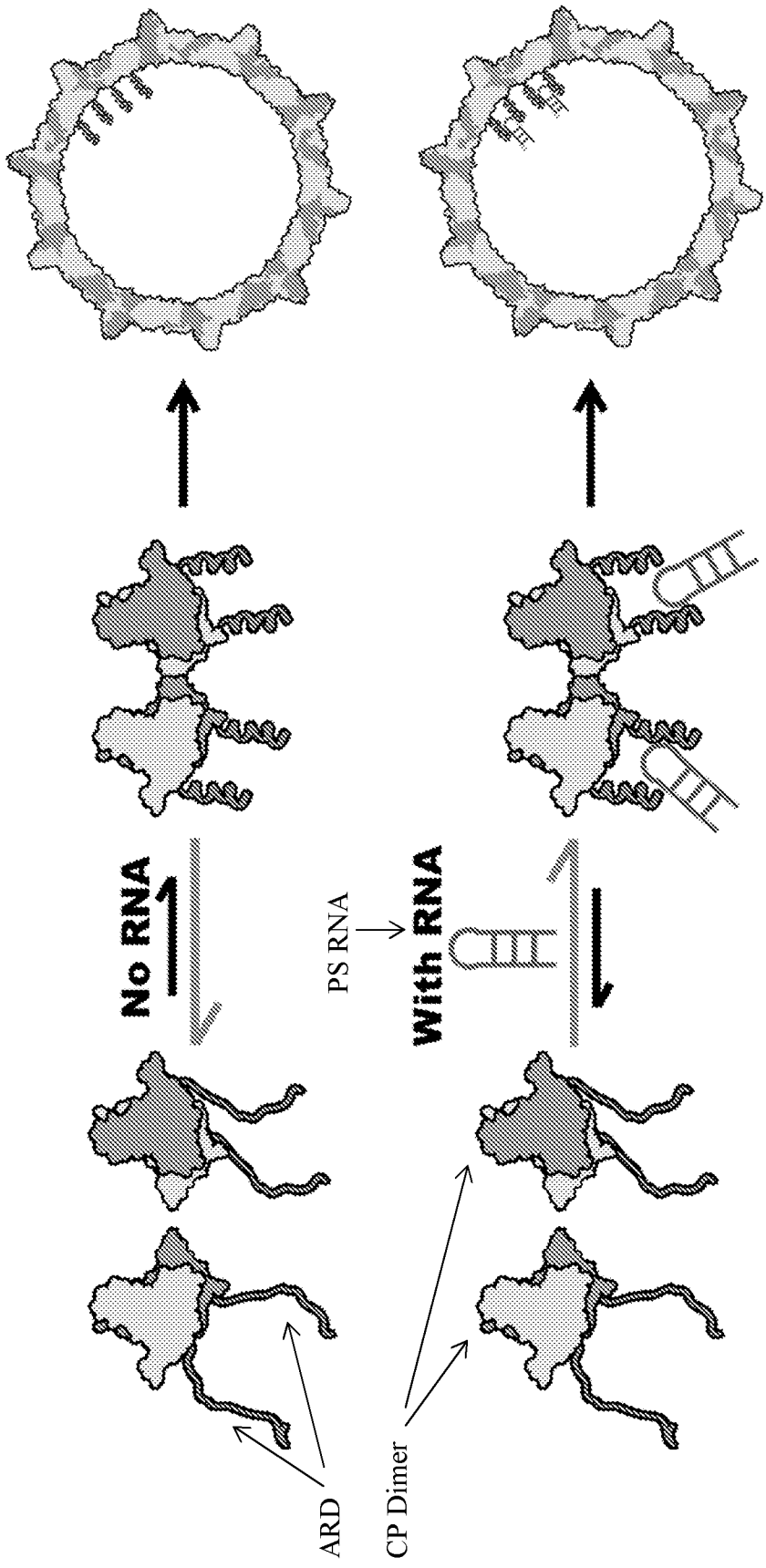

Figure 7

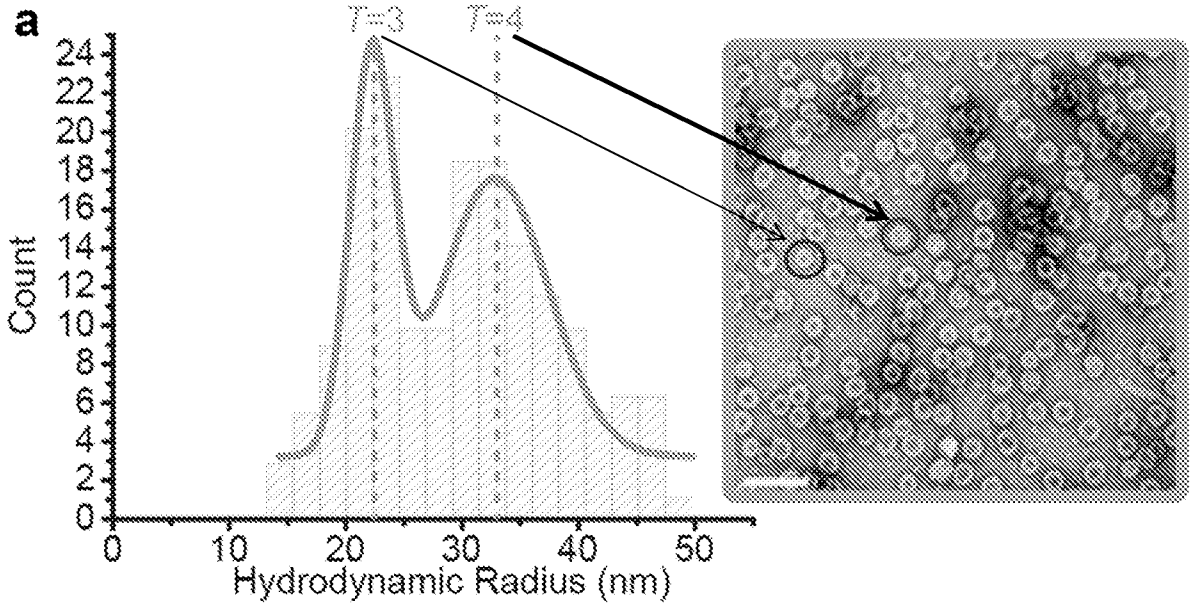
a
T=3
T=4
Count
0
2
4
6
8
10
12
14
16
18
20
22
24
0
10
20
30
40
50
Hydrodynamic Radius (nm)

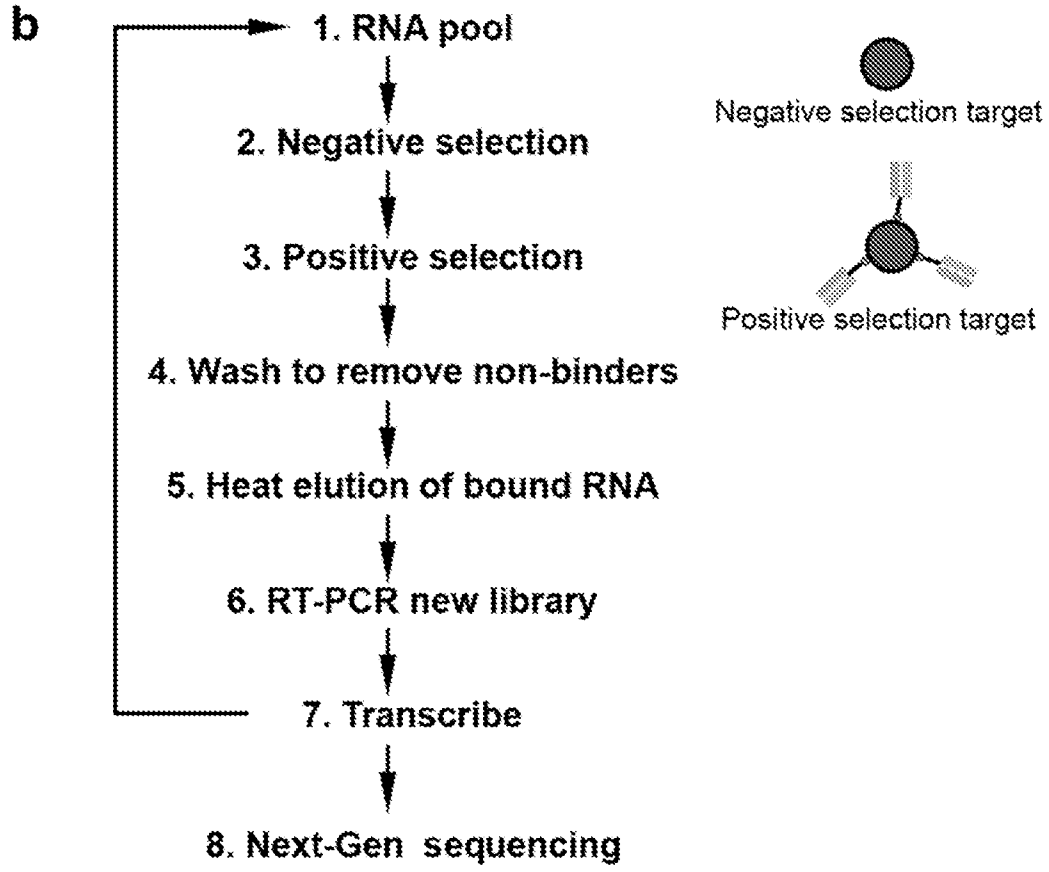
b
1. RNA pool
2. Negative selection
3. Positive selection
4. Wash to remove non-binders
5. Heat elution of bound RNA
6. RT-PCR new library
7. Transcribe
8. Next-Gen sequencing
Negative selection target
Positive selection target

Figure 8

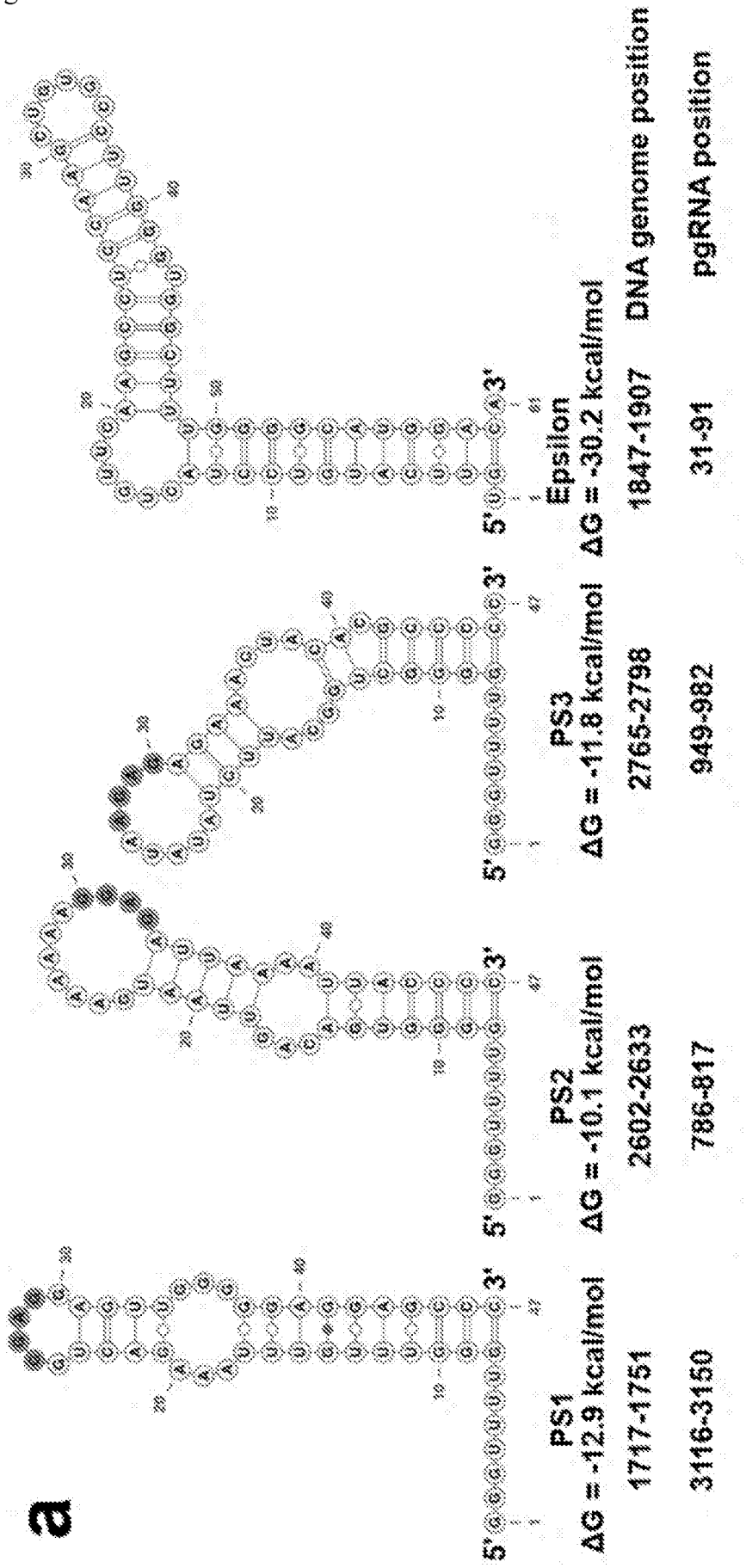
a
PS1
ΔG = -12.9 kcal/mol
1717-1751
3116-3150
PS2
ΔG = -10.1 kcal/mol
2602-2633
786-817
PS3
ΔG = -11.8 kcal/mol
2765-2798
949-982
Epsilon
ΔG = -30.2 kcal/mol
1847-1907
31-91
DNA genome position
pgRNA position

Figure 8 continued

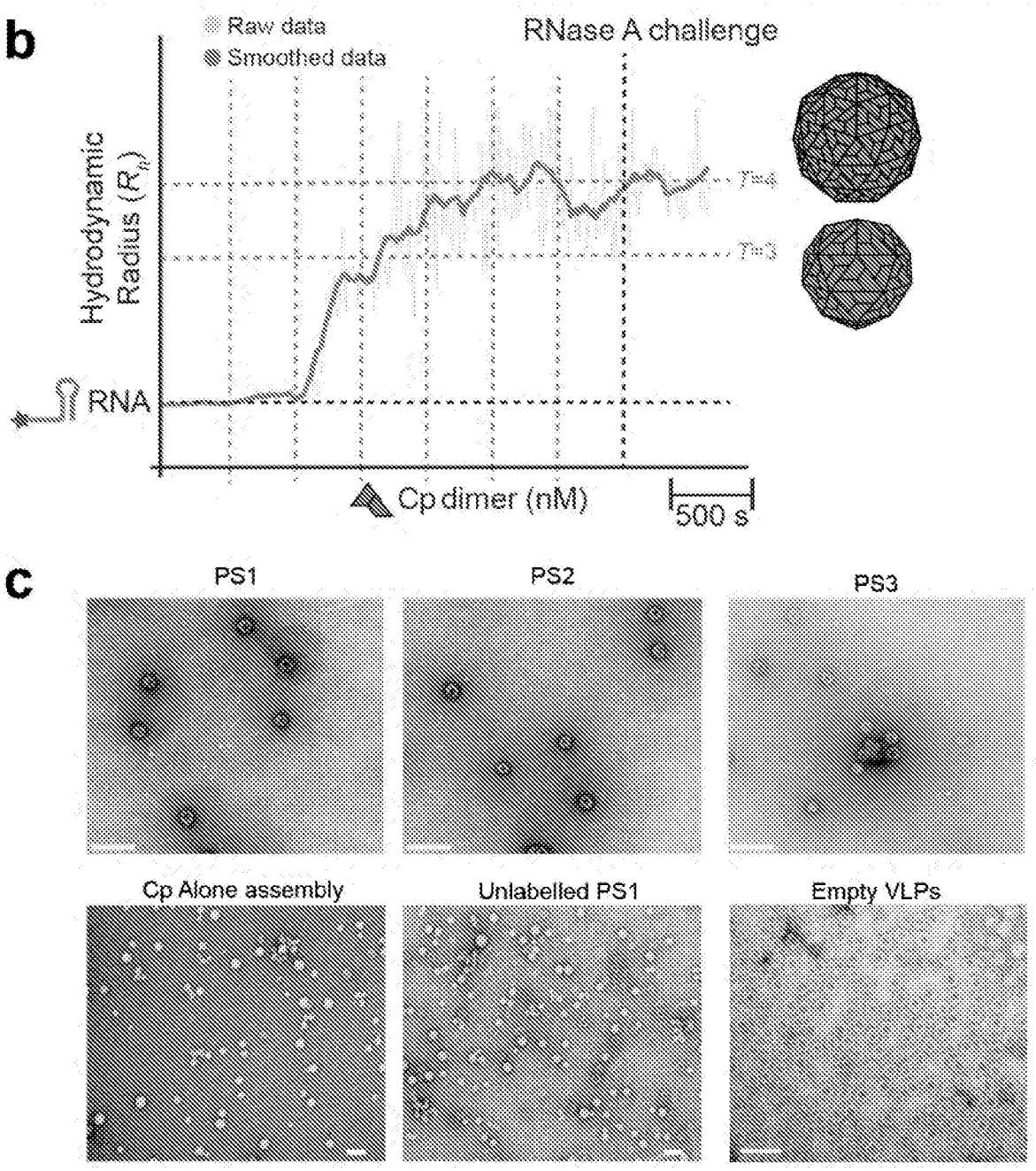

Figure 9

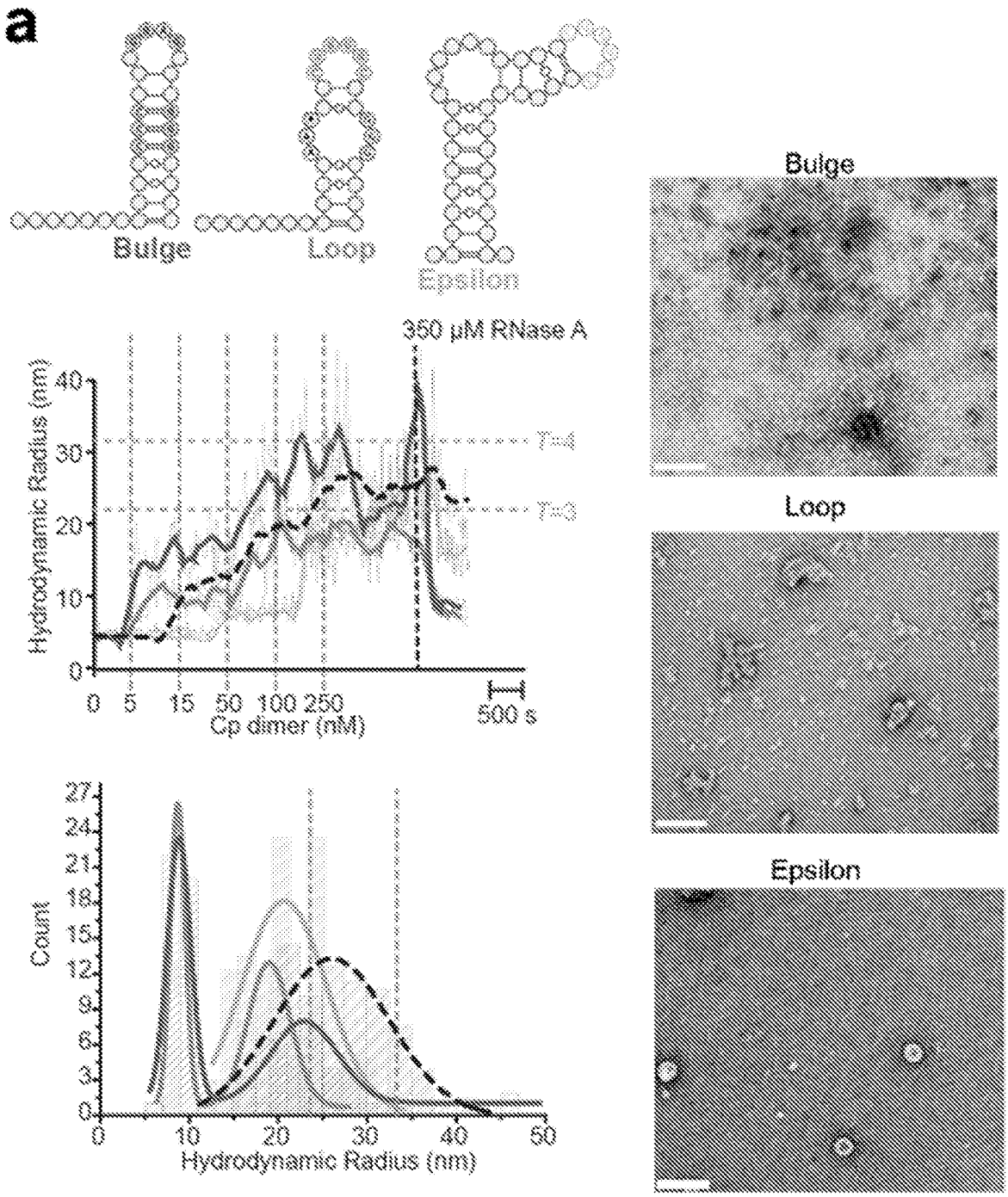
a
Bulge
Loop
Epsilon
350 μM RNase A
Hydrodynamic Radius (nm)
40
30
20
10
0
T=4
T=3
0 5 15 50 100 250
Cp dimer (nM)
500 s
Count
27
24
21
18
15
12
9
6
3
0
0 10 20 30 40 50
Hydrodynamic Radius (nm)
Bulge
Loop
Epsilon

Figure 9 continued

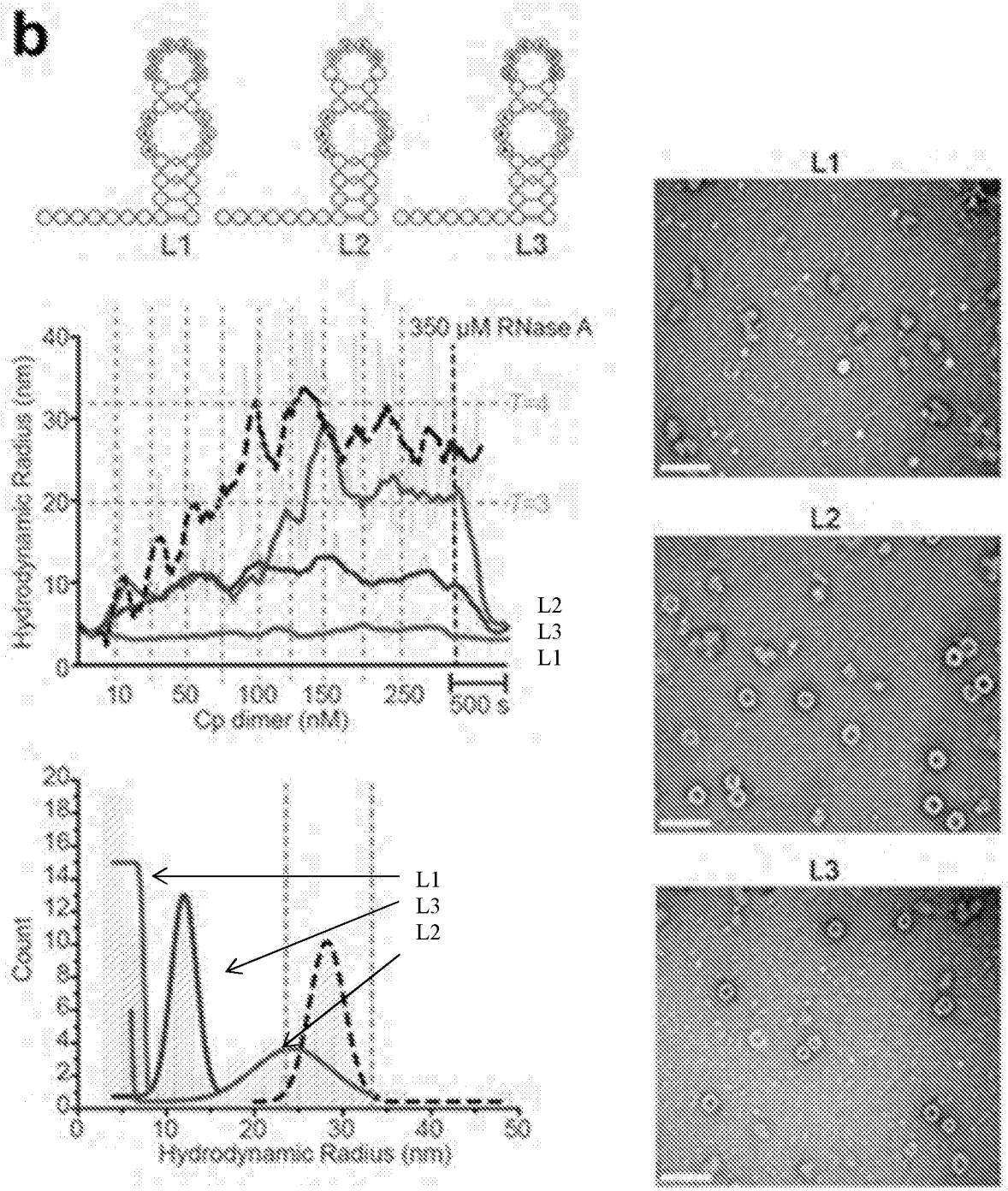

Figure 9 continued

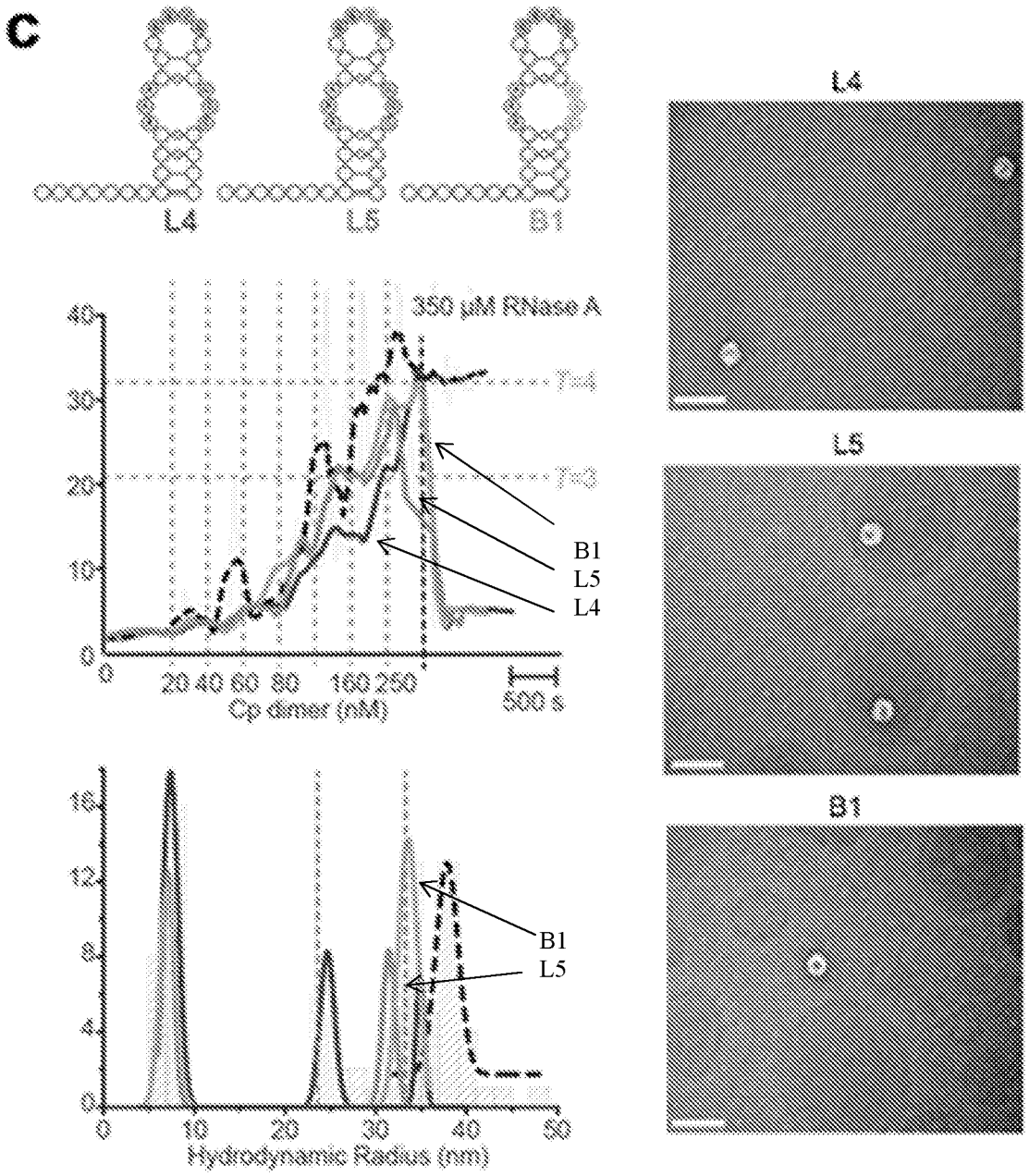

Figure 9 continued

d

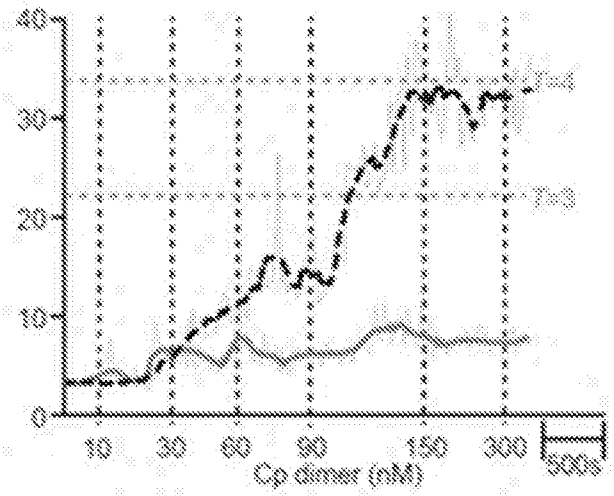

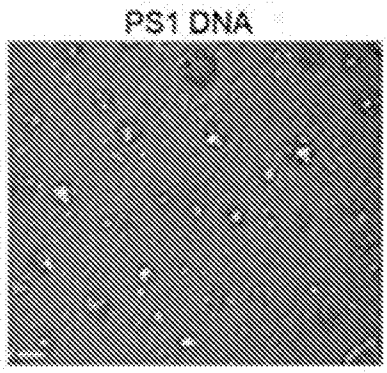

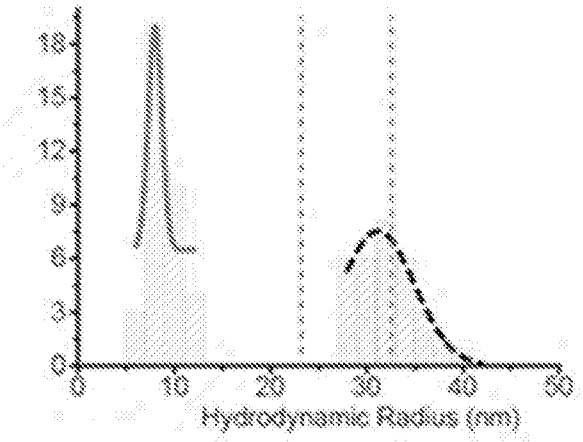

Figure 10

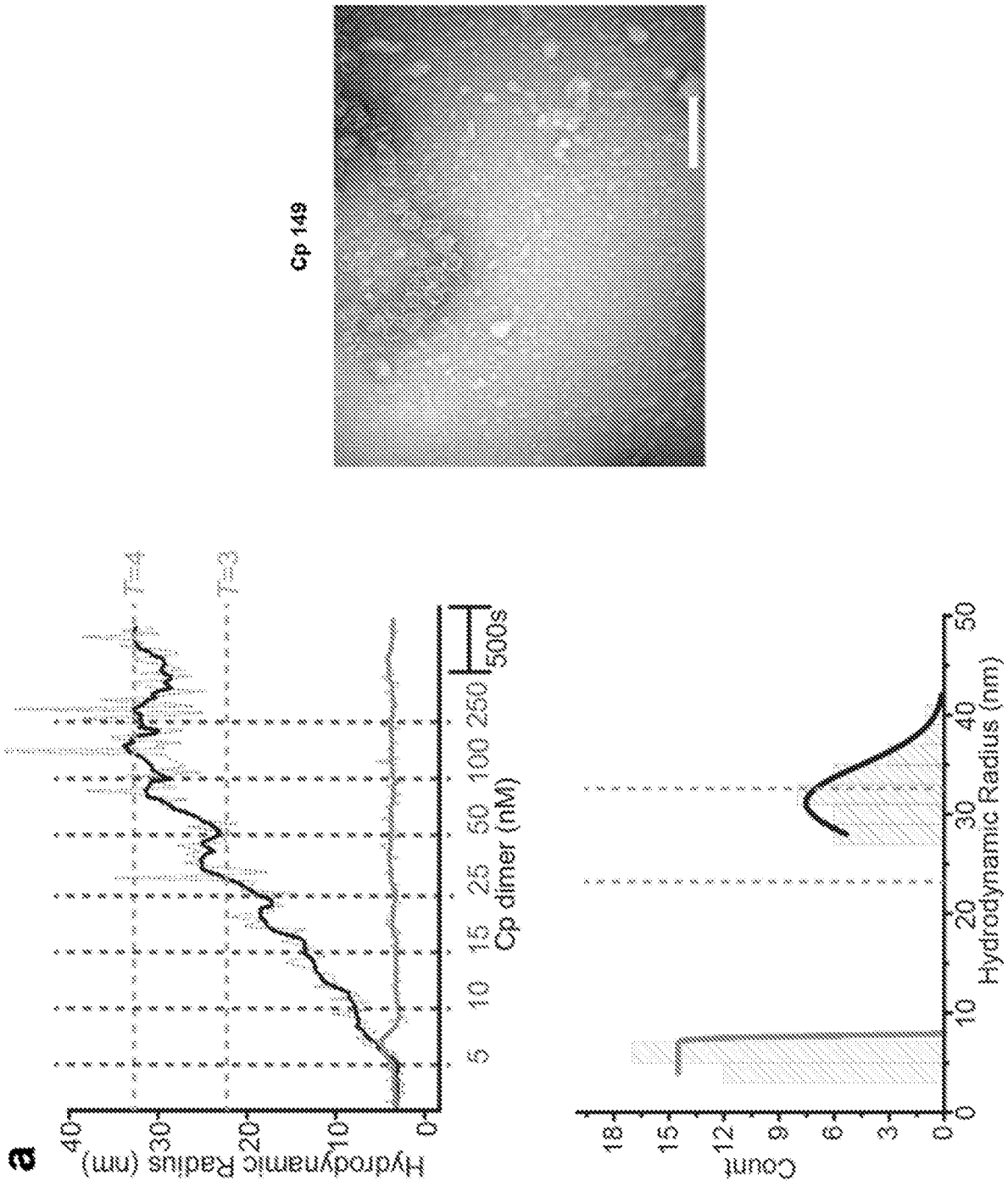
Cp 149
a
Hydrodynamic Radius (nm)
Cp dimer (nM)
T=4
T=3
500s
Count
Hydrodynamic Radius (nm)

Figure 10 continued

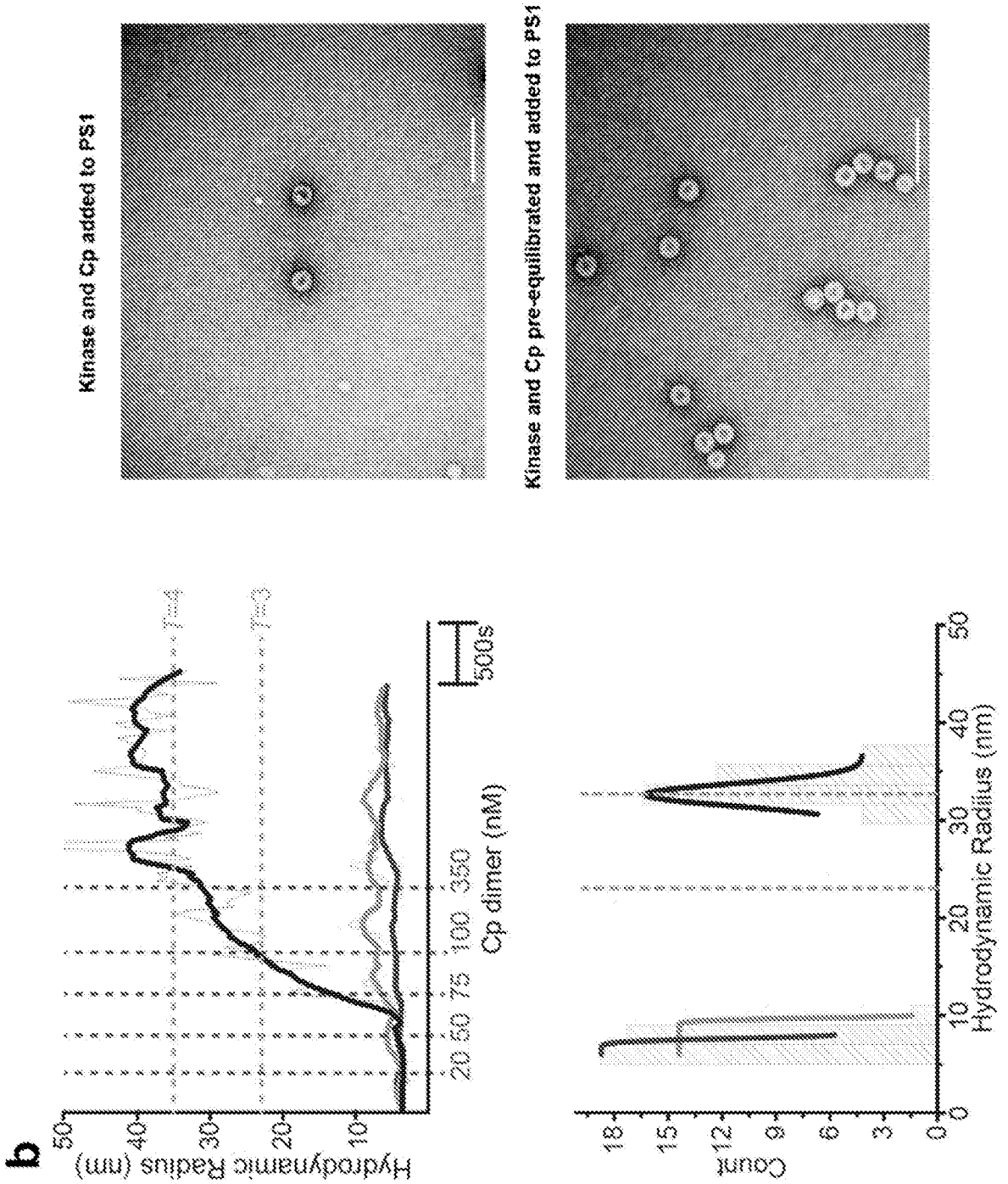

Figure 11

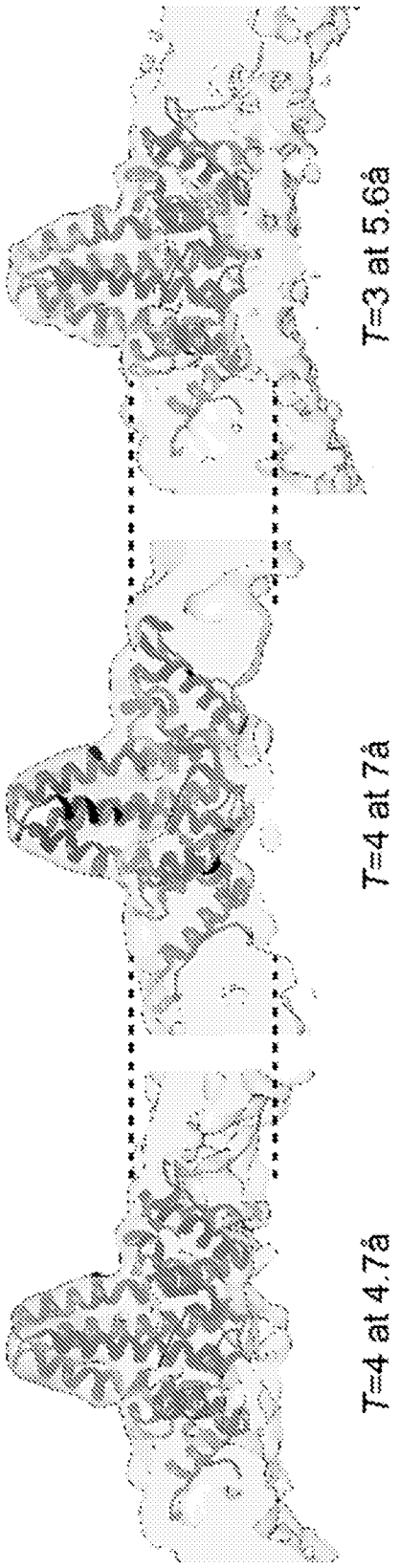

Figure 12

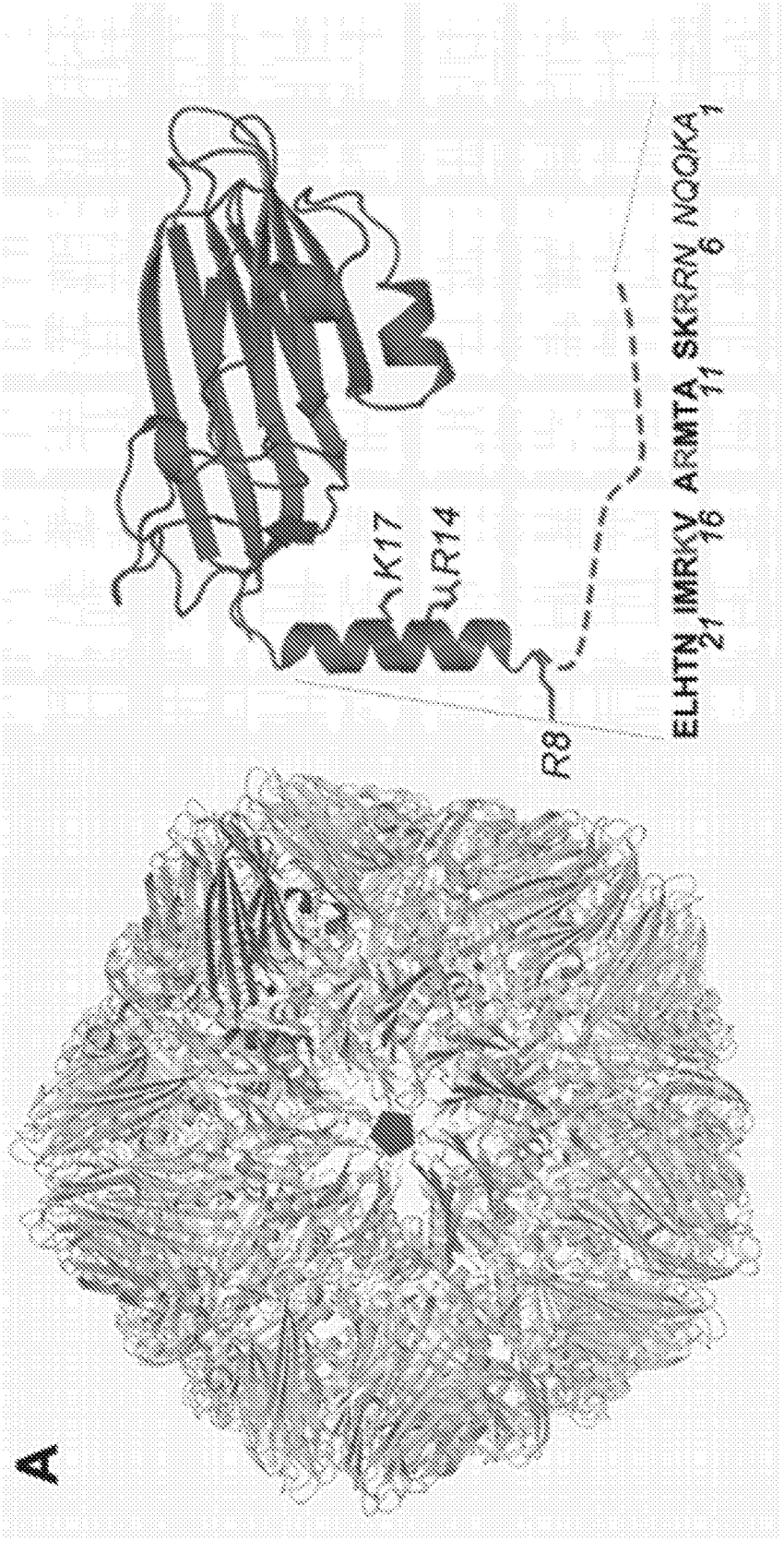

Figure 12 continued

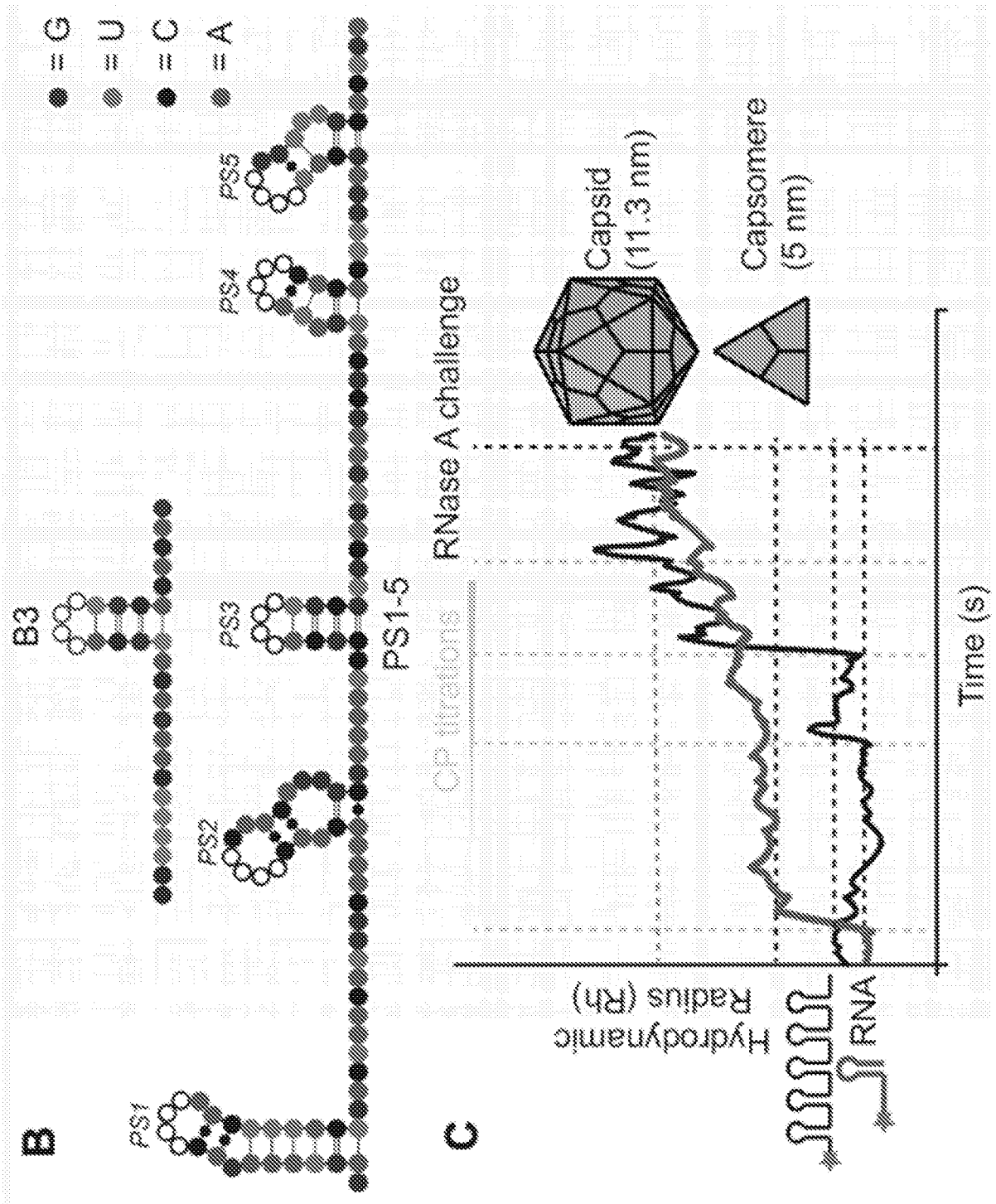

Figure 13

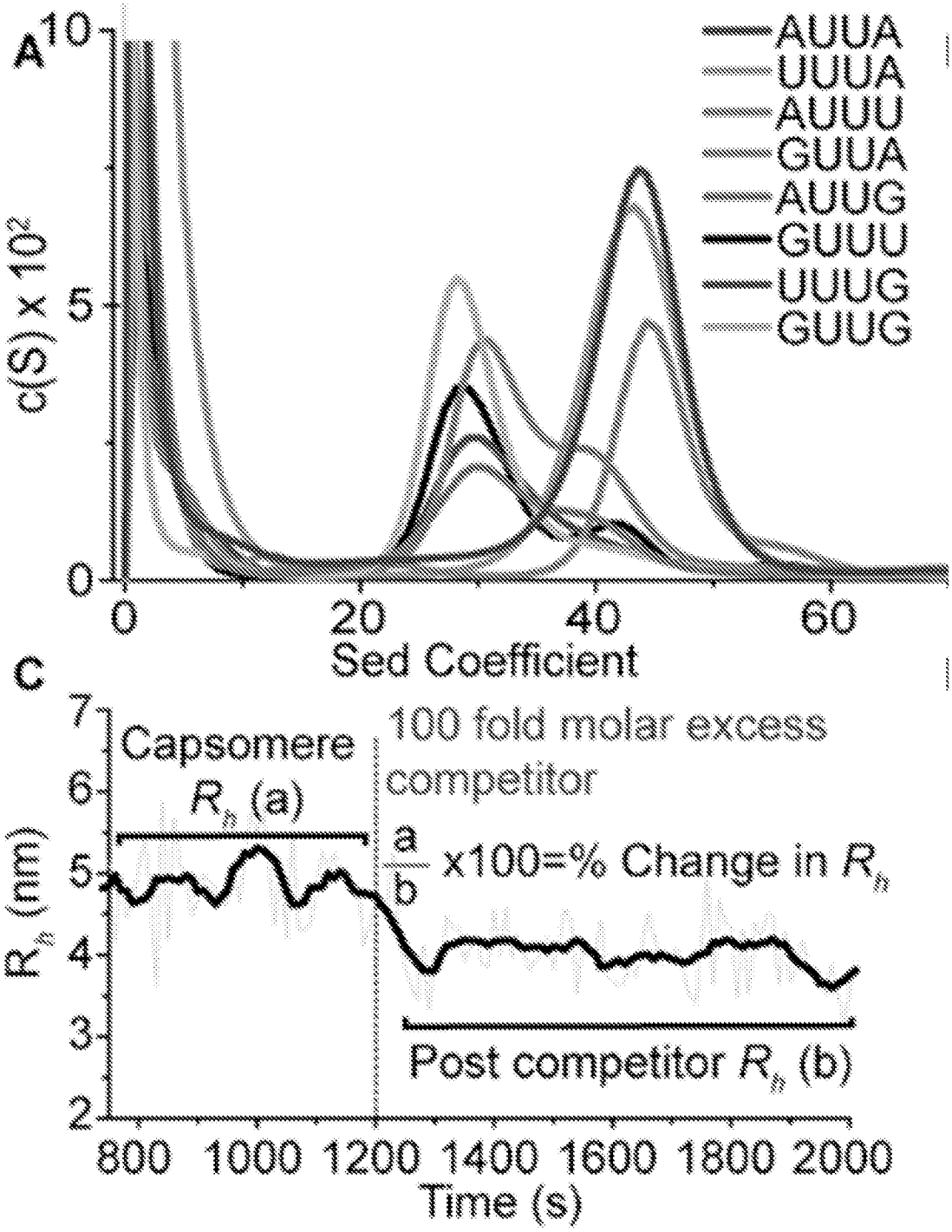
A
c(S) x 10²
10
5
0
0
20
40
60
Sed Coefficient
AUUA
UUUA
AUUU
GUUA
AUUG
GUUU
UUUG
GUUG
C
Rh (nm)
7
6
5
4
3
2
Capsomere
Rh (a)
100 fold molar excess
competitor
a/b x100=% Change in Rh
Post competitor Rh (b)
800
1000
1200
1400
1600
1800
2000
Time (s)

Figure 13 continued

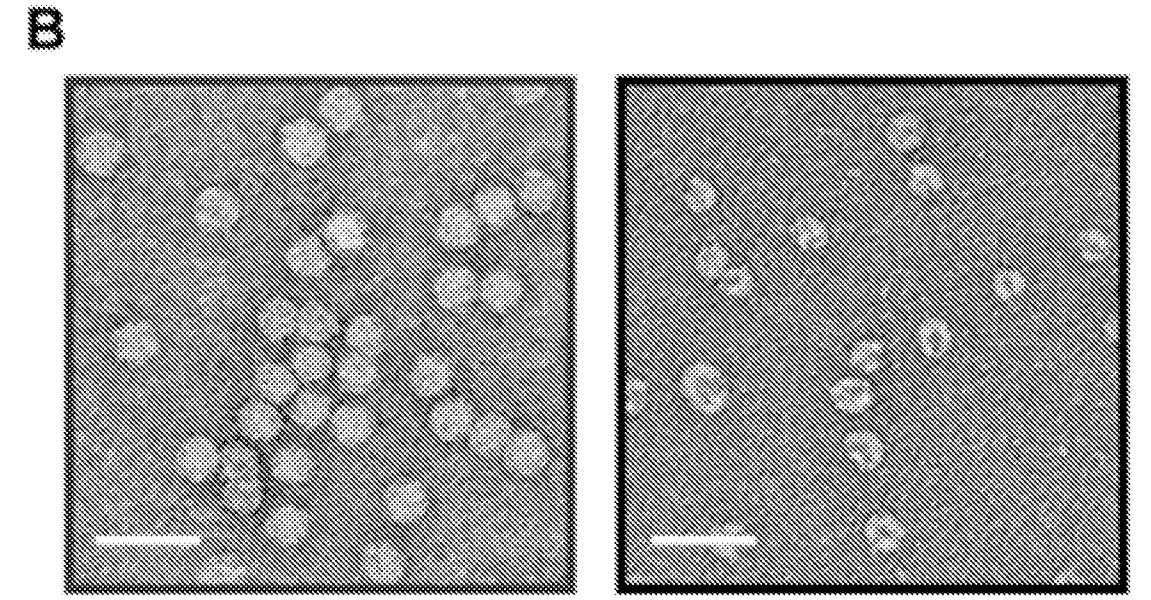

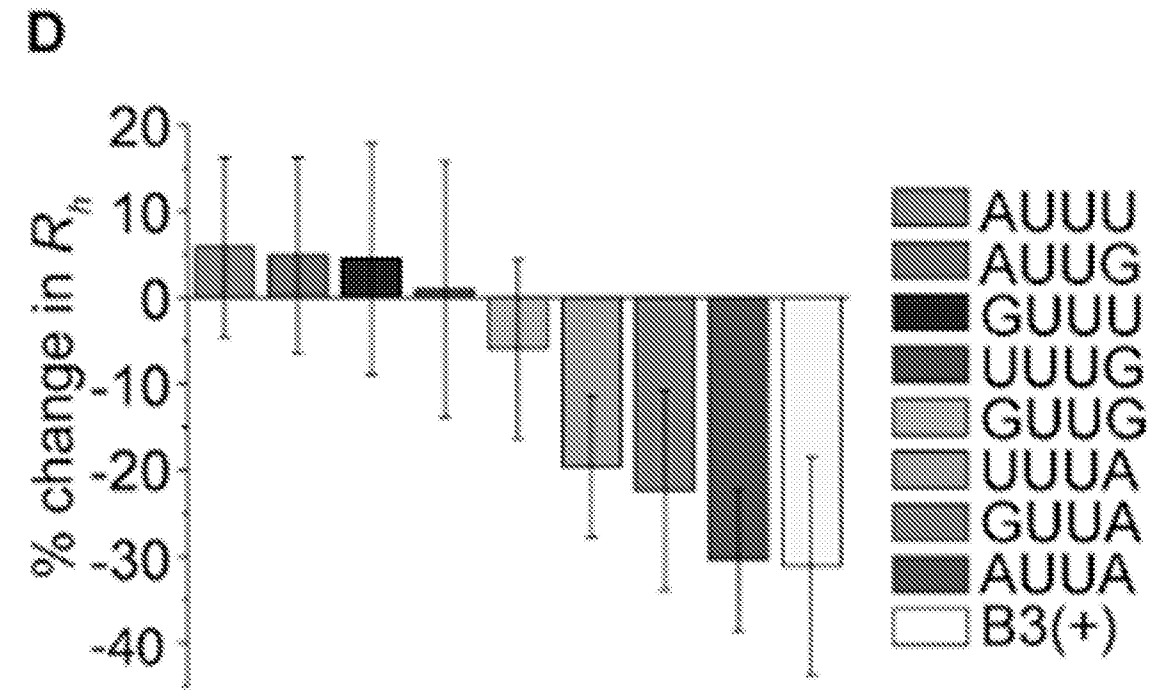

Figure 14

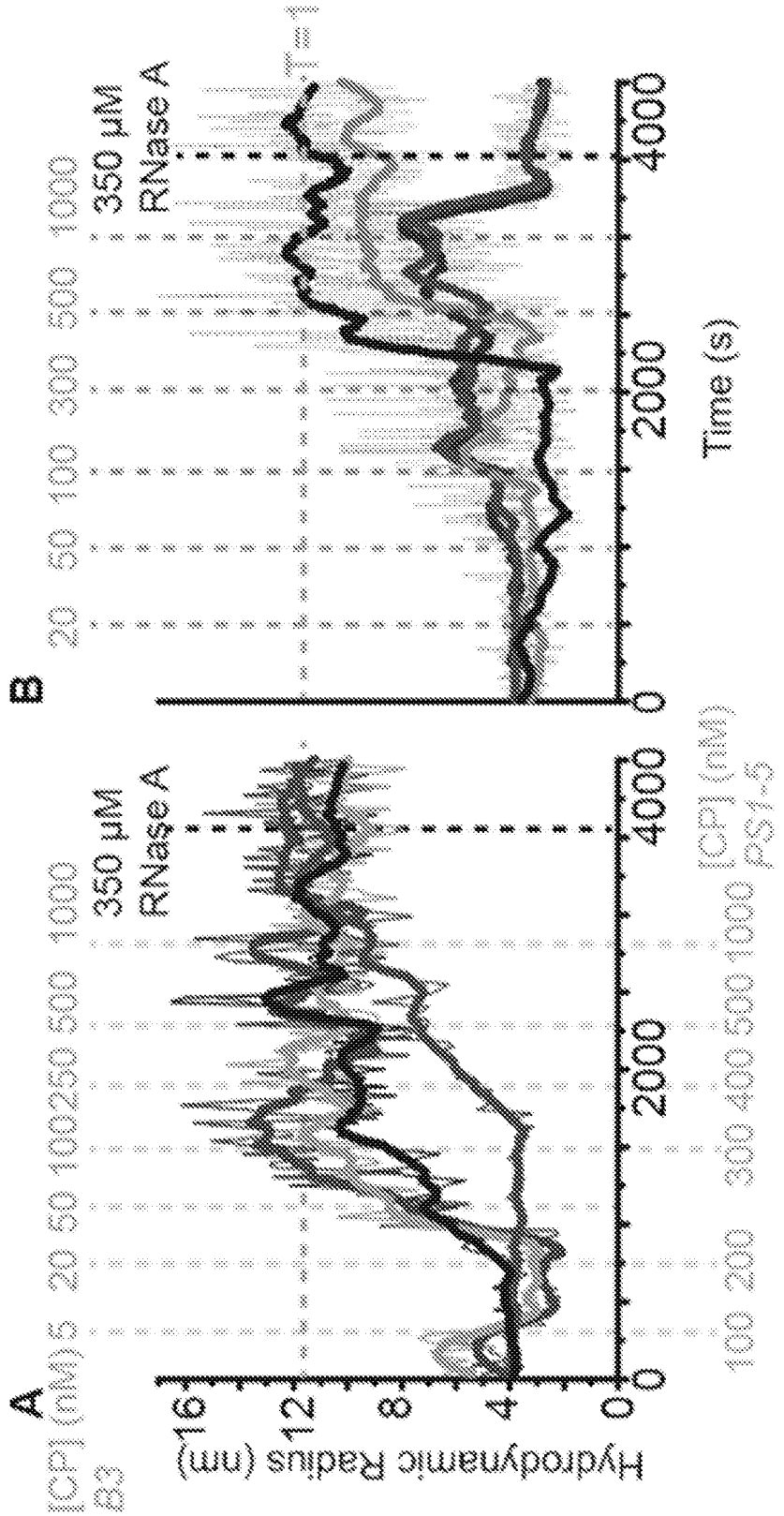
A
B
[CP] (nM) 5 20 50 100 250 500 1000
B3
350 µM
RNase A
Hydrodynamic Radius (nm)
16
12
8
4
0
2000
4000
Time (s)
T=1
20 50 100 300 500 1000
100 200 300 400 500 1000
[CP] (nM)
PS1-5

Figure 15

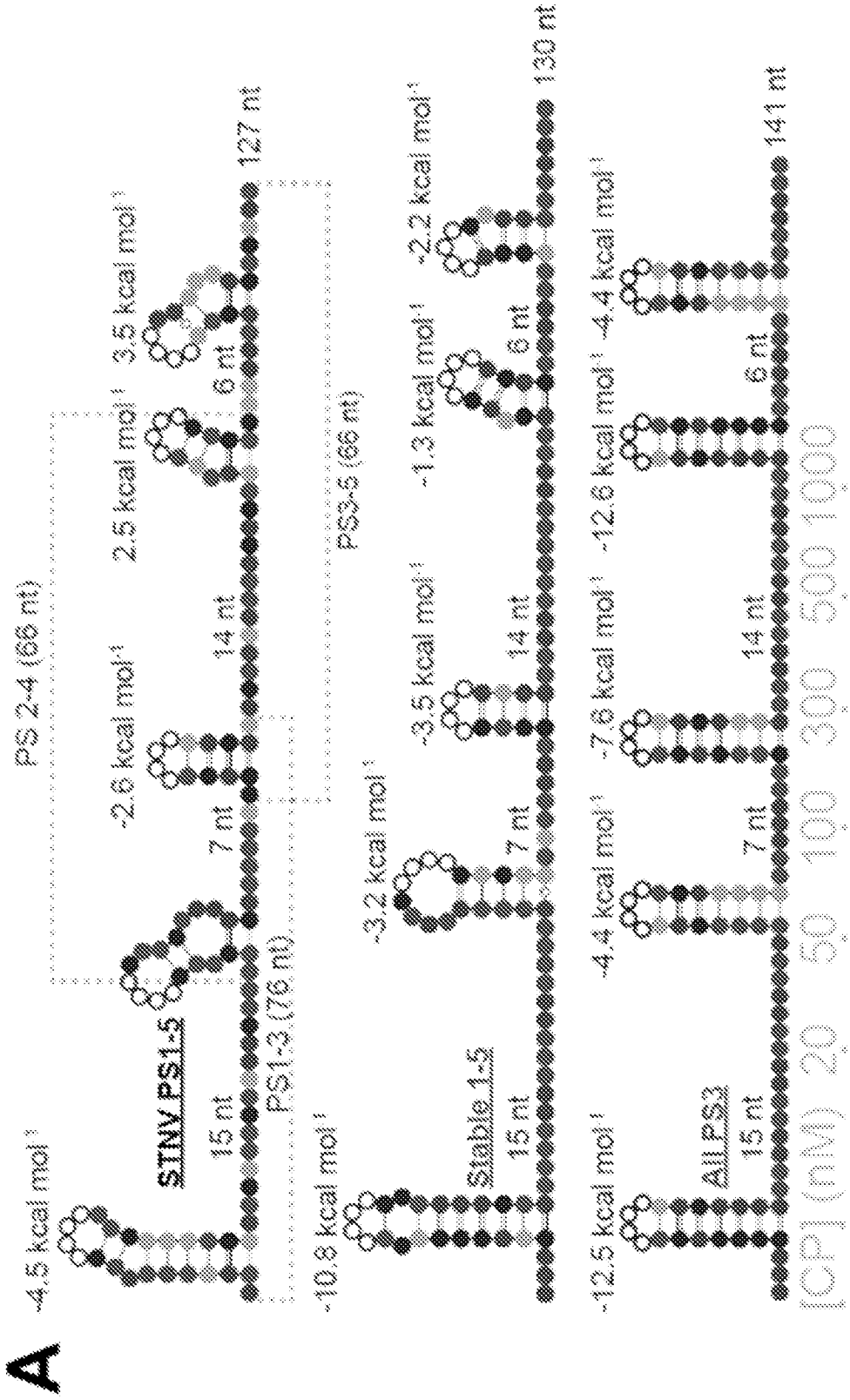
A
-4.5 kcal mol⁻¹
STNV PS1-5
15 nt
-2.6 kcal mol⁻¹
7 nt
2.5 kcal mol⁻¹
14 nt
3.5 kcal mol⁻¹
6 nt
127 nt
PS 2-4 (66 nt)
PS1-3 (76 nt)
PS3-5 (66 nt)
-10.8 kcal mol⁻¹
Stable 1-5
15 nt
-3.2 kcal mol⁻¹
7 nt
-3.5 kcal mol⁻¹
14 nt
-1.3 kcal mol⁻¹
6 nt
-2.2 kcal mol⁻¹
130 nt
-12.5 kcal mol⁻¹
AllPS3
15 nt
-4.4 kcal mol⁻¹
7 nt
-7.6 kcal mol⁻¹
14 nt
-12.6 kcal mol⁻¹
6 nt
-4.4 kcal mol⁻¹
141 nt
[CPI (nM) 20 50 100 300 500 1000

Figure 15 continued

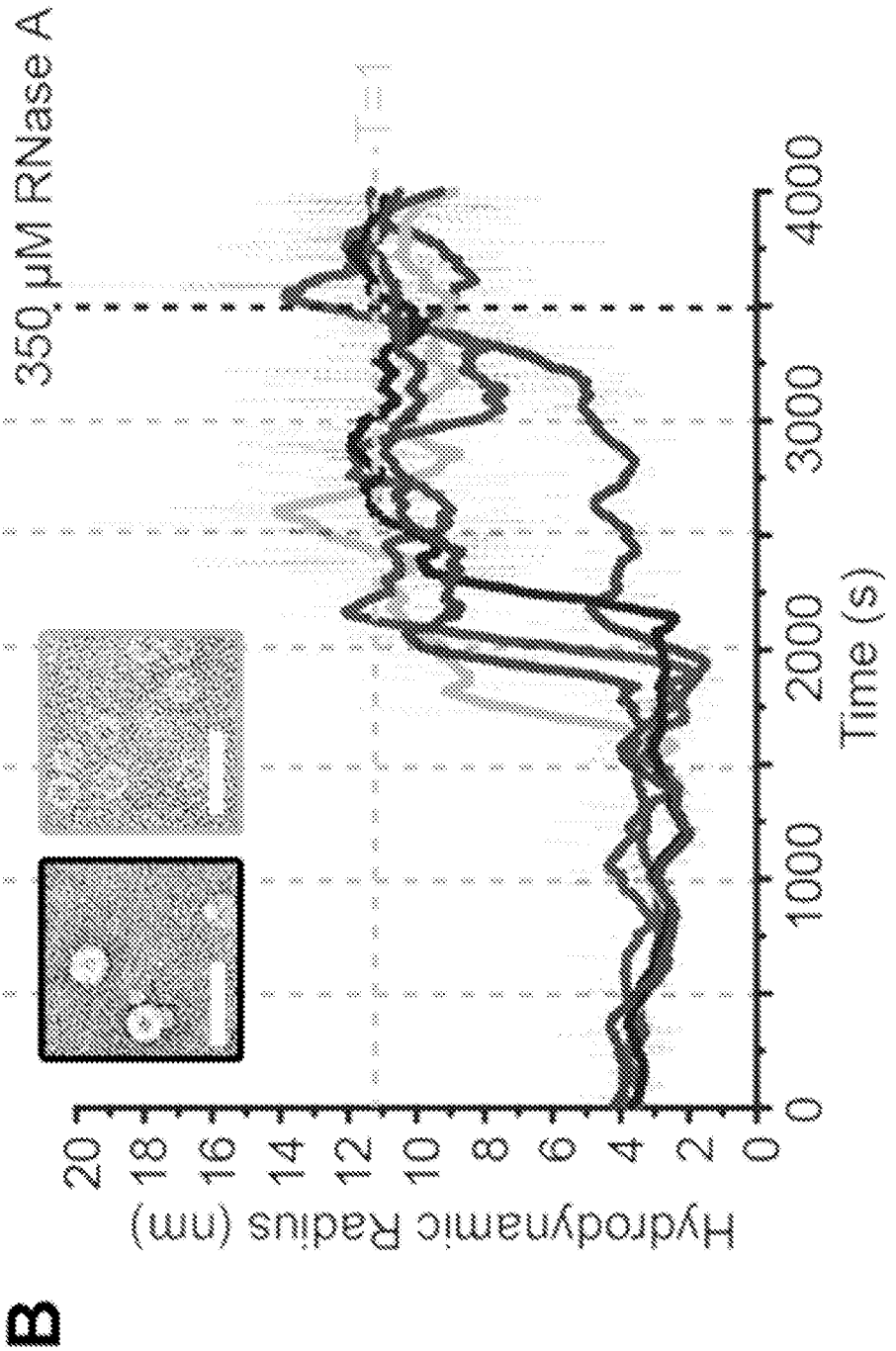

Figure 16

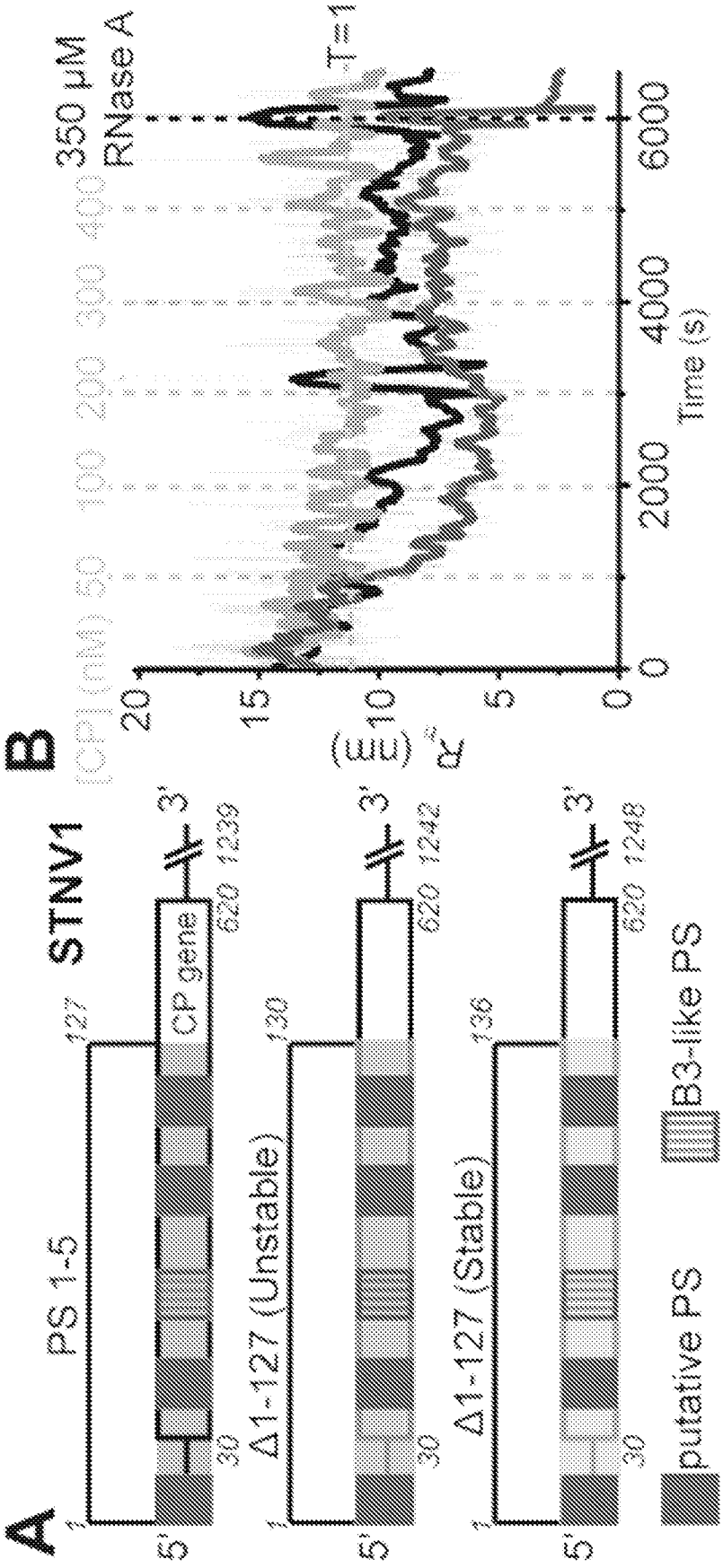
A
STNV1
PS 1-5
CP gene
Δ1-127 (Unstable)
Δ1-127 (Stable)
putative PS
B3-like PS
B
350 μM RNase A
[CP] (nM) 50 100 200 300 400
T=1
R_H (nm)
Time (s)

Figure 16 continued

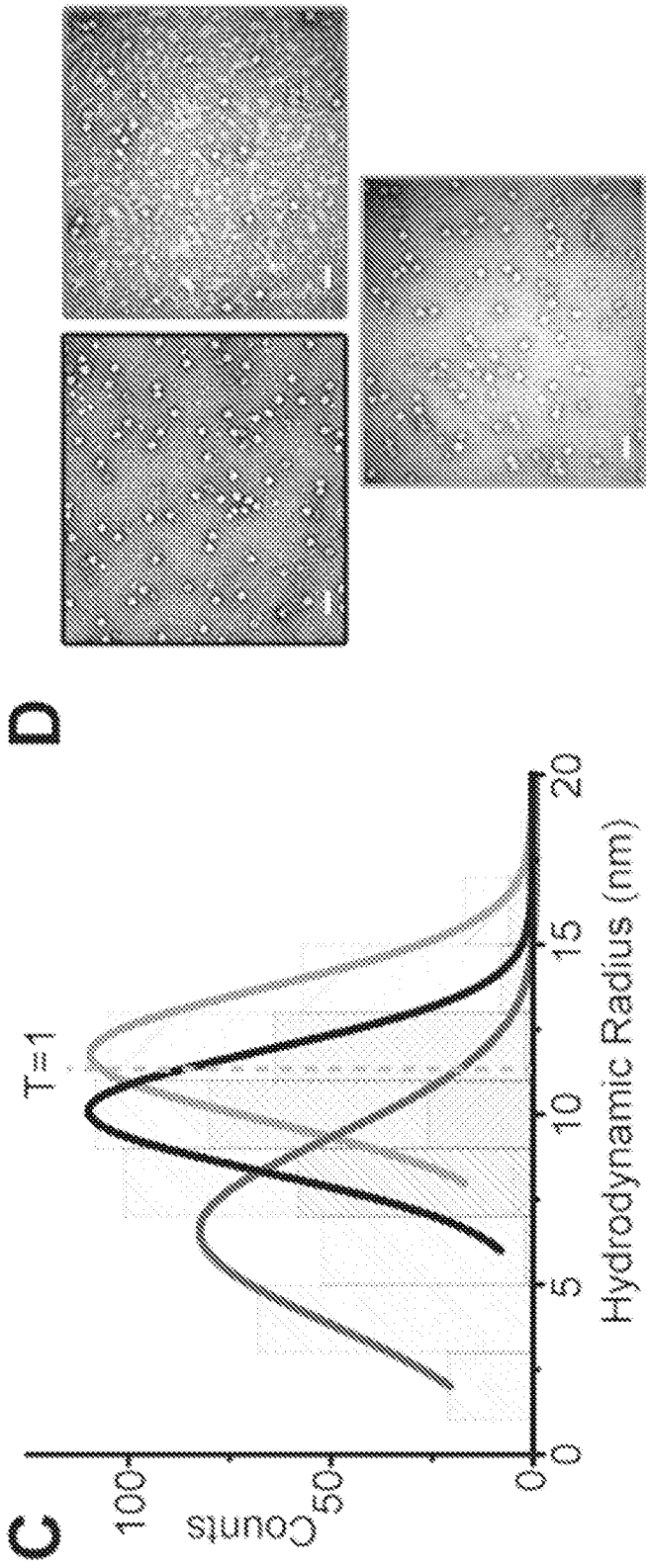

Figure 17

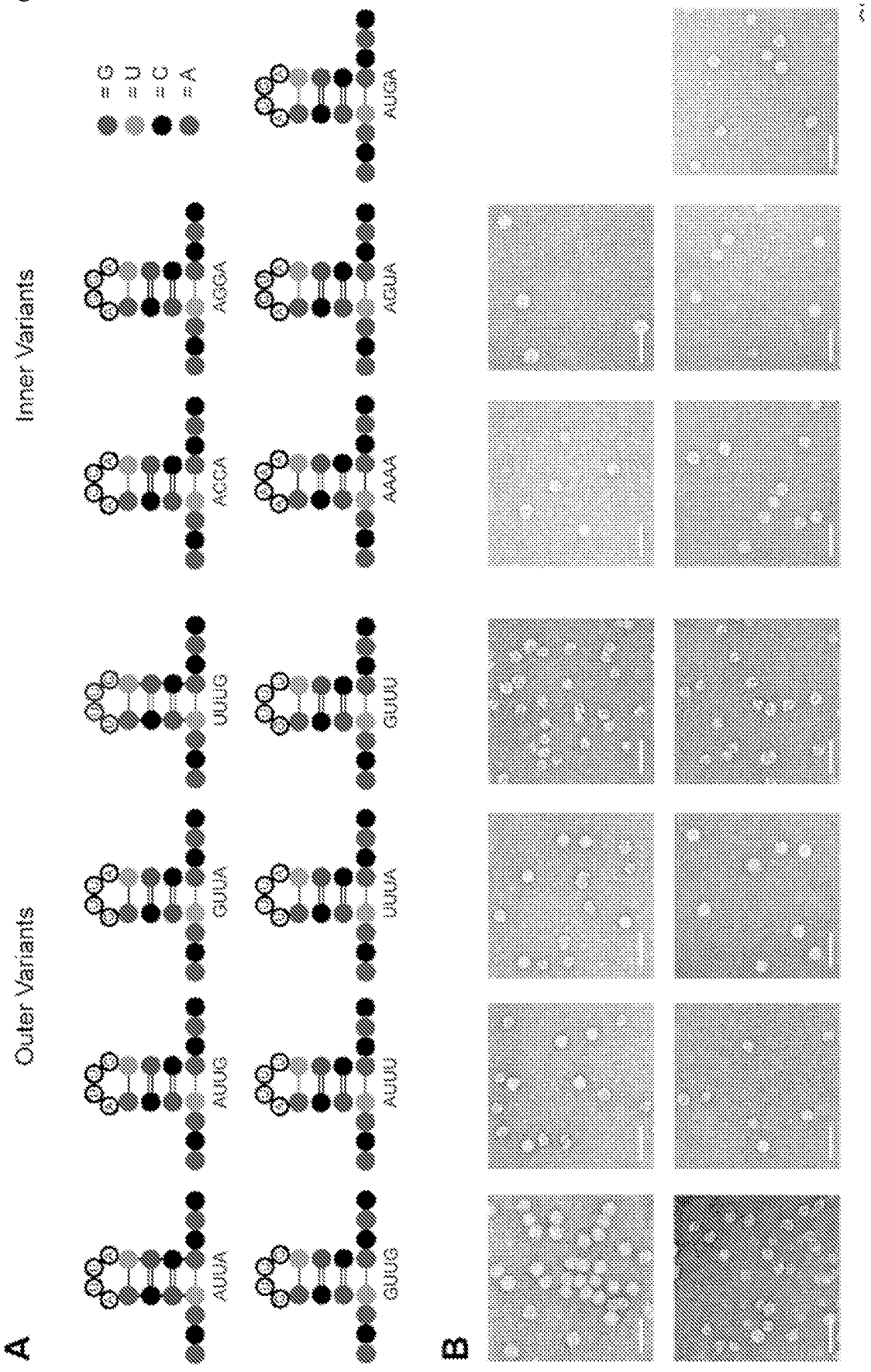
A
Outer Variants
Inner Variants
G = U = C = A
AUUA
AUUG
AUUU
AUUC
GUUA
GUUG
GUUU
GUUC
UUUA
UUUG
UUUU
UUUC
AGGA
AGGG
AGGU
AGGC
AGUA
AGUG
AGUU
AGUC
ACGA
ACGG
ACGU
ACGC
AAAA
AAAG
AAAU
AAAC
B

Figure 17 continued

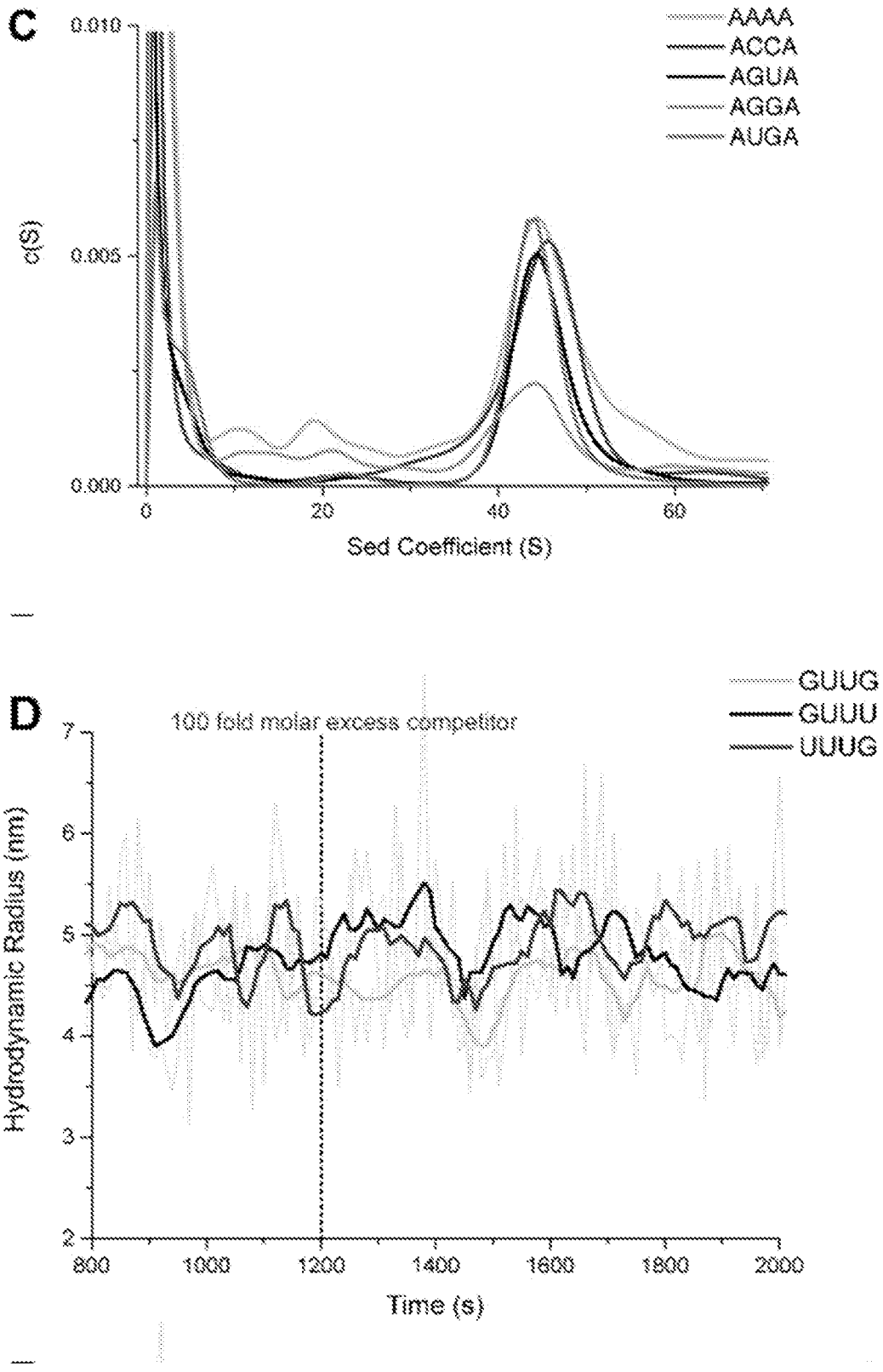

Figure 17 continued

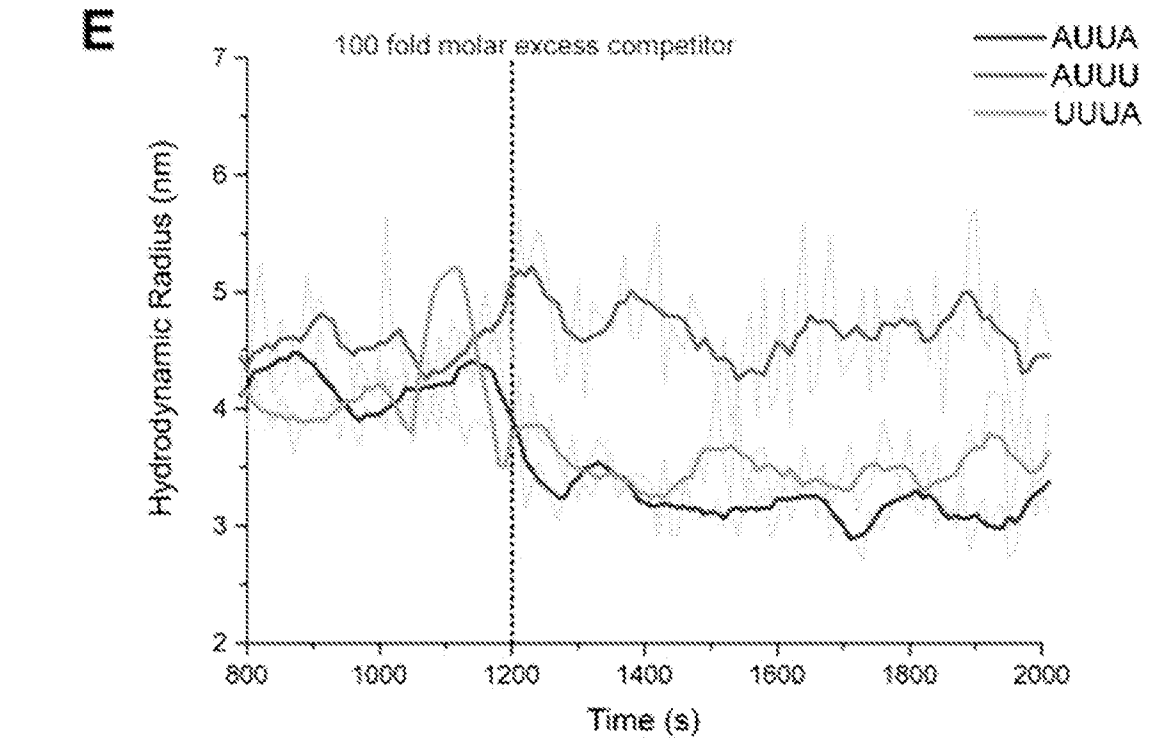

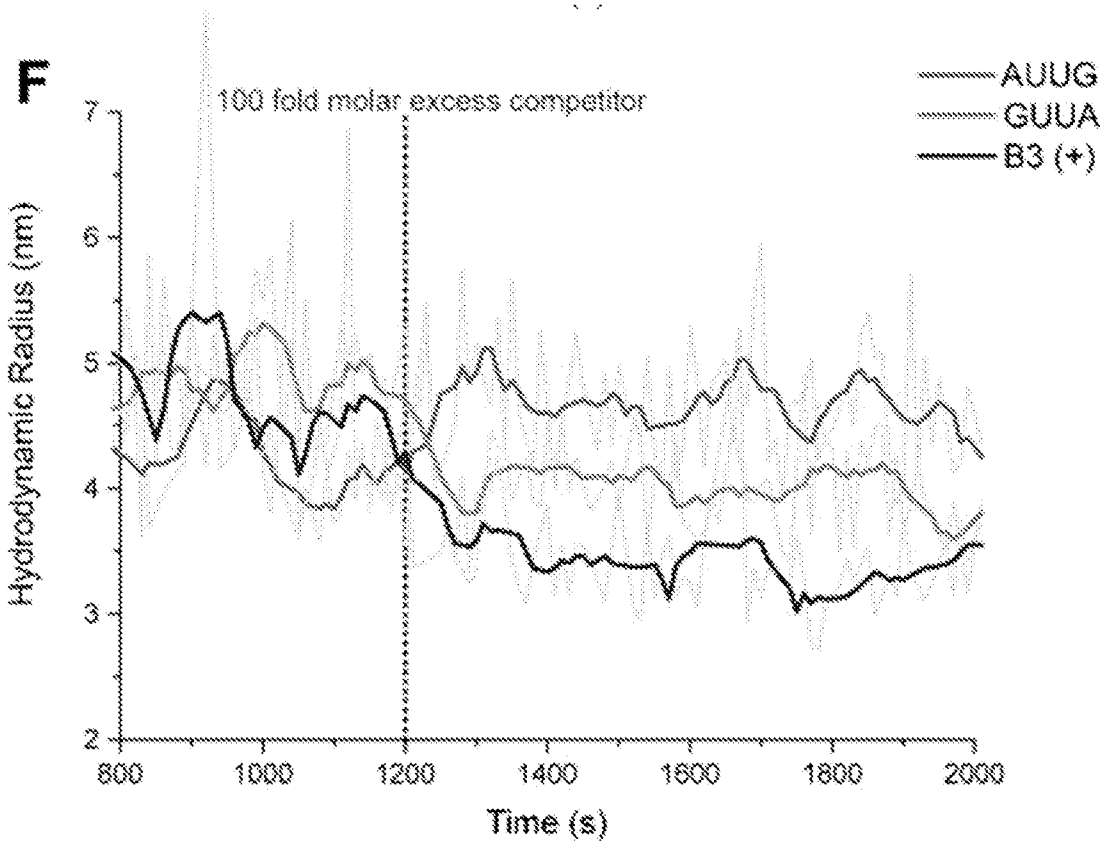

Figure 18

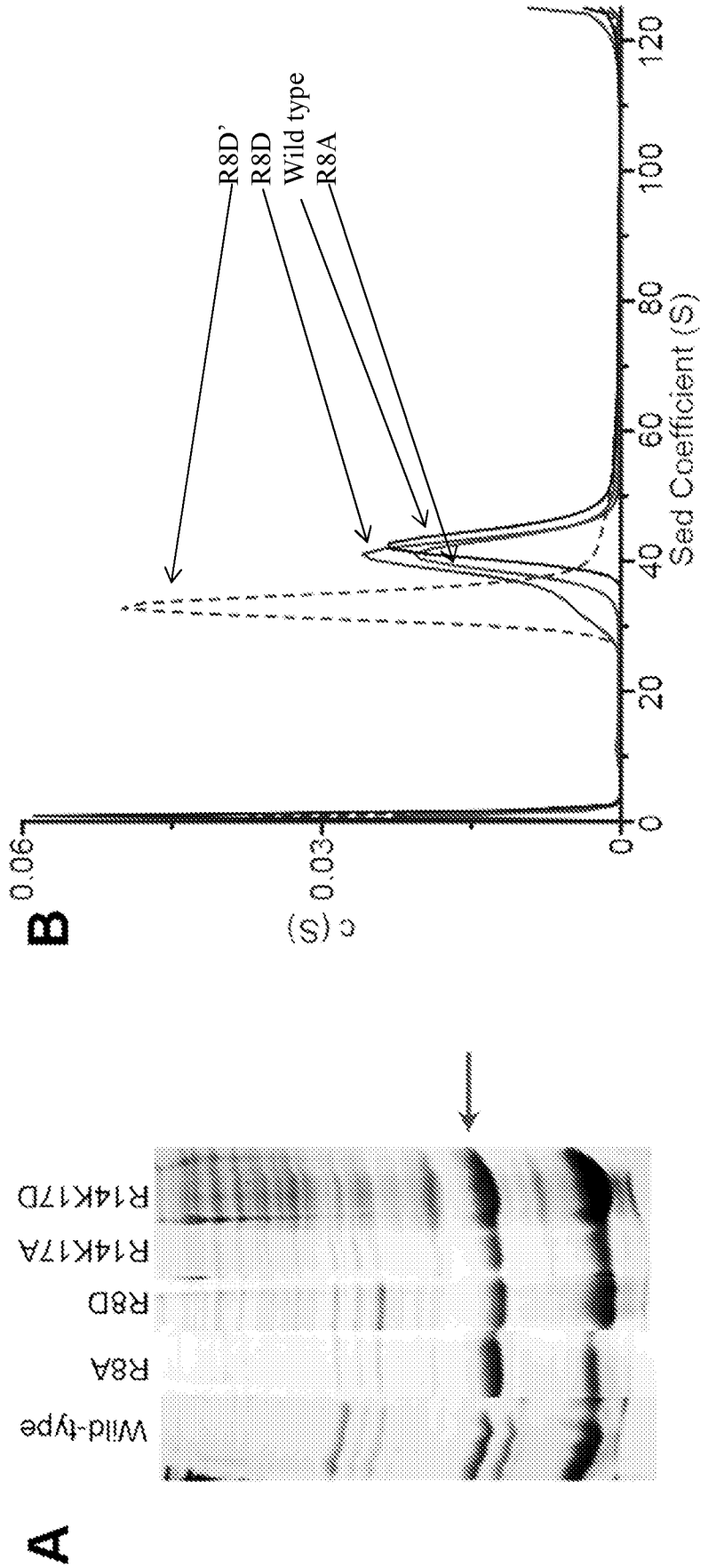
A
Wild-type
R8A
R8D
R14K17A
R14K17D
B
R8D'
R8D
Wild type
R8A
c (S)
0.06
0.03
0
0
20
40
60
80
100
120
Sed Coefficient (S)

Figure 19

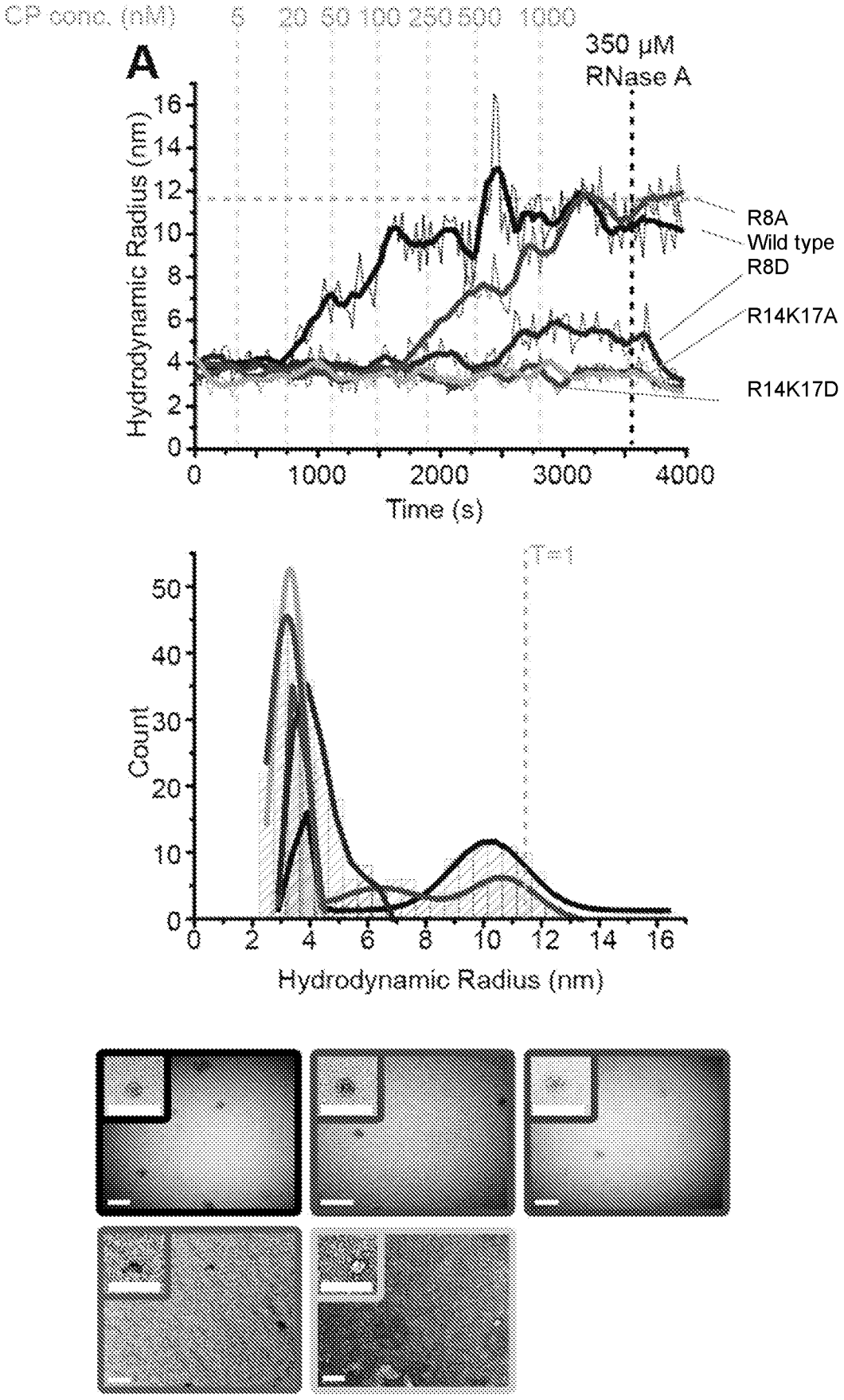
CP conc. (nM)
5
20
50
100
250
500
1000
A
350 μM
RNase A
Hydrodynamic Radius (nm)
Time (s)
R8A
Wild type
R8D
R14K17A
R14K17D
T=1
Count
Hydrodynamic Radius (nm)

Figure 19 continued

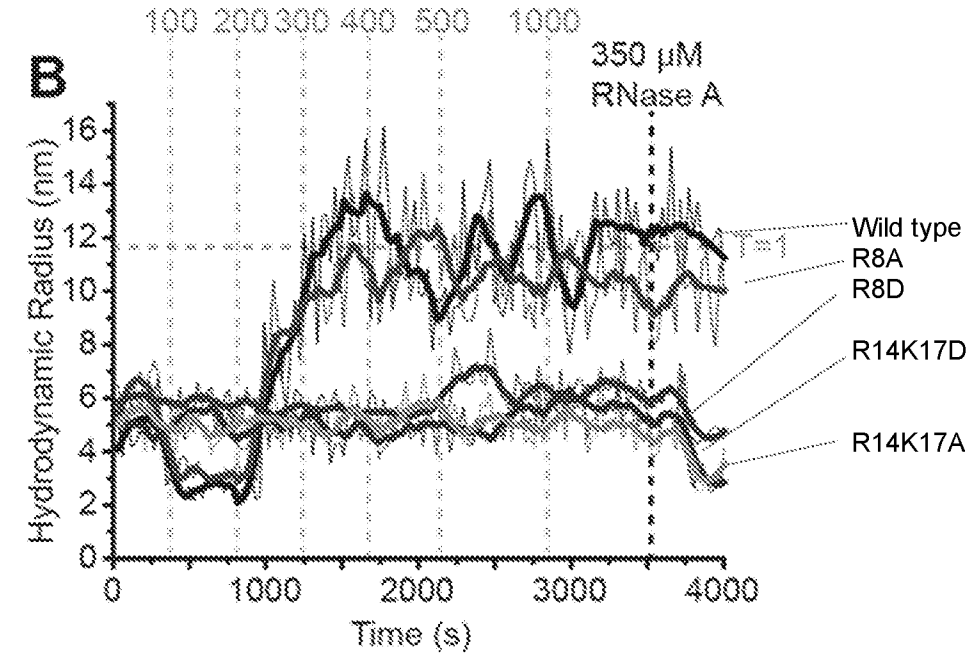

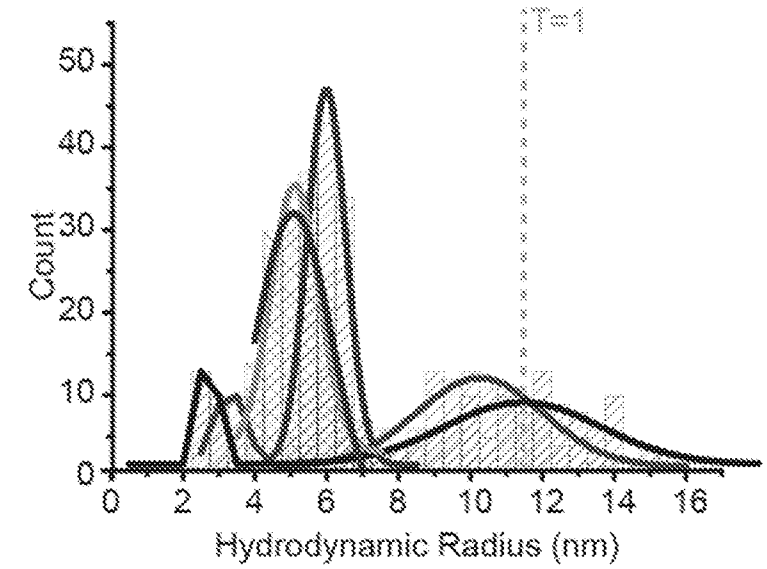

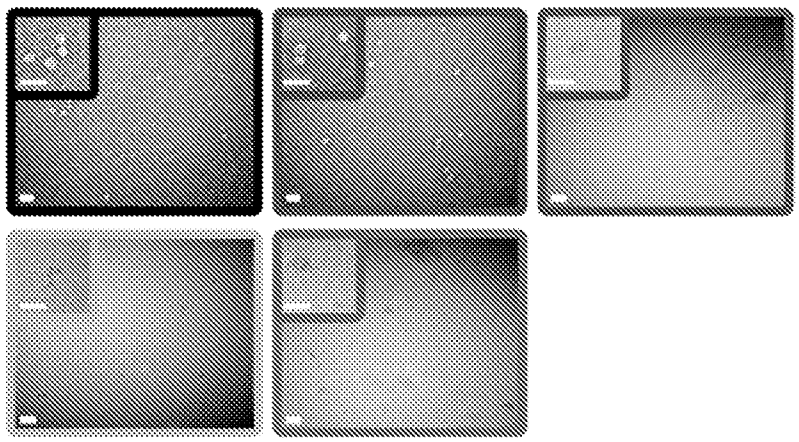

Figure 20

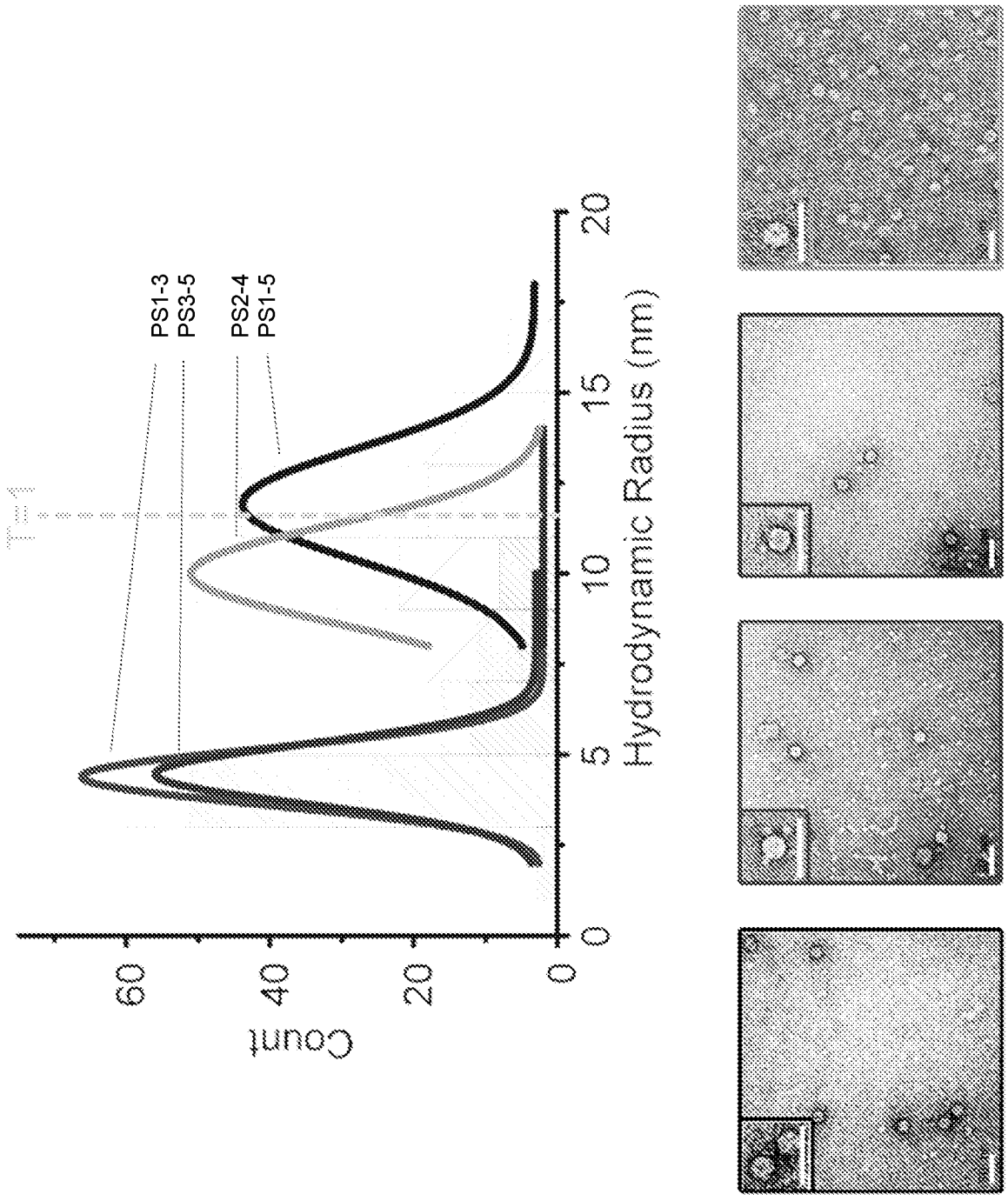
PS1-3
PS3-5
PS2-4
PS1-5
Count
Hydrodynamic Radius (nm)
0
20
40
60
0
5
10
15
20

Figure 21

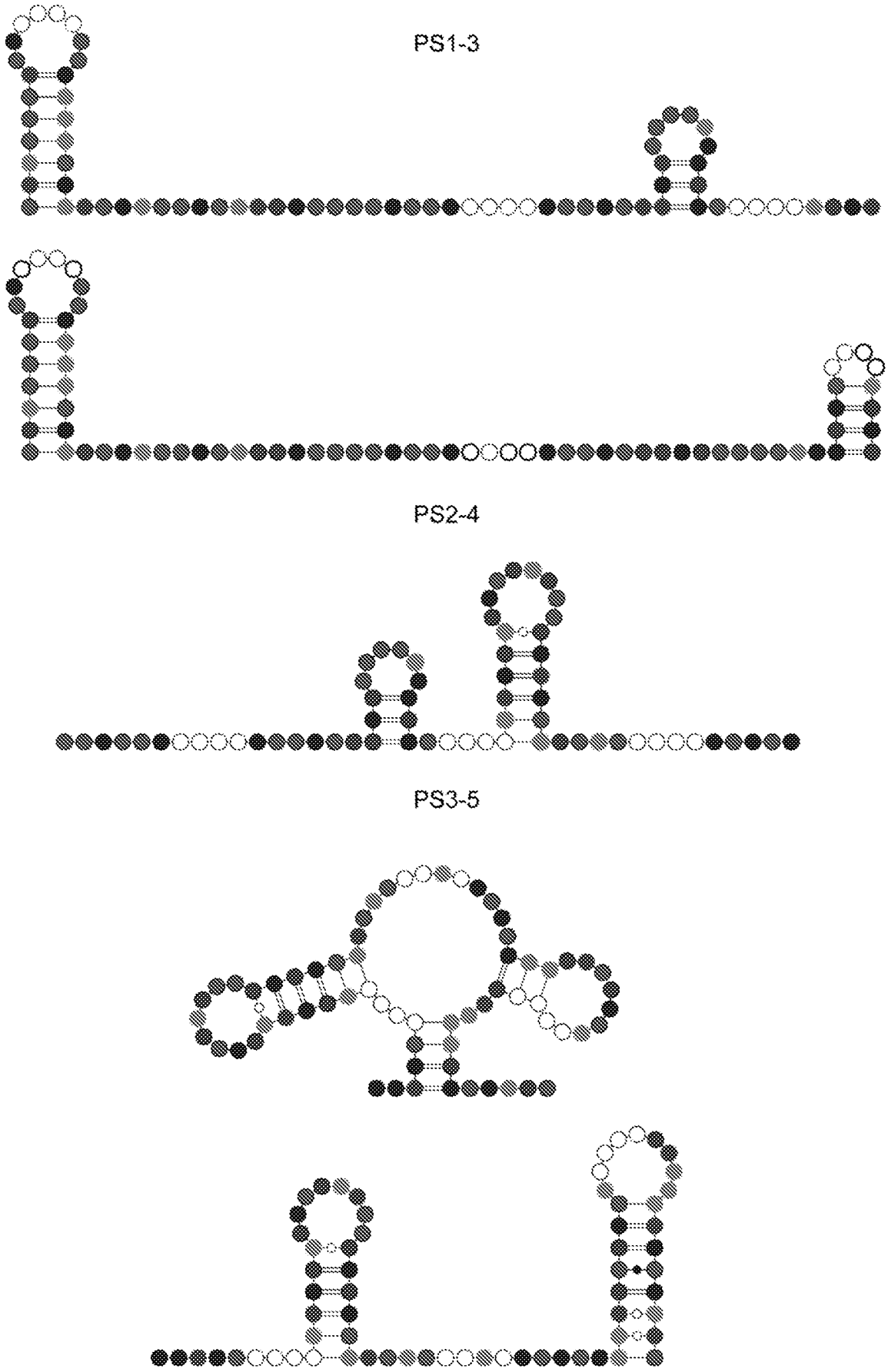

Figure 22

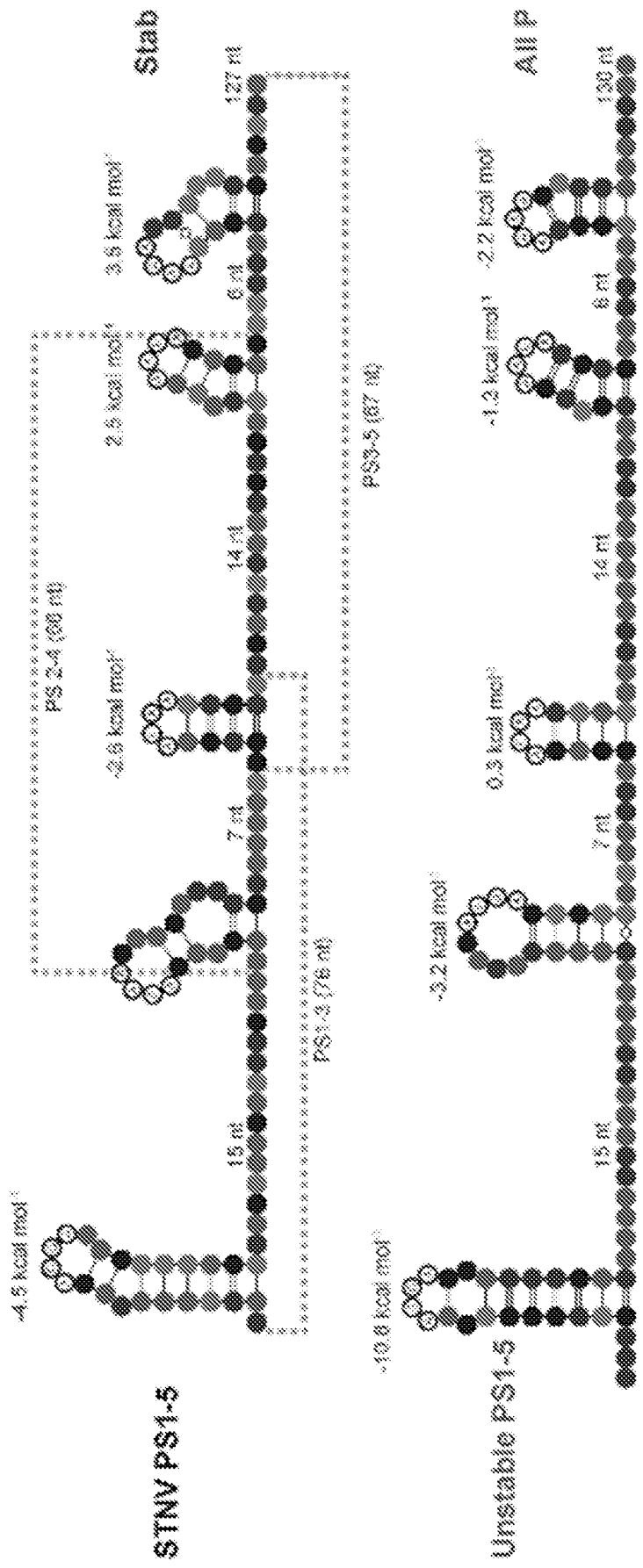
Stab
All P
STNV PS1-5
Unstable PS1-5
-4.5 kcal mol-1
-2.6 kcal mol-1
2.6 kcal mol-1
3.6 kcal mol-1
-10.6 kcal mol-1
-3.2 kcal mol-1
0.3 kcal mol-1
-1.2 kcal mol-1
-2.2 kcal mol-1
15 nt
7 nt
14 nt
6 nt
127 nt
130 nt
PS 2-4 (90 nt)
PS1-3 (76 nt)
PS3-5 (67 nt)

Figure 22

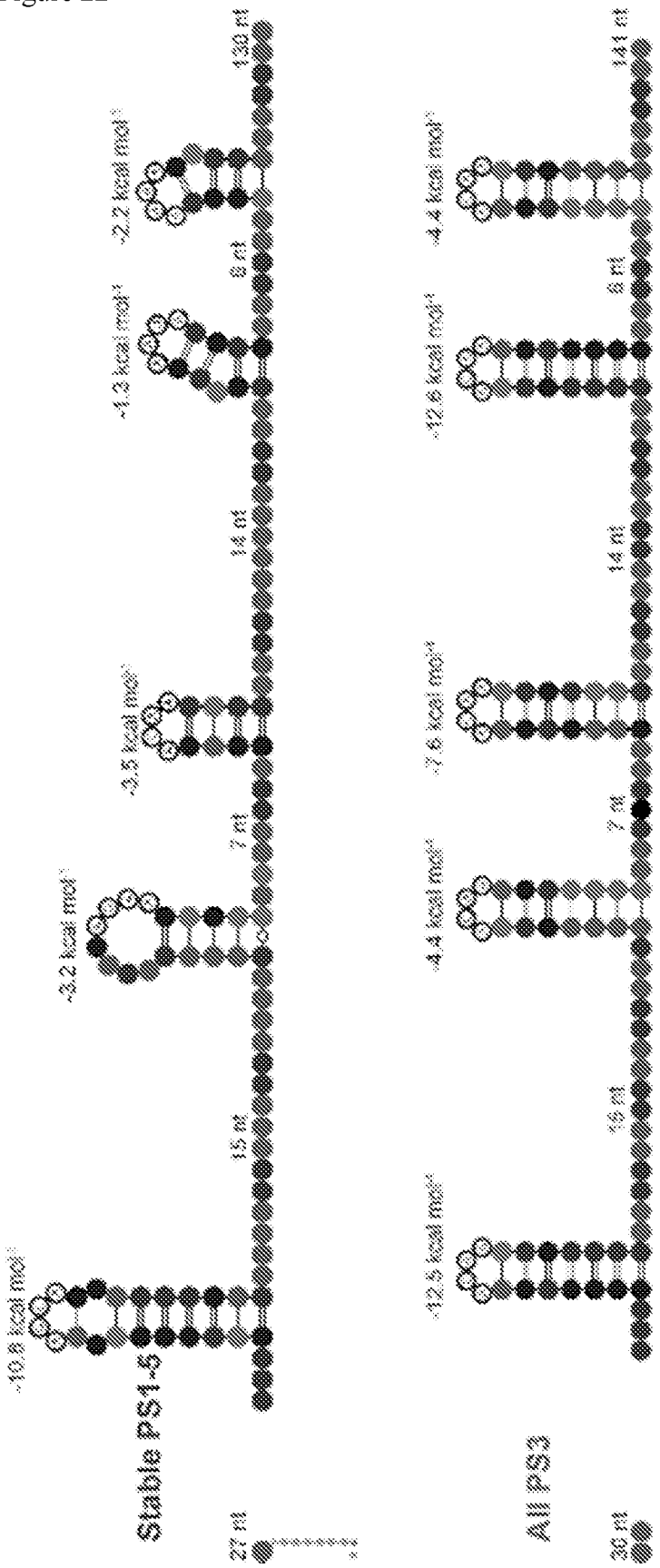
-10.6 kcal mol-1
-3.2 kcal mol-1
-3.5 kcal mol-1
-1.3 kcal mol-1
-2.2 kcal mol-1
15 nt
7 nt
14 nt
8 nt
130 nt
Stable PS1-5
27 nt
-12.5 kcal mol-1
-4.4 kcal mol-1
-7.6 kcal mol-1
-12.6 kcal mol-1
-4.4 kcal mol-1
15 nt
7 nt
14 nt
8 nt
141 nt
All PS3
39 nt

Figure 22 continued

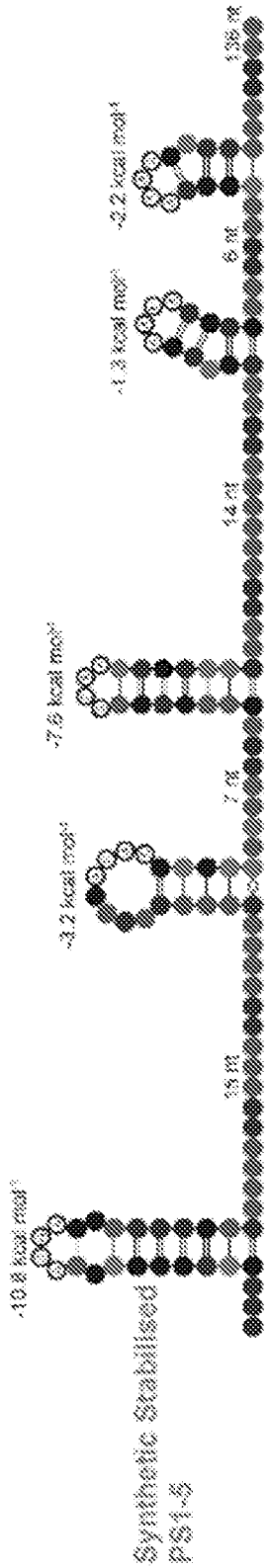

Oligonucleotide	Free Energy of Folding (kcal mol^{-1})				
	PS1	PS2	PS3	PS4	PS5
PS1-5	-4.5	N/A	-0.3	2.5	3.5
Unstable PS1-5	-10.8	-3.2	0.3	-1.3	-2.2
Stable PS1-5	-10.8	-3.2	-3.5	-1.3	-2.2
All PS3	-12.5	-4.4	-7.6	-12.6	-4.4
Synthetic, Stable PS1-5	-10.8	-3.2	-7.6	-1.3	-2.2

Figure 23

A

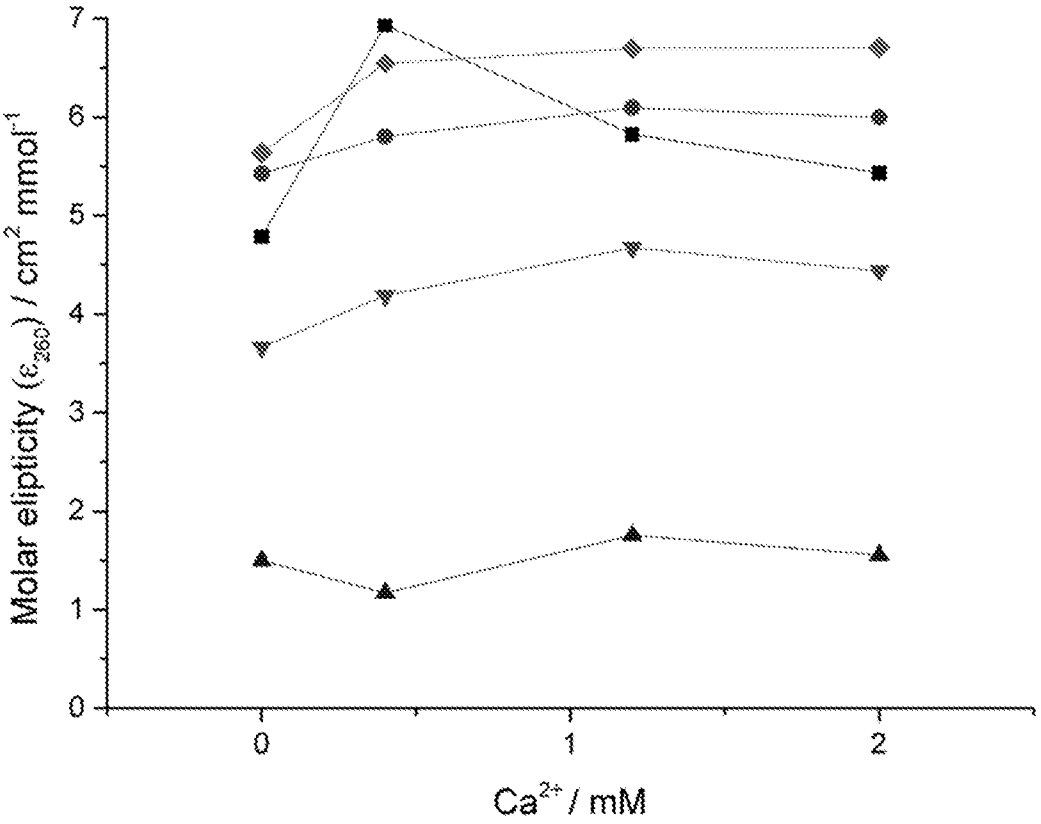
Molar elipticity (ϵ_{260}) / cm^2 mmol^{-1}
0
1
2
3
4
5
6
7
0
1
2
Ca^{2+} / mM

B

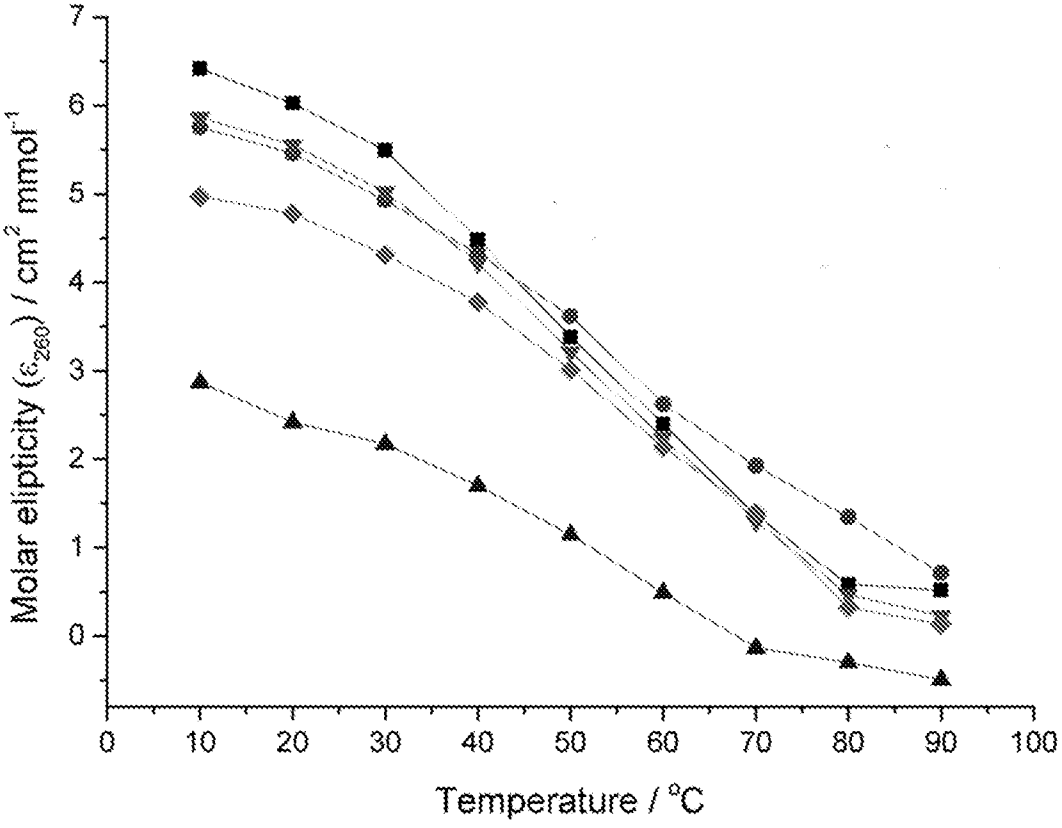
Molar elipticity (ϵ_{260}) / cm^2 mmol^{-1}
0
1
2
3
4
5
6
7
0
10
20
30
40
50
60
70
80
90
100
Temperature / °C

Figure 24

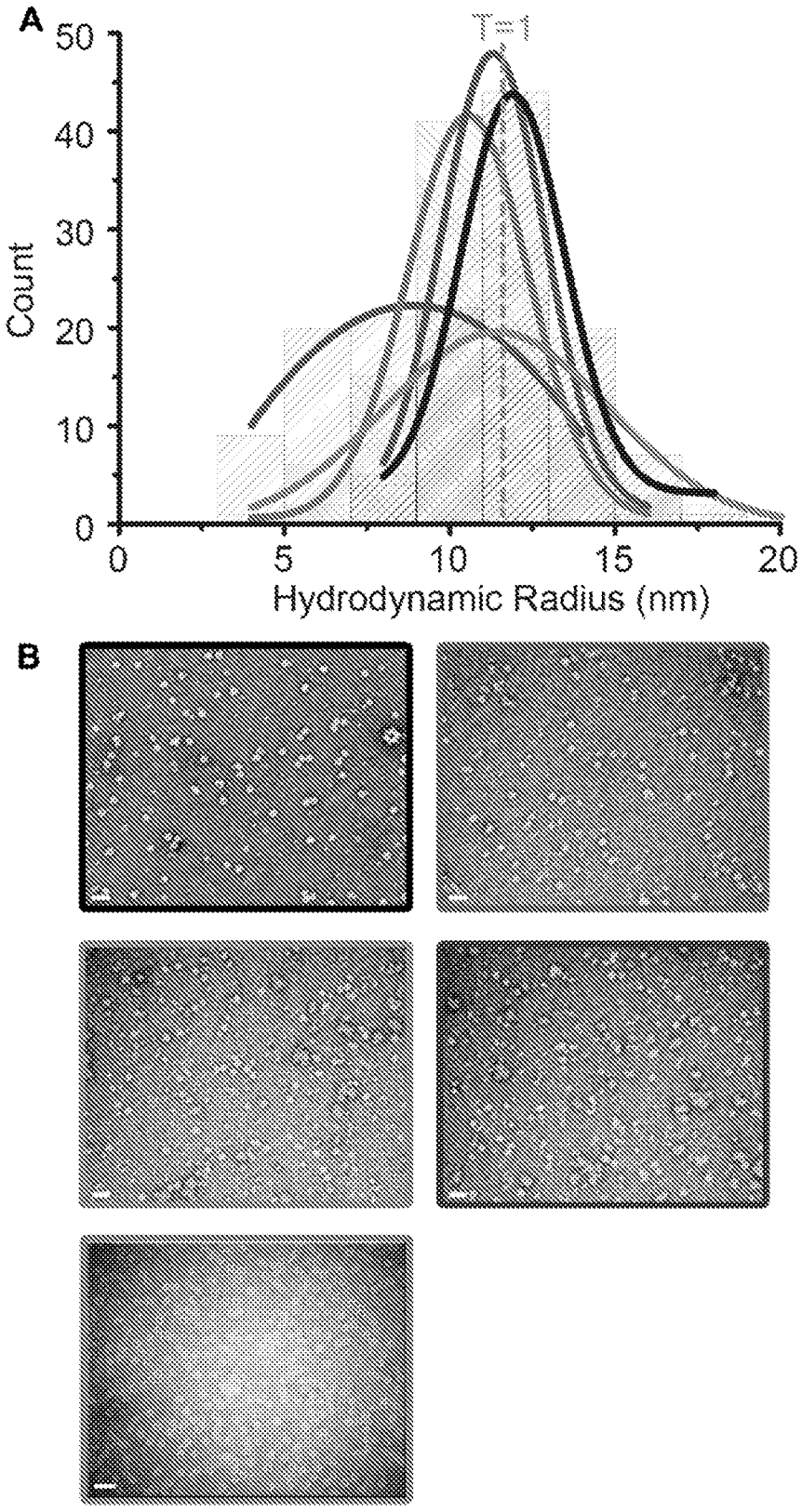

Figure 25

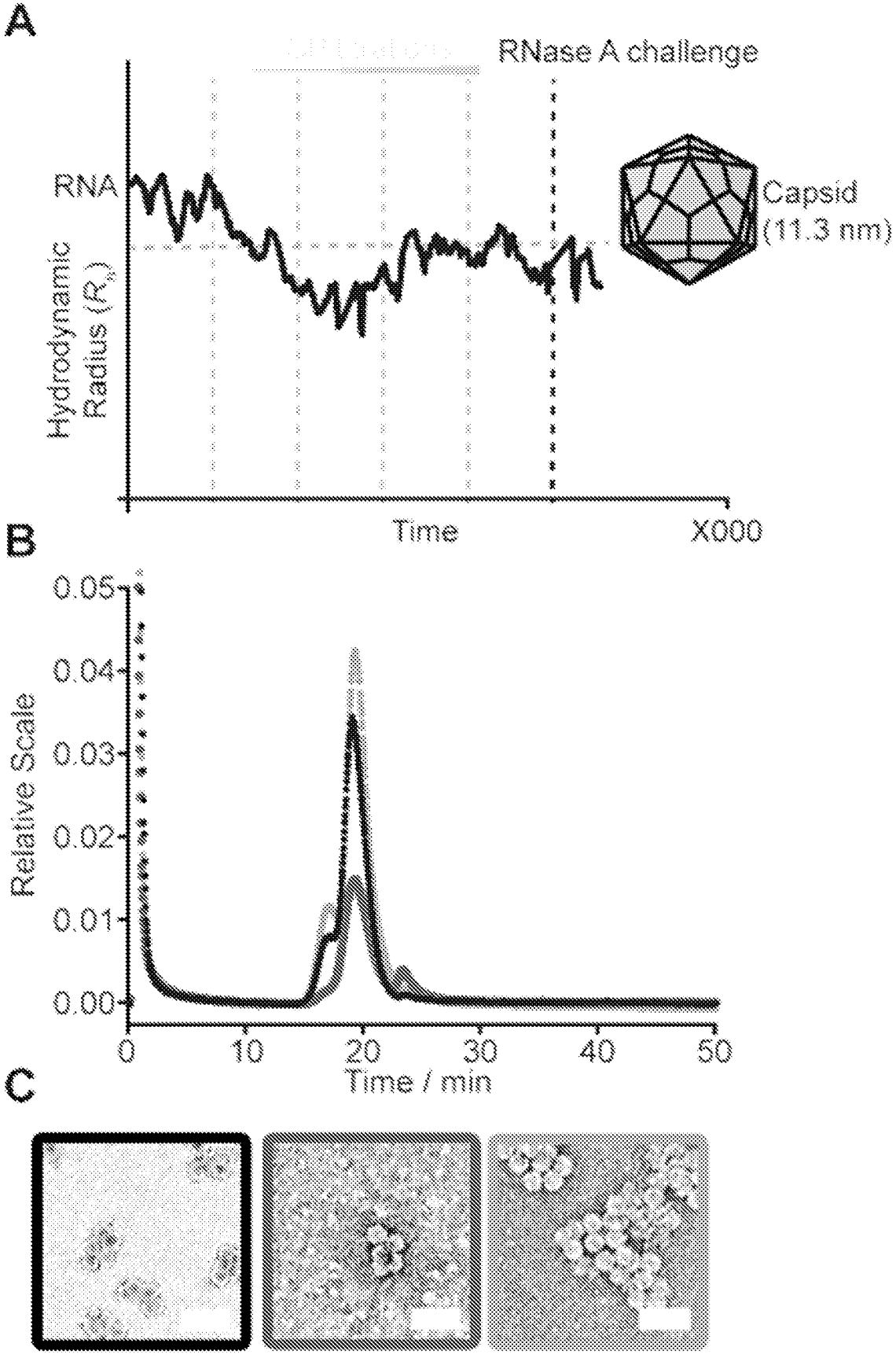
A
RNase A challenge
RNA
Hydrodynamic Radius (R_h)
Capsid (11.3 nm)
Time
X000
B
Relative Scale
0.05
0.04
0.03
0.02
0.01
0.00
0
10
20
30
40
50
Time / min
C

INTERNATIONAL SEARCH REPORT

International application No
PCT/GB2018/051475

A. CLASSIFICATION OF SUBJECT MATTER
INV. A61K31/7088 C12N15/113
ADD.

According to International Patent Classification (IPC) or to both national classification and IPC

B. FIELDS SEARCHED

Minimum documentation searched (classification system followed by classification symbols)
A61K C12N

Documentation searched other than minimum documentation to the extent that such documents are included in the fields searched

Electronic data base consulted during the international search (name of data base and, where practicable, search terms used)
EPO-Internal, WPI Data, BIOSIS, Sequence Search, EMBASE, CHEM ABS Data

C. DOCUMENTS CONSIDERED TO BE RELEVANT

Category*	Citation of document, with indication, where appropriate, of the relevant passages	Relevant to claim No.
X	E. C. DYKEMAN ET AL: "Solving a Levinthal's paradox for virus assembly identifies a unique antiviral strategy", PROCEEDINGS OF THE NATIONAL ACADEMY OF SCIENCES, vol. 111, no. 14, 24 March 2014 (2014-03-24), pages 5361-5366, XP055444531, US ISSN: 0027-8424, DOI: 10.1073/pnas.1319479111	1-18, 28-47
A	page 5361 - page 5366	19-27

-/--

[X] Further documents are listed in the continuation of Box C.

[X] See patent family annex.

* Special categories of cited documents :

"A" document defining the general state of the art which is not considered to be of particular relevance

"E" earlier application or patent but published on or after the international filing date

"L" document which may throw doubts on priority claim(s) or which is cited to establish the publication date of another citation or other special reason (as specified)

"O" document referring to an oral disclosure, use, exhibition or other means

"P" document published prior to the international filing date but later than the priority date claimed

"T" later document published after the international filing date or priority date and not in conflict with the application but cited to understand the principle or theory underlying the invention

"X" document of particular relevance; the claimed invention cannot be considered novel or cannot be considered to involve an inventive step when the document is taken alone

"Y" document of particular relevance; the claimed invention cannot be considered to involve an inventive step when the document is combined with one or more other such documents, such combination being obvious to a person skilled in the art

"&" document member of the same patent family

Date of the actual completion of the international search	Date of mailing of the international search report
25 July 2018	13/08/2018

Name and mailing address of the ISA/	Authorized officer
European Patent Office, P.B. 5818 Patentlaan 2 NL - 2280 HV Rijswijk Tel. (+31-70) 340-2040, Fax: (+31-70) 340-3016	Seranski, Peter

1

Form PCT/ISA/210 (second sheet) (April 2005)

C(Continuation). DOCUMENTS CONSIDERED TO BE RELEVANT

Category*	Citation of document, with indication, where appropriate, of the relevant passages	Relevant to claim No.
X	H. STEWART ET AL: "Identification of novel RNA secondary structures within the hepatitis C virus genome reveals a cooperative involvement in genome packaging", SCIENTIFIC REPORTS, vol. 6, no. 1, 14 March 2016 (2016-03-14), XP055494881, DOI: 10.1038/srep22952	1-18, 28-47
A	pages 1-10; figures 3-5	19-27

X	ROLFSSON ÓTTAR ET AL: "Direct Evidence for Packaging Signal-Mediated Assembly of Bacteriophage MS2", JOURNAL OF MOLECULAR BIOLOGY, ACADEMIC PRESS, UNITED KINGDOM, vol. 428, no. 2, 1 December 2015 (2015-12-01), pages 431-448, XP029407036, ISSN: 0022-2836, DOI: 10.1016/J.JMB.2015.11.014	1-18, 28-47
A	page 431 - page 445	19-27

A	PREVELIGE PETER E ED - LU TIMOTHY K ET AL: "Follow the Yellow Brick Road: A Paradigm Shift in Virus Assembly", JOURNAL OF MOLECULAR BIOLOGY, ACADEMIC PRESS, UNITED KINGDOM, vol. 428, no. 2, 18 December 2015 (2015-12-18), pages 416-418, XP029407038, ISSN: 0022-2836, DOI: 10.1016/J.JMB.2015.12.009 the whole document	1-47

A	WO 2015/033155 A1 (UNIV YORK [GB]; UNIV LEEDS [GB]; UNIV HELSINKI [FI]) 12 March 2015 (2015-03-12) the whole document	1-47

X,P	NIKESH PATEL ET AL: "HBV RNA pre-genome encodes specific motifs that mediate interactions with the viral core protein that promote nucleocapsid assembly", NATURE MICROBIOLOGY, vol. 2, 19 June 2017 (2017-06-19), page 17098, XP055494815, DOI: 10.1038/nmicrobiol.2017.98 the whole document	1-47

1

INTERNATIONAL SEARCH REPORT

Information on patent family members

International application No
PCT/GB2018/051475

Patent document cited in search report	Publication date	Patent family member(s)	Publication date
WO 2015033155 A1	12-03-2015	EP 3041480 A1	13-07-2016
		US 2016326529 A1	10-11-2016
		WO 2015033155 A1	12-03-2015